POLITECNICO DI TORINO

Collegio di Ingegneria Meccanica, Aerospaziale, dell'Autoveicolo e della Produzione

Master Degree Course in Automotive Engineering

Master Thesis in Automotive Engineering

Investigating the mechanical behavior of carbon fiber single lap joints utilizing structural adhesive: experimental and numerical analyses

Supervisor
Ing. Ciardiello Raffaele
Co-supervisor
Ing. Tridello Andrea
Ing. Boursier Niutta Carlo

Company Tutor
Ing. Actis Grosso Moreno

Candidate
Bettoni Edoardo
S303290

Academic Year 2022/2023

List of figures

List of tables

Acknowledgement

This thesis would not have been possible without the guidance and the help of several individuals who in one way or another contributed and extended their valuable assistance in the preparation and completion of this study, which is just the termination of several years of study in this university.

I would like to start to thank my academic supervisor Raffaele and his colleagues Andrea and Carlo who assisted me for this research, they all guaranteed guidance, support and expertise that enabled me to complete the hard work of this thesis. Big thanks also go to my company side tutor Moreno who assisted me daily ensuring a rigorous approach which enabled me to learn many new competences on the simulation field, as well as Ugo which guided the project and followed closely the work.

I then thank my parents for always letting me choose with my mind, for better or worse. They have always been an example for me of strength and determination, in work as well as in life, for teaching me to always give my best, without being afraid to make mistakes, and that any goal is achievable with commitment and passion.

Thanks also to Virginia who is living with me daily since a couple of years, thus she is always supporting and enduring me every single day, when I get home. Big decisions on our future are made together and achieving this big goal of mine was also thanks to her.

Then I would like to thank all my friends that assisted me during this long but eventful journey.

A kind thought goes to a special friend, that in his own way contributed to my success sharing its happiness with me and all the others surrounding him, which today is looking at us from high in the sky, thank you for everything Ugo.

Abstract

The automotive field has always been one of the driving fields for mechanical research and development for many years. This brought many new complex and expensive solutions to be investigated and developed mainly in racing or high-end applications and then commercialized on road or commercial vehicles later on.
Composite materials are a great example of this trend and in particular in the last decades a lot of research went into adhesive bonding, a technique used to join similar or dissimilar materials of any kind. Adhesive bonding applied to composites reduced drastically the weight of assemblies usually made of many components, which traditionally were made out of metals and joined by welding or bolted connections which increased a lot the weight of the structures. This outcome allowed for an increase in performance in the racing field, a decrease in fuel consumption and consequently a decrease in emissions in road vehicles, which is a crucial factor in these years.

The following thesis work aimed to characterize a structural adhesive and the relative joints and correlate numerical simulations with experimental tests.
The adhesive used for this research is a toughened and high impact-resistant bi-component adhesive with an epoxy and amine base for the two components respectively.
The adhesive has been tested with different loading conditions through the Double Cantilever Beam test (DCB) on metal substrates, Single Lap Joint test (SLJ) made with carbon fiber substrates and Doge Bone test on pure adhesives specimens.
Different adhesive thicknesses were tested in order to understand property trends by varying this parameter, knowing in advance that too high thickness can bring a high degradation of the mechanical properties of the joint.
The parameters needed to validate a numerical Finite Element Method (FEM) model were determined for a further study of the adhesive joint configurations. The final goal was to have a clear understanding of the adhesive behavior, to be able to simulate any kind of structure in any loading condition, achieving accurate results.

1. Introduction

Adhesive connections have been used by humans in the past ever since any sort of civilization was established, for many different uses.

Initially these kinds of connections have been used for buildings on very rough structures, by using natural materials like mud and clay. Then finer techniques were discovered and the way to join different elements was improved. Nowadays it is common to find cement as a joining material in modern buildings, which is not so different from the joining techniques explained before and used thousands of years ago.

With iron workability obtained by metal forging bolted connections became of common use to join utensils, mechanical structures, objects, mechanical tools and so on.

In the last centuries, with the advent of more refined mechanical jobs, after the industrial revolution, new joining techniques have been developed, mainly for metals applied to structural applications. An example is the use of welding techniques to join similar materials.

Then, in the last decades, the further increase in research of mechanical performance and development of new solutions brought adhesive bonding in the structural field, while before was only used for the general joining of simple structures under the form of adhesive tape mainly or sticky glue applied on paper, wood or easy working materials.

Despite the introduction on the market of adhesives for some decades already, research and development are still growing and of great importance to achieve the desired mechanical performances required by very high-quality standards.

The target of the following study is to understand the mechanical behavior of an epoxy bi-component structural adhesive, which is a widespread material used in high-quality joints for mechanical structures. Many different adhesive makers are present in the market, with a wide range of different kinds of adhesives, based on each different application, properties of the adhesive itself and other categories. It is clear how the choice of the correct adhesive for a given application is crucial for an effective and high-quality joint.

In this research, various mechanical tests have been performed on the adhesive of study in order to understand the adhesive properties and mechanical behavior under different loading conditions.

The driving factors of engineering research have always been performance improvement, reduction of costs and overall quality increase. Product testing in the design phase is of critical importance since allows to understand the actual behavior, characteristics and aspect of the actual component. Physical testing is a time-demanding and expensive way to perform this. Since the market is moving faster and faster, requiring shorter lead times and reduced costs to increase profits, this led to the development of virtual testing over physical testing to reduce the time and costs of production of the final products. Virtual simulations are very common nowadays in any field, from electrical to thermal, from mechanical to aerodynamics, and from economical to managerial.

In the mechanical field, to simulate the behavior of structures Finite Element Analysis (FEA) is performed, in which the model is discretized and replicated in the virtual environment, then the problem is numerically solved and results are analyzed.

Thus, another goal of this research was to perform a Finite Element Analysis (FEA) to correlate experimental tests with virtual simulations. Two different software have been used to perform the virtual simulation, so an interesting comparison between the two will be presented in this work.

This thesis work has been developed at Podium Advanced Technologies as part of their research program, while experimental tests and specimen manufacturing have been carried out in the Department of Mechanical and Aerospace Engineering (DIMEAS) at Politecnico di Torino.

2. Adhesive

2.1 General adhesive concepts

An adhesive is a polymeric material that, applied on the surfaces of two or more components, allows a permanent joint among them. Adhesives can be used to join many different materials like metals, plastics, ceramics, wood, rubbers and composites.
Adhesives can be classified by many different characteristics like their source, chemical composition, physical aspect, technological application, method of application or curing method.
One key feature of adhesive bonding is the ability to join together different materials (unlike welding), this allows the use of new innovative materials with more traditional ones to achieve better mechanical performances. A great example that is now widespread in the automotive field is the joining of composites materials with metals, to reduce weight, thanks to the low density of Carbon Fiber Reinforced Plastic (CFRP), to increase mechanical resistance, in case of high-performance CFRP, to have high corrosion resistance, to have low thermal conductivity or to improve other properties.
Adhesives can be thermoplastic or thermoset. Thermoplastic adhesives are one-component and cure due to cooling after being applied in a liquid state on the bonding area. Usually, these kinds of adhesives are not used for structural applications since their mechanical resistance is quite low compared to thermosetting ones. They also have to work in a restricted temperature range since at high temperatures they lose their properties, but these kinds of adhesive can be melted and reused at the end of their working life several times before losing their properties, so in terms of environmental impact they offer a good solution.
Thermoset adhesives instead cannot be melted and reused, due to their chemical composition, since before bonding their monomers are unlinked and after mixing and curing the process cannot be reversed by applying heat to the adhesive. One-part and two-component thermosetting adhesives have an acrylic, polyurethane, epoxy, vinyl or silicon base usually [1].

Their cure process happens by common ageing, in fact, storage usually is done in a cooled environment since the curing process is accelerated by temperature increase following more or less the Arrhenius equation rate. Handling time can be significantly reduced by a slight increase in temperature (even just 10°C). For the same reason oven curing at high temperatures can reduce the curing time of the adhesives, which depending on the type and composition can take from several minutes to several days to fully cure, while an oven cure can last a few minutes if performed at sufficiently high temperature.

Two-part resins cure due to the mixing of a base polymer and a catalyst, with the same influence of temperature discussed above, these are the most used types for structural applications since they have a higher handling time compared to one-part ones usually, although precise mixing ratios have to be used to properly get the desired final properties of the joint.

Handling time is the necessary time taken by the adhesive to cure up to a point in which its strength is sufficient to hold the joint in place if subjected to small accelerations as for handling it, such strength is said to be handling strength. As for the full cure process, this can be affected by air temperature, humidity and general ambient conditions.

In general, there are countless types of adhesives with a lot of variability that allows designers to pick the most adequate adhesive for a given application, depending on the manufacturing process, working life, mechanical performances, particular properties, working conditions, environmental conditions and so on.

Their use can be limited on applications with temperatures below 180°C, since above this temperature polymers start to degrade and lose their properties.

Compared to traditional joining methods such as welds, rivets, and bolts, the weight of a bonded structure is significantly less, given the same constraints and requirements for the joint.

Mechanical properties of the bonded structure depend on the characteristics of the bond forces developed inside the adhesive (Cohesive forces), bond forces developed between adherend and adhesive (Adhesive forces), mechanical properties of the two substrates and from the interface surface between adherend and adhesive.

By looking at a bond section some terms used in this field can be distinguished:

- Adherend (or substrate): solid material on which the adhesive is applied to realize the bond.
- Adhesive zone (or interface): contact plane between two different materials. The bigger the interface the stronger the bond is.
- Transition zone: volume of material where distinct properties of a material are not recognizable since interactions between the two happen.
- Cohesive zone: area in which the bond material is applied and its intrinsic properties prevail.
- Overlap: Overlap area between the adherends, where the adhesive is applied.

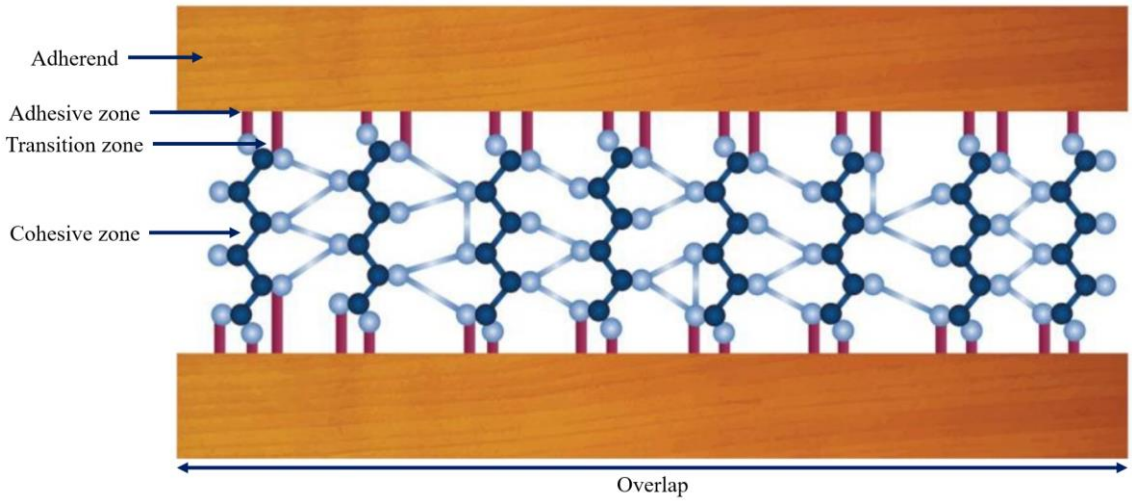

Figure 1. Adhesive joint section [2].

An advantage in the use of adhesive bonding can be seen when the two substrates, made of different materials, are subjected to a variation of temperature, thanks to its compliance, the adhesive, can compensate different expansions between the two substrates that have different thermal expansion coefficients, without inducing internal stresses to the system.

When choosing the appropriate adhesive for the application the bond itself should be even stronger than the substrates, so much so that the wanted failure should happen in the components and not in the adhesive layer.

Due to their low stiffness, some adhesives are able to absorb a lot of energy and damp the system they are attached to, by dissipating it through heat.

The laying of the adhesive layer and its cure doesn't induce internal stresses as a welding operation would do, avoiding distortion of the substrates in extreme cases.
In order to obtain a good quality adhesion it is necessary to prepare the substrate's surfaces in a proper way prior to bonding. Usually, the process is made up of two main phases: degreasing and abrasion. The goal is to obtain a homogenous surface with deep enough furrows so that the adhesive can grip well to the surface and provide good mechanical resistance. Sometimes abrasion can be replaced with chemical etching, which is a process that can alter the surface by removing material from it, exploiting the chemical interaction between the substrate's surface and the etching substance. Typically the process is carried out in the following order: degreasing – abrasion – degreasing - bonding.
The curing process can happen in several modes depending on the adhesive type: through chemical reactions engaged by heat, pressure, chemical agents, cooling of molten liquid or solvent evaporation.
During bonding manufacturing the adhesive can be laid during the application time, in which it has low viscosity and good wettability and allows the bond to be realized correctly. After this phase the adhesive starts to thicken and viscosity drops, starting its transition from liquid state to gel, which is an intermediate state before reaching the solid state. In the first part of the fixture time, the gel state can guarantee a certain stability to the bond, so that it can be carried around maintaining the substrates' relative positions. Once the bond reaches the handling strength it can provide enough strength for very light loads, while after the post-curing phase its full strength is achieved and the bond can be exploited fully for its application.
The curing process is an exothermic process so when working with the liquid mixture an excess in the volume of the mixture can cause a buildup of heat that cannot be dissipated, so adhesive temperature rises and the working time of the mixture reduces since the speed of the curing reactions increases.
When designing an adhesive joint it is necessary to take into account that by increasing adhesive thickness the joint resistance reduces, by increasing the overlap length the joint resistance increases, by increasing the width of the joint the joint resistance increases.

2.2 Adhesive bonding applications

Adhesive bonding applications are widespread, including not only the automotive and aerospace industries but also various other structural fields.

Many applications instead do not require particular strength of the bonding, others are considered only for aesthetics, and others are following sustainability criteria, so a big part of adhesives is made considering these factors without the need for high strength and durability, leading to a reduction in time and costs related to the product itself and to the bonding process.

In general, adhesives have been used for centuries in building and construction, woodworking, paper bonding, and packaging applications. Thanks to technological advancements, this joining technique has been employed in a diverse range of engineering applications lately, considering again the automotive field one of the pioneering ones regarding research and development of the best quality products.

2.3 Adhesive bonding in automotive industry

In the automotive field both in racing and passenger vehicles the use of adhesive bonding increased exponentially in the last decades, mainly as a way to replace mechanical joints, such as welds, bolted or riveted assemblies, but also to exploit its capability to join together dissimilar materials.

In racing adhesive bonding has been used mainly to reduce weight to increase vehicle performance and reduce the number of components so as to decrease assembly operation complexity, while maintaining high reliability.

In passenger vehicles, instead main goal recently has been to reduce weight to achieve lower fuel consumption and pollutant emissions.

As an example nearly 20% of Greenhouse Gases come from the transportation system, with a 15% share given by road transport.

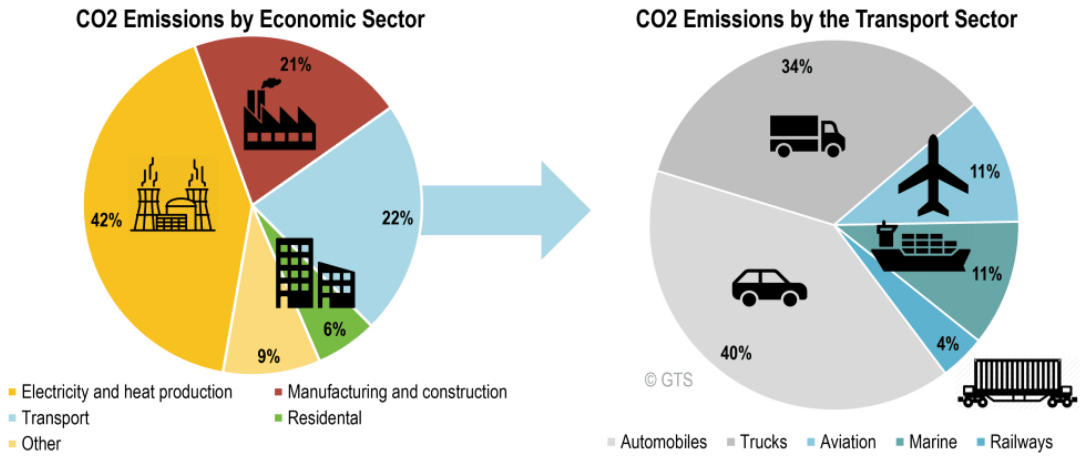

Figure 2. Global greenhouse gas emissions by the transportation sector [3].

In particular in Europe due to stricter EU regulations meeting targets for pollution has become a tough challenge, so the use of lightweight structures has become fundamental. In this field, it is widespread the use of structural adhesives that can cope with strong excitations maintaining their integrity to keep the component's functionality. These adhesives should also guarantee certain durability, especially in components that do not require replacement in the life of the vehicle.

Due to the long curing times at room temperature use of adhesives in large production volumes could be limited, but since the vehicle in the manufacturing line is taken through an oven for paint baking, this station can be used also to post-cure the adhesive and reduce the stock time needed to fully cure, reducing drastically the wait time and increase production efficiency.

2.4 Adhesive composition

The adhesive composition can vary to obtain a material with the desired properties and characteristics. The high number of components that are used to make an adhesive allows to obtain a wide variety of products with different properties, this allows the designer to properly choose the best fitting adhesive for its application basing its choice on substrate material, performances of the joint, loading conditions, curing process, manufacturing time, integrability with production process and so on.

The main components are:

- Binder: base of the adhesive, which contains the polymers that will link in the curing process. Possible bases are epoxy or acrylic resins.
- Hardener: they are employed in two-components thermoset adhesives that enhance the curing process and the formation of covalent bonds among polymeric chains which form the reticular structure.
- Catalyst: used in small quantities to control reaction speed between binder and hardener. They also control the working time of the mixed adhesive and cycle times.
- Solvent: its main role is to increase the bonding between adhesive and substrate reducing the viscosity of the mixture and improving its wettability. The volatility of the solvent acts also on the evaporation of the mixture.
- Diluents: they are employed to reduce mixture viscosity, they don’t evaporate but remain inside the adhesive even after curing, usually reducing the mechanical properties of the base resin.
- Fillers: these particles have the objective of decreasing the amount of resin needed in the mixture reducing costs, altering the thermal expansion coefficient, and thermal and electrical conductivity, mainly reducing thermal expansion during the curing process.
- Plasticizers: they increase the working time but reduce mainly the chemical resistance to other substances and thermal resistance [1].

Other substances can be used to manipulate the final properties, acting on corrosion resistance, thermal conductivity, electrical properties or mechanical ones.

2.5 Structural adhesives

As seen before, chemical composition and surface interactions between adhesive and substrate are very important to obtain a good adhesion. With the high use of composite materials in the last years, the combination of the base compound of the adhesive and resin matrix of the composite is a critical aspect to take into consideration in the design phase.

The general rule is that the substrate's material with a polymeric base, bonds well with adhesives of the same type. For this reason, the use of epoxy adhesives in combination with epoxy resin matrix for composites in the automotive world for structural purposes is very common.

The most used adhesives in this industry are based on epoxy, acrylic, urethane and cyanoacrylate. Each base has its pros and cons and the choice has to be taken based on the specific application, even though we can set some general trends that apply to these bases.

	Acrylic	Epoxy	Urethane	Cyanoacrylate
Peel strength	+	+++	++	+
Overlap shear strength - metals	++	++++	++	+
Overlap shear strength - composites	+++	++++	+++	++
Overlap shear strength - plastics	++++	++	++	+++
Impact toughness	+	++	++	+
Solvent resistance	+	+++	+	+
Temperature range resistance	++	+++	+	+
Flexibility	+	++	+++	+

Table 1. Main characteristics of adhesive bases [1].

As it is noticeable from the table above, epoxy-based adhesives can perform very well in a wide variety of properties, this is why they are the most popular type used in the automotive industry.

2.6 Epoxy adhesives

Epoxy resins have higher strength and toughness compared to other families of thermosets, so they are used in applications where high performances are required. Their density is quite low so they also offer a good strength/weight ratio for the bonding. Working time is satisfactory as can last from minutes to a few hours. They have high corrosion resistance and in general they maintain their properties high even if exposed to humidity, relatively high heat, or harsh environment. Epoxy base polymers reacting with hardeners form strong covalent bonds between chains that develop high stiffness and resistance of the final joint. Moreover, they are able to develop strong adhesive bonds with many substrate matrixes. During the curing process, they don't shrink much thanks to the low presence of volatile compounds and offer also good chemical resistance against most of the aggressive elements.
Often the curing process is carried out at a high temperature to reduce curing times and to increase the peak resistance, care must be taken to avoid thermal degradation of the material due to too high temperatures [4].

Here we can sum up the main advantages of this family of base resin:

- High mechanical properties after curing
- Good chemical stability
- Wide working temperature range (-150°C ÷ +200°C)
- Ability to vary mixture to obtain different properties
- Low shrinkage during curing
- Good adaptability to a wide variety of surfaces
- Long enough working time

Some disadvantages can also be found:

- High cost compared to other adhesives
- Long curing times at room temperature (several days usually)
- Impossibility to melt after cure and disassemble the joint without mechanical removal

- Care and sufficient knowledge of the manufacturing process is required to obtain satisfactory results

2.7 Mechanics of adhesion

Over the years many studies and theories about adhesion mechanics have been proposed and often it is difficult to associate a single mechanism to the creation of a joint, instead the bonding happens thanks to a combination of different mechanisms, each contributing to a greater or lesser extent.
Previous studies showed that each mechanism acts at a particular length scale (microscopic, macroscopic, atomic scale,…).
The most important mechanisms that can be highlighted are mechanical interlocking, electrostatic theory, weak layers, wettability, diffusion and chemical bonds [1][4].

Mechanical interlocking:
Based on the mechanical constraint theory, adhesion happens due to the penetration of the adhesive inside the substrate, thanks to surface irregularities, pores and cavities. When the adhesive solidifies the bonding happens thanks to crests and valleys of the surface that constrain the adhesive with the substrate.
Several studies confirmed that a rougher surface can guarantee a stronger bond than a smoother one, however, it is also possible to obtain good enough bonding capabilities on a smooth surface, so this theory cannot be used alone to explain adhesive bonding phenomena.
Bonding can be improved by correctly cleaning the surface with degreasing agents or mechanical removal, by increasing surface reactivity or by increasing the contact surface area. It is then possible to improve the joint by varying the physical properties of the bonding surface. Higher surface roughness brings a higher resistance, but lower fatigue resistance due to sharper peaks that can cause easier formation of cracks. Surface roughness has to go along with a good wettability of the adhesive, to reach all the pores and cavities, otherwise unsatisfactory results may happen.
Another aspect confirming a higher peak mechanical resistance of high surface roughness is the fact that if a crack starts at the tip of a crest its propagation area is limited and has to travel a rougher path to propagate along the surface, so this contributes to giving higher strength at peak loads when cracks are initiated.

Electrostatic theory:

Electrostatic theory is based on the fact that between two materials with different band electronic structure there is an electron transfer, this occurs to reach the Fermi level which is the last available energy level and causes the formation of a double layer of electrons that causes the emergence of electrostatic forces between adhesive and adherend.

According to some studies when detachment between adherend and adhesive happens a first increase of voltage and accordingly an increase in the resistant force up to a peak and then a decrease of both can be appreciated.

Weak layers:

This theory suggests the failure of weak cohesive bonds between the substrate's matrix and some superficial layers of material defined as weak layers. Weak layers can form due to the nature of the adhesive, of the adherend or the environment when impurities concentration bonds to the substrate. Some polymers inherently contain these impurities inside them, that will cause the formation of this weak layer. Contamination in the air can also cause this phenomenon, as well as air trapped into crevices due to not good wettability of the adhesive. Usually, the thickness of these layers is very small, in the range of nanometers from the surface.

Wettability:

According to this theory, adhesion happens thanks to a molecular contact between adhesive and adherend along with interface forces developed by the contact. Wettability is the necessary property to realize a continuous contact between liquid and solid. A necessary condition so that an adhesive is able to correctly wet a solid substrate is that the adhesive should have a lower surface tension with respect to the one of the solid. It is obvious how superficial treatment of the solid can favour this condition. Contact between two materials is important because the Van der Waals forces that rise among molecules lower significantly increasing the distance among them.

Van der Walls and acid-base Lewis forces included in this theory can be correlated to thermodynamics parameters such as the surface free energy of adhesive and adherend.

This theory has been developed trying to correlate the surface free energy to other material properties and then trying to estimate an adhesion work of the surface properties and then look for a relation between adhesion resistance and adhesion energy.

Diffusion theory:

According to this theory, an adhesive bond is developed thanks to the molecular interdiffusion between adhesive and adherend, this is true when both components have a polymeric base and involved polymers are constituted of long molecules with high freedom of movement. Both the nature of the materials and physical conditions influence the adhesion and its strength. This interdiffusion phenomenon happens in a vary thin layer at the interface between the two materials in a narrow range (1 ÷ 100 nm). High resistance of adhesive bond is achieved when the two materials are soluble in one another.

Since the diffusion is enhanced at higher temperatures, also the adhesive bond strength is a function of the temperature.

An other important factor in this theory is the viscosity of the adhesive base since the motion of the molecule can be inhibited by the difficult path encountered and entanglements of other chains in the surroundings, which reduce the interdiffusion.

Chemical bond theory:

The strongest chemical bonds between adhesive and substrate, those with the highest binding energy, are defined as primary. These primary bonds are covalent, ionic and hydrogen. Secondary ones are instead Van der Walls and London forces.

Types of interaction that form depend on chemical composition at the interface and surface reactivity. Adhesion resistance depends instead on the number of chemical bonds that form their nature, and from other mechanisms that contribute previously listed.

Covalent and ionic bonds give the highest contribute to the adhesion resistance and mainly form on the substrate's surface that contains polar groups. Covalent is the strongest and most long-lasting bond but requires chemical compounds that are mutually reactive, so polar groups enhance their formation.

Surfaces of thermosetting coatings of plastics or composites contain functional groups that usually generate a covalent bond with the adhesive material. These conditions can be created through superficial treatments that use flame or plasma.
Dipole-dipole bonds are secondary interactions that occur following the trend of polar molecules to align so that the molecule's positive charge is near the negative charge of adjacent molecules.
A hydrogen bond forms between two molecules when a hydrogen atom, linked to a small and highly electronegative one, gets attracted by a couple of electrons of another molecule.
The acid-base bond arises between an acid and a basic substance, like the hydrogen bond between two water molecules.
London forces develop from instantaneous dipoles that form due to electron position change during their path around the atomic nucleus. The bigger the atoms and the most number of electrons per atom, the stronger the bond will be, due to a higher polarity of the molecule.
In general adhesive coatings tend to form stronger bonds with substrates that are made of the same type of functional group, with high reactivity.

The wide variety of different phenomena involved in the mechanics of adhesion , the different typologies of substrates and adhesives themselves, make the adhesion principle a very complex and intricate matter, but the great advantages brought by a high quality bond make this field of research actual and worthwhile, especially virtual modelling and joint simulation through finite element method.

2.8 Surface preparation

The application of an adhesive to a surface often requires its preparation, aimed firstly at cleaning it, but also at modifying the chemical and physical properties that are important for adhesion, which then improve the mechanical performance of the bond.
The surfaces to be bonded have surface layers characterized by impurities: in metals, a surface oxide layer can lead to the absorption of molecules through hydrolysis; in ceramics or polymers, organic molecules are absorbed into the surfaces. On some metal components, lubricants and oils may be present on the surface due to machining operations or any other production process, 3D printed parts or plastics may have powder laying on the surface, and dirt of any kind may have deposited on any material's external surface. So due to these various kinds of surface contaminations and others, a good surface preparation process is needed to obtain a high-quality bond.
These external layers are poor in terms of adhesion and it is necessary to carry out surface treatments, which can be both chemical or mechanical. It is important to point out that these treatments do not go deep into the component but only affect a thin layer on the surface of the part. Any specific treatment has a direct impact on the quality of adhesion, the properties of static and dynamic fatigue and corrosion resistance can also be improved.
The treatments to be carried out depend on the adhesive, the substrate and the contaminants and are characterized by a limited duration in time.
The surfaces can be treated in three main different ways and, above all, the application of one treatment does not exclude the other: preparation, pre-treatment, post-treatment.

Surface preparation:
Removal of surface contaminants such as oil, grease, organic compounds, etc. Cleaning agents or solvents can be used for these operations. Cleaning agents are the most economical and easiest to use. They are almost always applied by spraying. However, they can react with the surfaces of some metals, so it is very important to know the chemistry of the substrates. Solvents have an organic base and are applied through a soaked cloth. Depending on the substrates, different chemical species are used, the most

frequently used are Acetone, which may be too aggressive on some polymers or plastic material and iso-propyl alcohol which is less aggressive and can be used also on most polymers. The removal of impurities must always precede any other surface treatment, either mechanically, as sanding in the presence of impurities pushes them further and further into the surface, making adhesion more difficult, or chemically, as the impurity layer prevents solutions from attacking the surfaces.

Surface pre-treatment:

Strongly absorbed layers on the surface are removed by mechanical, physical and chemical measures:

- Mechanical treatments: these include, abrasion with sandpaper, sandblasting, scratching with metal brushes or scrapers. The use of these instruments allows an increase in surface roughness and as previously seen in the adhesion theories, this property influences mechanical adhesion and the modification of surface wettability. However, during grinding, contaminating particles of the abrasive, the surface layer is to be ground off and the material itself is detached and rests on the external surface of the component, so they must be removed later with further processes. This process is mainly used for removing oxide layers, rust and fouls.

- Chemical treatments: this treatment is carried out by immersing the piece in tanks containing a chemically active, purely acidic solution and passing electricity through it. Electrochemical deposition takes place by immersing the metal substrate in a bath, whose chemistry depends on the desired coating. The cathode is often the piece to be treated, especially if it is of a constant size, while the anode can be soluble, like nickel, or insoluble, like graphite. By applying current in an electrolytic solution, the metal ions are deposited on the part to be treated and form a stable porous oxide layer that modifies the electrochemical properties and favours adhesion.

- Physical treatments: treatments in which the surface is chemically altered by exposing it to high-energy charges or other ionic species. These treatments are more efficient for metal substrates. A first example is flame treatment: A flame generated with propane or acetylene is introduced into the atmosphere or air. Both fuels contain oxygen-containing groups which absorb into the surface after treatment and increase the polarity and thus the wettability. The following example is plasma treatment. The gases from which the plasma is generated can be argon or nitrogen as well as oxygen. Another example is crown treatment, in which the substrate is placed in a flat capacitor: The voltage is applied to the electrode, while the other plate takes the form of an electrically earthed roller. The build-up of voltage ionizes the air, which increases the surface tension of the substrate. Energetic species and polar groups, that can adhere to the surface, are introduced into the atmosphere of the treatment.

Surface post-treatment:

This includes the application of adhesion promoters such as primers to improve adhesion and protect the surface. The main purpose of primers is the interaction between adhesion and adhesive due to their chemical properties, which make it possible to create bonds with both. They are applied as thin films on the adhesive so that they bond closely with it, changing the surface tension or polarity of the substrate. The use of primers improves cut and peel resistance. The chemistry of the primer used is often related to the adhesive to be used and is usually an organic, thermosetting solvent with low solids content. The downside of adhesion promoters is that they are treated with solvents that are often organic, leading to environmental and disposal problems.

2.9 Adhesive application

Adhesive application is of particular importance to avoid gaps and voids in the bonding area.

Liquid adhesives can flow well and fill all the cavities, resulting in a homogeneous spread of the adhesive itself and easier manufacturability. Thick and viscous adhesives instead may lead to more difficult joint manufacturability, since the adhesive cannot flow as well.

Even if viscous, some mono-component adhesives and bi-component one extruded by using a cartridge and a mixing nozzle can present no voids or air bubbles trapped in the adhesive's volume if mixed well. Instead, if hand mixed sometimes due to the nature of the adhesives, voids and air trapped inside its volume can cause some defects in the adhesive layer.

In some cases degassing can be used to remove air bubbles present in the adhesives, this technique consists of applying a vacuum and is particularly effective on liquid and low-viscosity adhesives, but on thicker ones, it can be tricky to get all the air out of the mixed adhesive.

Taking for granted the correct mixing, air can still be trapped in the adhesive layer if an incorrect application of it is performed, closed and circular patterns must be avoided, as well as parallel lines of application, instead single lines or undulated ones are preferred. On top of this adhesive should always be applied on both sides that have to be bonded, to guarantee a correct spread of the adhesive on all areas of interest and to avoid again formation of air pockets.

2.10 Adhesive failure

Joint failure can happen in many different ways, depending on the loads applied to the joint itself, the good practices adopted in the manufacturing of the joint, the actual design parameters chosen, the type of adhesive chosen, chemical properties at the bonding interface and many other parameters, so when analyzing the fracture surfaces it is not so straightforward a correct and rapid assessment of the causes of failure.
In general joint failure can happen in various modes:

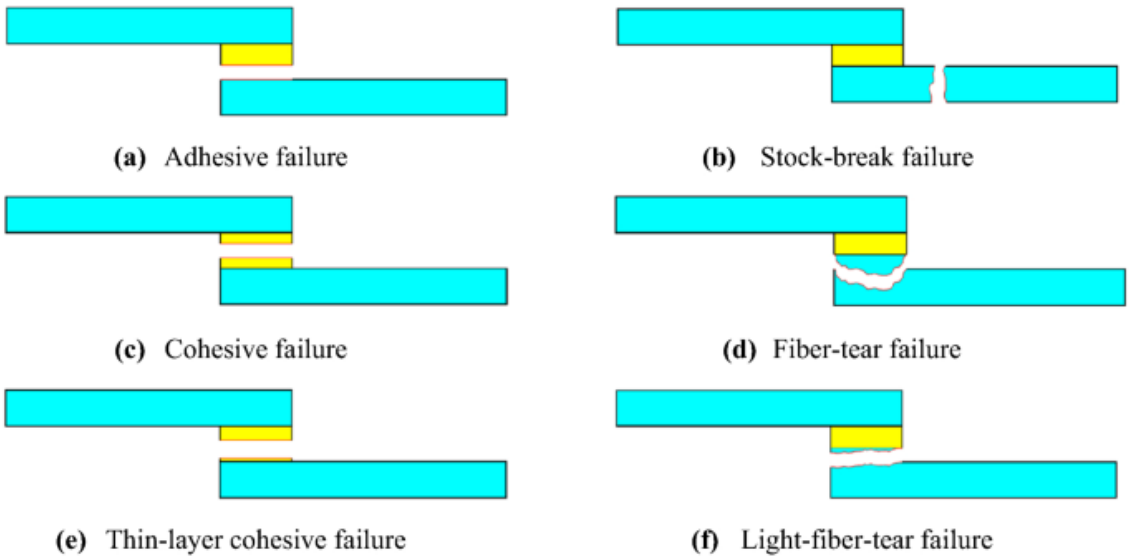

Figure 3. Failure modes [5].

- Adhesive failure: failure in correspondence of the effective interface between the adhesive and the substrate. This failure is often due to incorrect preparation of the joint, compatibility problems between adhesive and adherends or in some cases a cohesion force greater than that of adhesion.
- Stock-break failure: failure does not evolve in the overlap area, but happens entirely in the substrates. This means that the joint is stronger than the substrate and the full potentialities of the joint are exploited.
- Cohesive failure: failure for which an adhesive layer remains integral to the surface of both adherends. This is the desirable failure during experimental tests

in which the goal is to get adhesive properties. This mode highlights a good adhesive layer, that is stronger than the cohesive one.

- Fiber-tear failure: can only occur in the case of composite material. Here the failure does not occur in the adhesive but in the fibers of the substrate's material along the overlap area. This could be caused by adhesive strength greater than that of the fibers' adhesion or due to particular loading out of the plane of the fibers, which makes them work in an unwanted direction, causing premature failure.
- Thin-layer cohesive failure: failure similar to purely cohesive (c), but with an unequal adhesive distribution on the substrates. This can be caused by low bond forces between the cohesive layer and the adhesive one.
- Light-fibre-tear failure: breakdown of the fibres of the material, as in mode (d), but with failure closer to the interface between adherend and adhesive. The causes of this failure can be similar to the mode (d).

In real applications the wanted failure should be the stock-break one so that the bond is fully exploited and the adhesive can resist even more than the component itself, this is achievable with proper adhesive selection, design and manufacturing. In testing the wanted failure mode is the cohesive one, but in most cases however, the obtained failure is of the mixed mode, due to local inaccuracies and joint complexity.

A common practice in actual component production to increase the overall bonding strength is to use more bonding areas or longer overlap, to achieve the same resistance wanted in the design phase.

2.11 Stresses on adhesives joint

Depending on the loading of the structure the adhesive can be subjected to different tensional states:

- Compression: it is applied by a force that is in-plane, straight and towards the bond. The load is distributed across the entire area of the bond line.
- Tension: the pull direction is straight, in-plane and away from the adhesive bond. The load is distributed across the entire area of the bond line.

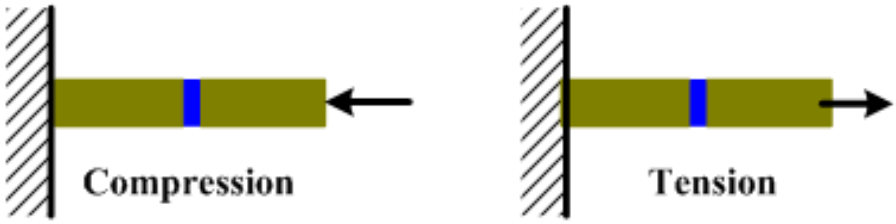

Figure 4. Compression and tension loading condition [6].

- Shear: it is a pull away from the adhesive bond in a parallel plane with a certain offset, forcing the substrates to slide one over the other. The load is distributed across the entire area of the bond line.
- Bending: it is caused by a force applied perpendicular to the bond area, with the components pivoting around two supports which will induce compression on the upper half and tension on the lower half of the joint.
- Torsion: it is a stress caused by a moment applied in a direction perpendicular to the bond area. Traceable to shear loading condition. The load is distributed across the entire area of the bond.

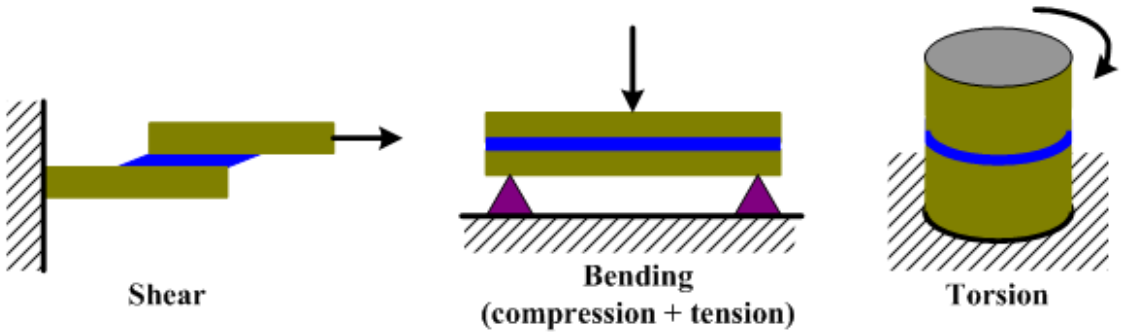

Figure 5. Shear, bending and torsion loading condition [6].

- Cleavage: it is a pull concentrated at one edge of the joint perpendicular to the bond area, exerting a prying force on the bond. While one end of the adhesive is experiencing concentrated stress on the leading edge, the other is theoretically under zero stress. This type of stress occurs with two rigid substrates.
- Peel: as in the previous case, peel is a pull that is also concentrated at one edge of the joint perpendicular to the bond area. In this case one of the substrates is flexible, resulting in even more concentration at the leading edge than with a cleavage joint.

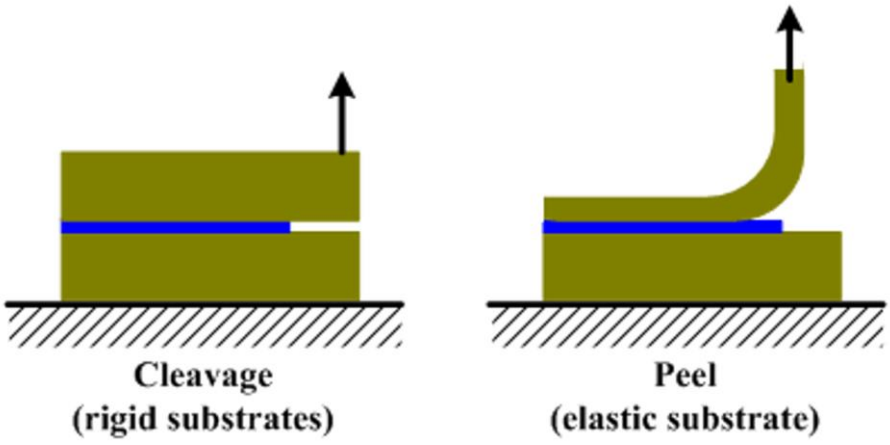

Figure 6. Cleavage and peel loading condition [6].

2.12 Joint configuration

Joint configuration is another important factor that determines the loading of the bonded area. Different configurations can lead to different failures for the same boundary conditions since stresses inside the adhesives can be different. Asymmetry in the joint can cause rotation and induce a higher peel contribution concerning shear, enhancing the mixed loading mode of the adhesives, this is particularly effective in the end zones of the bonding area where border effects are more evident.

In the following the various types of joints are shown:

- Butt joint: used on thick substrates, easiest joint to manufacture, but shows poor capabilities
- Scarf joint: Stronger than butt joint due to increased bonding area, but brings additional complexity, with limited capabilities.

Figure 7. Butt and scarf joint [6].

- Single lap joint: usually adopted in case of structural thin sheets bonding.
- Double lap joint: usually adopted in case of thin sheets bonding where high strength and symmetry loading is required.

Figure 8. Single and double lap joint [6].

- Single strap joint: adopted for aesthetic reasons since the joint is completely flat on one side.
- Double strap joint: stronger and stiffer solution since straps are added on each side of the panels to be joined.

Figure 9. Single and double strap joint [6].

3. Adhesive of study: SikaPower - 1277

SikaPower-1277 is a structural 2-component epoxy adhesive produced by Sika Industry, which cures at room temperature. It is designed for high strength and impact-resistant bonding of metallic substrates, like steel and aluminium, as well as of composite substrates, like GFRP and CFRP laminates. The adhesive has good non-sag properties and contains glass beads of 0.3 mm to ensure an optimal bonding thickness.

Component	**A**	**B**	**Mixed**
Chemical base	Epoxy	Amine	-
Color	Red	White	Light red
Density	1.08 g/cm^3	1.06 g/cm^3	1.07 g/cm^3
Mixing ratio by weight	2	1	-
Viscosity	430 Pas^A	100 Pas^A	-
Application temperature	15 – 35 °C		
Open time	1 hour		
Handling time	11 hours		
Curing time	24 hours		
Tensile strength	30 MPa		
E modulus	2000 MPa		
Elongation at break	4 %		
Tensie lap shear strength (Steel specimens)	28 MPa		
Glass transition temperature	67 °C		
Shelf life	24 months		

Table 2. SikaPower 1277 datasheet [7].

SikaPower-1277 is suitable for structural bonding applications in transportation and general industry. It can also be used for repair applications in combination with spot welding, riveting or clinching. The product is applied as a contact adhesive (2-side application).

This product is suitable for professional experienced users only. Tests with actual substrates and conditions have to be performed to ensure adhesion and material compatibility.

SikaPower-1277 cures by chemical reaction of the two components at room temperature. The cure rate is accelerated and the final glass transition temperature, as well as the tensile and shear strengths, may be significantly increased at higher curing temperatures.

The following curing cycles are suggested by the manufacturer:

- 24 hours at 23 °C
- 60 minutes at 60 °C
- 30 minutes at 80 °C

Figure 10. SikaPower – 1277 cartridge [8].

4. Experimental research

Since the goal of this study is to characterize the adhesive and to correlate experimental tests to numerical simulations the following properties were of particular interest:

- E, modulus of the pure adhesive
- Tensile strength of the pure adhesive
- Elongation at break of the pure adhesive
- Gic, fracture energy parameter in mode I and II
- Tensile lap shear strength on CFRP specimens

Further explanation on why these parameters have been chosen will be given in the next chapter: 5 Numerical simulation.

Different adhesive thicknesses have been the object of study, to understand if an increasing trend of thickness could have brought to a high degradation of the mechanical properties of the joint. The studied thicknesses have been:

- 0.3mm: the minimum thickness of the adhesive considered the glass beads present inside its volume (representing an optimal bonding).
- 0.8mm: intermediate value between min and max and similar to a reference standard.
- 1.1mm: maximum thickness obtainable during manufacturing due to very large components and low controllability of the thickness (representing a low-quality bonding in terms of thickness control).

Since many different properties have been selected to study, various tests have been planned to get all the required properties. In particular, the following tests have been performed:

- Tensile test on dog bone specimens made of pure adhesive
- Double Cantilever Beam (DCB) on steel substrates
- Single Lap Joints (SLJ) on CFRP substrates.

The tests have been performed with two different machines, depending on the test performed:

- Instron 8801 servo-hydraulic testing machine with a force capacity of up to 100 kN. The data acquisition has been done with dedicated software from Bluehill.
- Zwick/Roell Z050 electromechanical drive testing machine with a force capacity of up to 50 kN. The data acquisition has been done with dedicated software from Zwick/Roell.

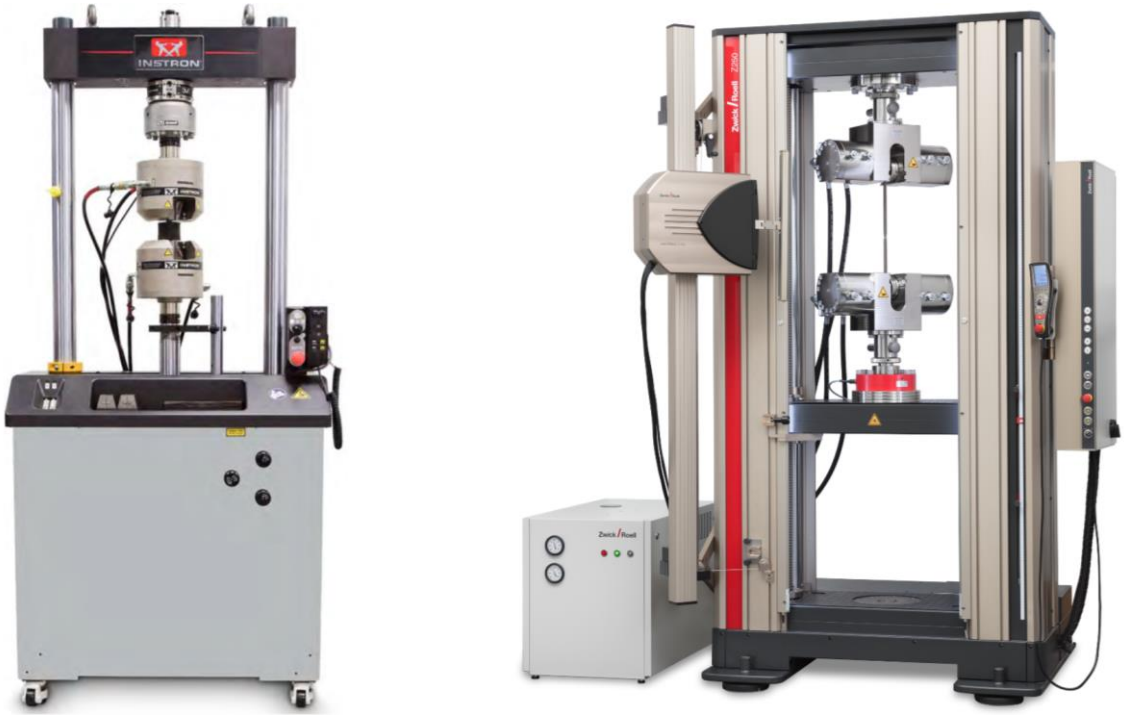

Figure 11. Instron 8801 machine (left) and Zwick/Roell Z050 machine (right)

4.1 Dog Bone test

4.1.1 Requested properties

The following properties, related to the adhesive, have been evaluated through tensile dog bone tests:

- E modulus of the pure adhesive
- Tensile strength of the pure adhesive
- Elongation at break of the pure adhesive

4.1.2 Test requirements and standards

The preparation and testing of these specimens have been done following the International standard ISO 527-3-2018, which is a test method for the determination of tensile properties of plastic materials including adhesives.

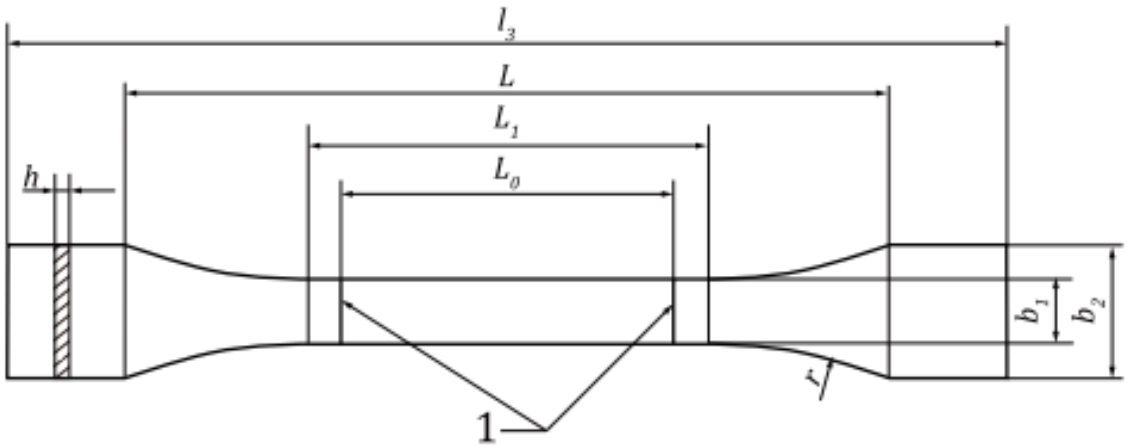

Figure 12. Specimen specifications according to ISO 527-3-2018

4.1.3 Manufacturing

Adhesive mixing has been done by hand following the weight ratio given by the manufacturer of 2:1 (Part A:Part B). The specimens have been realized by spreading the mixed adhesive on a specifically designed Teflon die, pre-treated with a release

agent in order to avoid sticking the adhesive on the walls and surfaces after the curing cycle, thus inducing high stresses on the specimen in the removal operation out of the die.

Figure 13. Release agent application on Teflon die

Since on the adhesives datasheet different curing cycles were present, we decided to manufacture these specimens following the three different curing cycles suggested by the manufacturer, listed in the previous section, to understand if any mechanical property change was noticeable with different curing times and temperatures:

- 24 hours at 23 °C
- 60 minutes at 60 °C
- 30 minutes at 80 °C

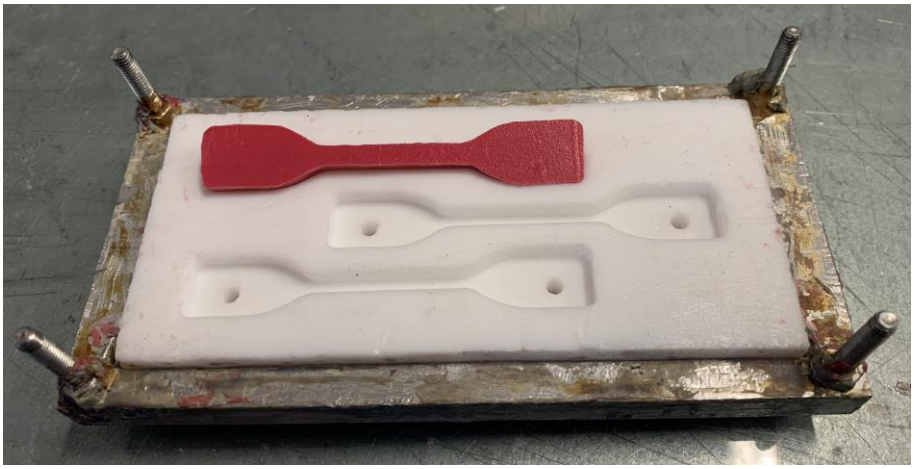

Figure 14. Teflon die with cured specimen

For repeatability reasons, three samples for each configuration have been produced. Adhesive curing has been performed in an OV301 precision benchtop curing oven from Easycomposites, using a ramp-up initial phase to reach the curing temperature and then a constant temperature phase for the duration of the curing cycle.

Figure 15. Curing oven OV301 easycomposites

4.1.4 Testing

Testing of the specimens was carried out with the Zwick/Roell machine.

Specimens have been placed in the machine in an upright position, ensuring their centring on the grips of the machine. Then clamping on the extremities has been done

with mechanical leverages of the machine, to avoid slippage of the specimen during the test. Then the test has been performed with the head of the machine moving at 2mm/min and Force-Displacement data have been acquired from the machine with a data acquisition frequency of 50 Hz. A dedicated laser integrated into the machine, served as an extensometer measuring the displacement of a 10mm section of the specimen so that strains could be precisely evaluated.

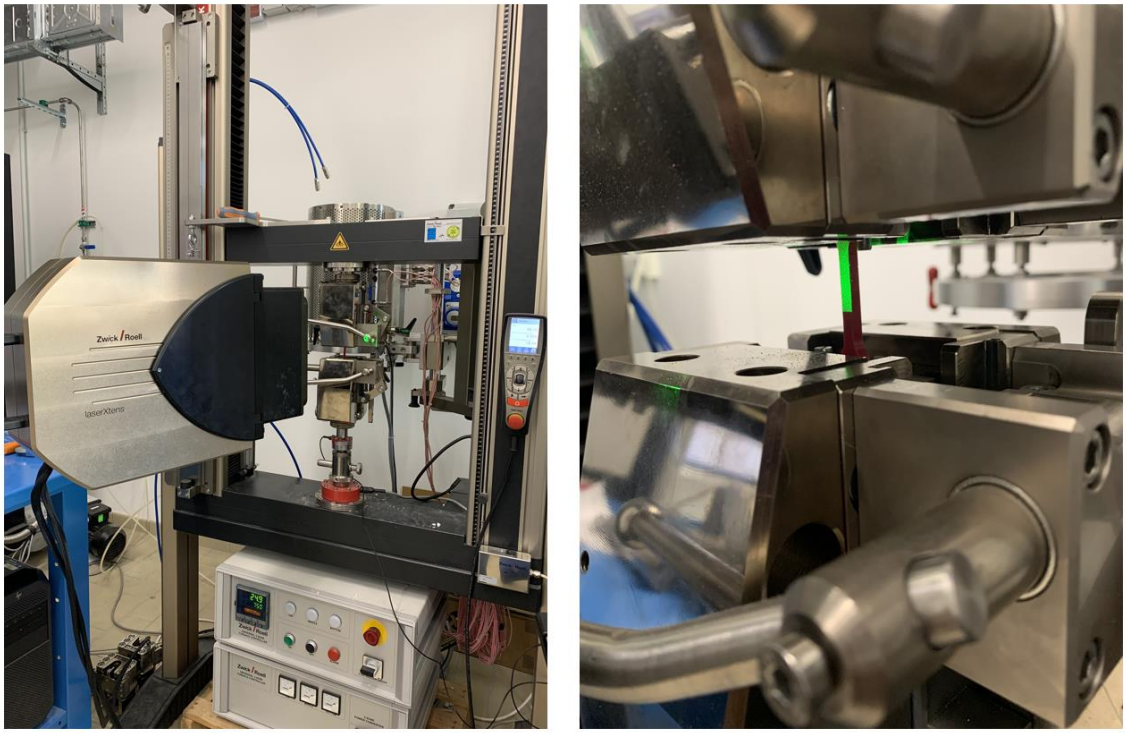

Figure 16. Laser Xtens machine (left) and tested specimen (right)

4.1.5 Results and fracture analysis

In this section, the fracture surfaces of the broken specimens have been analyzed, as well as Stress-Strain curves for each sample.

From data acquisition, Force-Displacement curves have been displayed, but since on each sample tested relevant defects present inside the failure cross-section were present, Stress-Strain curves were more capable of representing a consistent trend across the various specimens tested.

All the specimens showed very small bubbles of air trapped inside the adhesive and spread across the entire surface, probably coming from the mixing phase where air is introduced in the adhesive due to the manual mixing, but every failure happened in correspondence with bigger voids present in the volume of the adhesive, probably coming from the laying of the adhesive in the tight spaces of the die where overlapping of the adhesive caused air to be trapped inside. With a dedicated tool and the use of a microscope actual resistant area has been evaluated over the nominal area, to achieve more accurate results.
These considerations are valid for all the tested specimens in the different curing cycles.

- 24 hours at 23 °C

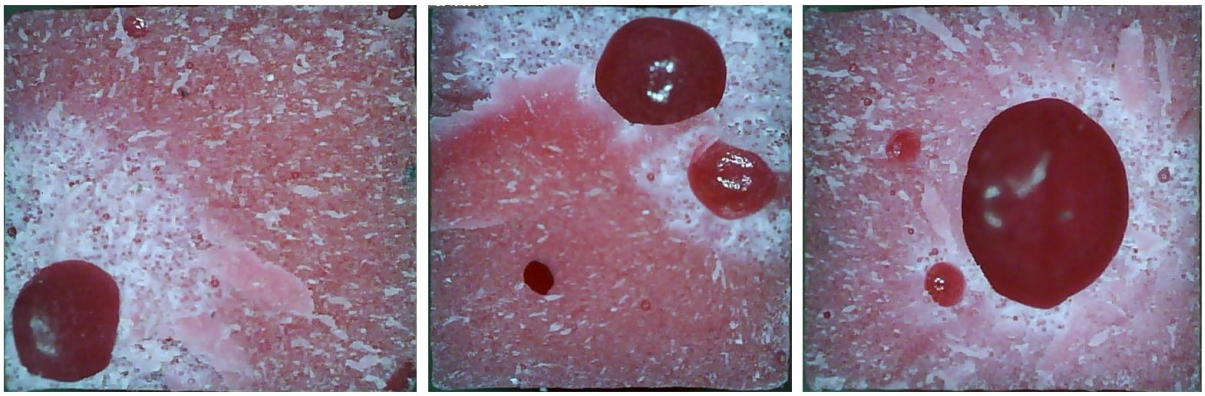

Figure 17. Fracture surface of the three specimens cured for 24 hours at 23°C

Actual resistant areas for the three specimen were respectively : 70% - 65% - 60%

- 60 minutes at 60 °C

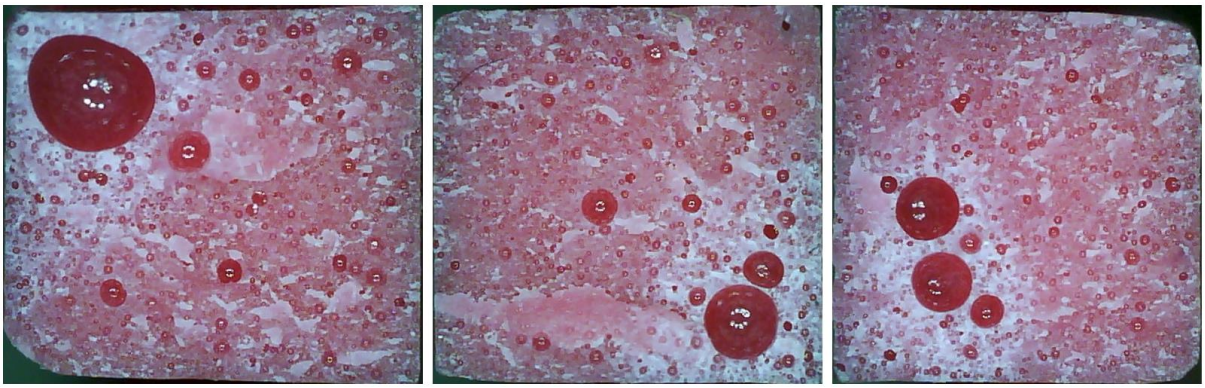

Figure 18. Fracture surface of the three specimens cured for 60 minutes at 60°C

Actual resistant areas for the three specimen were respectively : 60% - 65% - 65%

- 30 minutes at 80 °C

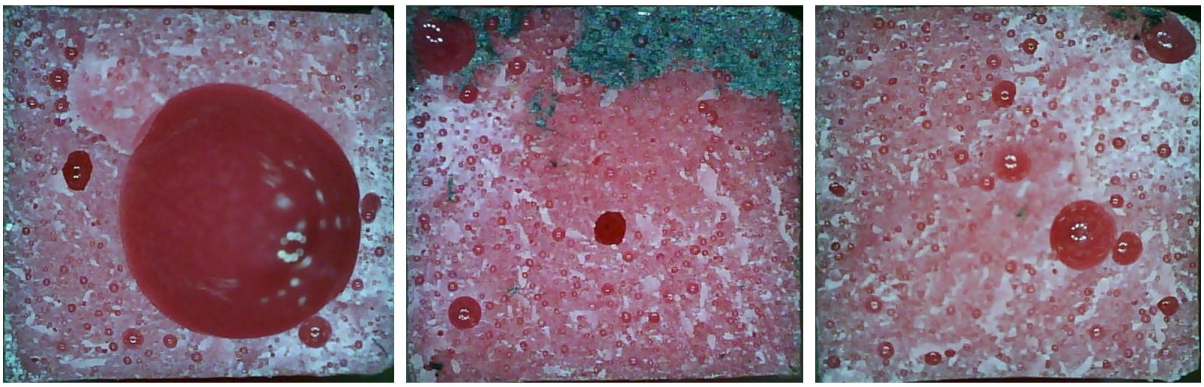

Figure 19. Fracture surface of the three specimens cured for 30 minutes at 80°C

Actual resistant areas for the three specimen were respectively : 40% - 60% - 60%

In the following some considerations about the obtained results will be presented.

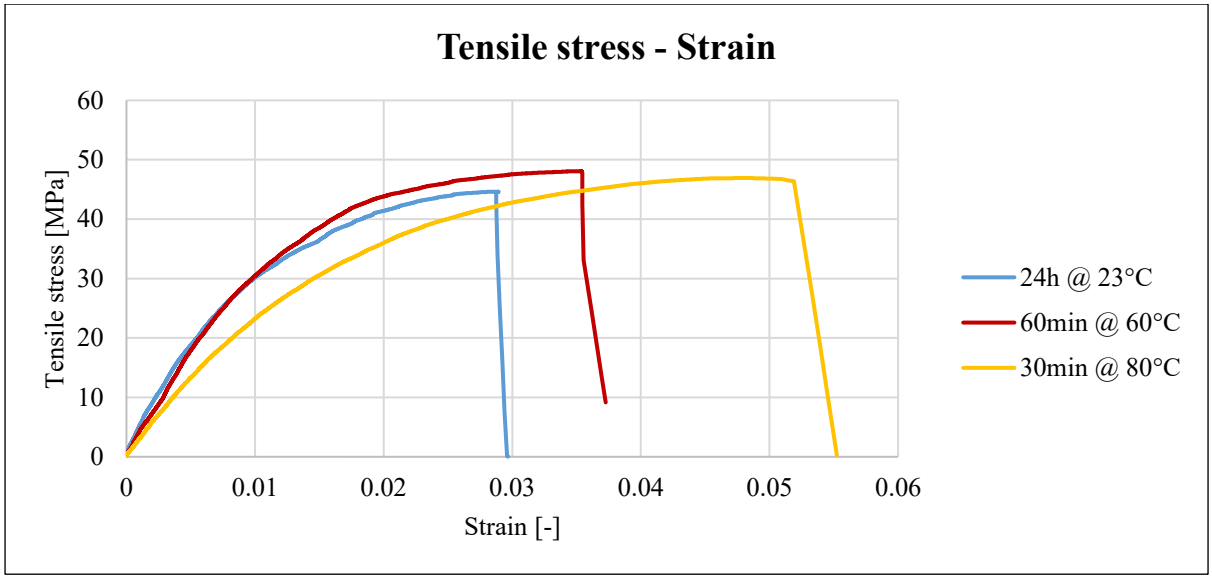

Figure 20. Tensile stress - Strain chart

In the Stress-Strain graph, only the most representative curve for each curing cycle has been displayed. From the curves, a reduced stiffness is clearly visible for the third curing cycle, as well as higher tensile strength for the second curing cycle and a higher elongation at failure for the first curing cycle.

A more detailed display of all the evaluated properties for each sample tested will be presented in the following graphs.

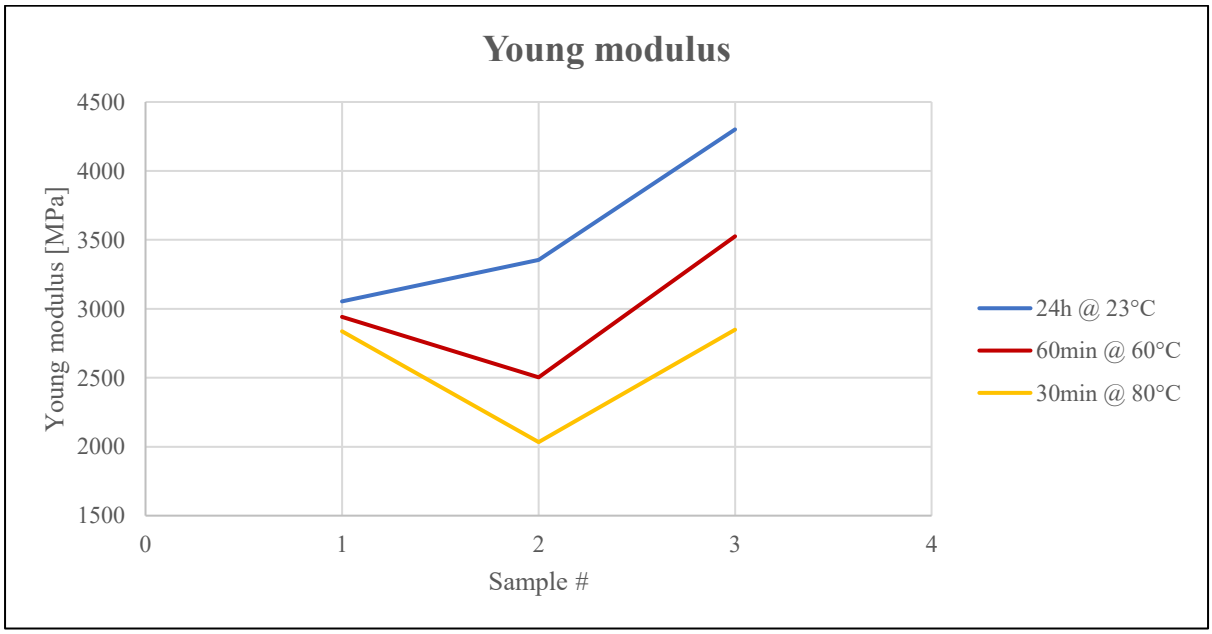

Figure 21. Young modulus chart

A noticeable difference in the Young modulus has been observed with the highest values obtained for 23°C curing cycle. A constant trend is visible, that is the Young modulus decreases as the curing temperature increases. All the samples showed higher values compared to the one given in the datasheet from Sika Industries, where the reference value was 2000 MPa.

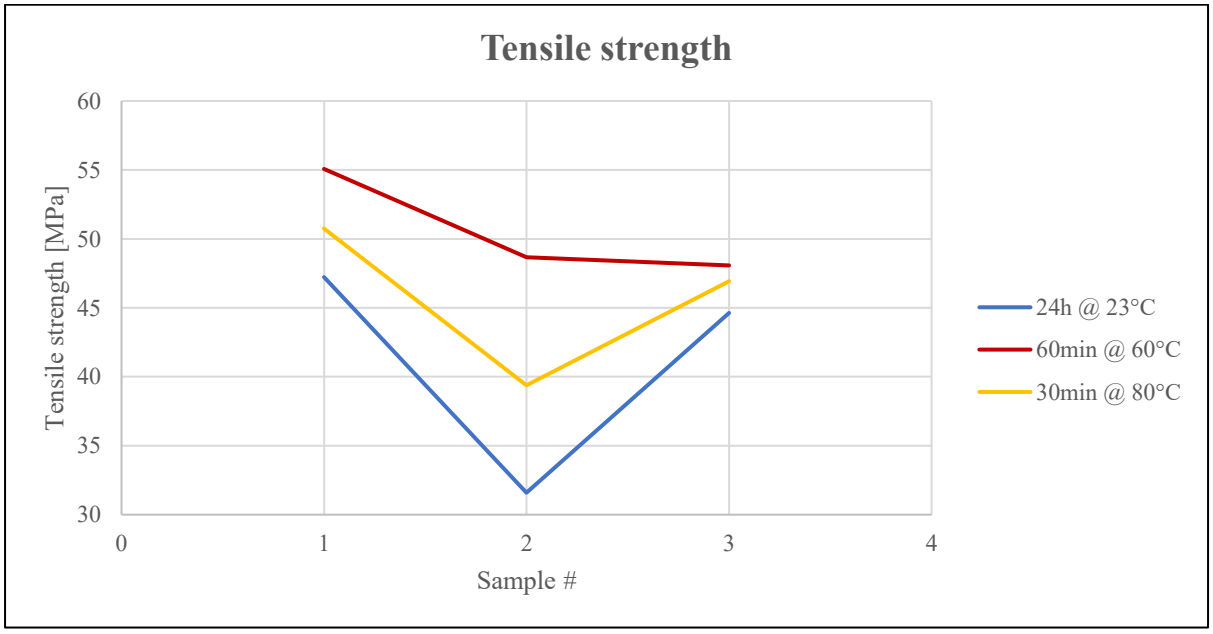

Figure 22. Tensile strength chart

A noticeable difference in the tensile strength has been observed with the highest values obtained for the 60°C curing cycle. Lowest values have been obtained with the room temperature cure. Despite the lower values obtained in the room temperature curing cycle, all the values are above the specifications given in the datasheet by Sika Industries, where the reference value was 30 MPa.

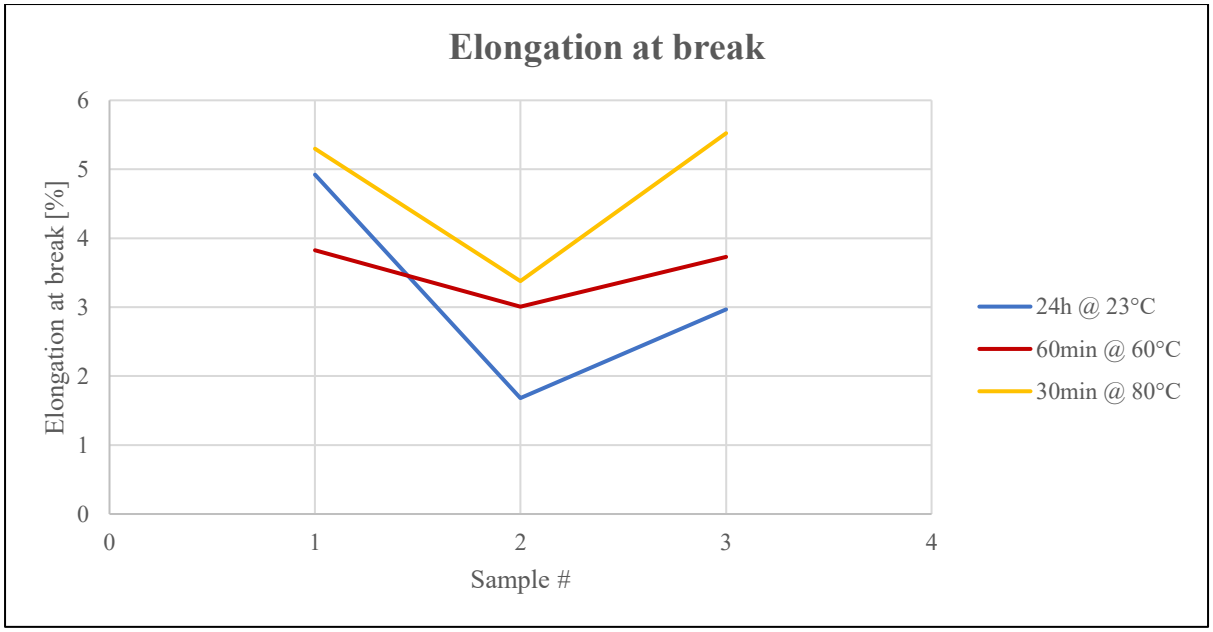

Figure 23. Elongation at break chart

A noticeable difference in the elongation at break has been observed with the highest values obtained for the 80°C curing cycle. The lowest values have been obtained with the room temperature cure. The samples showed some variance in the obtained result with some values higher and others lower than the expected one. The average elongation at break obtained from the experimental test is a bit lower than the one given in the datasheet by Sika Industries, where the reference value is 4%.

In general all the obtained results on the pure adhesive, for the different curing cycles, were either higher or comparable to the datasheet values, which is a desirable condition to achieve.

4.2 DCB test

4.2.1 Requested properties

The following properties, related to the adhesive, have been evaluated through double cantilever beam tests:

- Gic, fracture energy parameter in mode I

4.2.2 Test requirements and standards

The preparation and testing of these specimens have been done following the British standard ISO 25217:2009, which is a test method for the determination of the mode I adhesive fracture energy of structural adhesive joints using double cantilever beams and tapered double cantilever beam specimens.

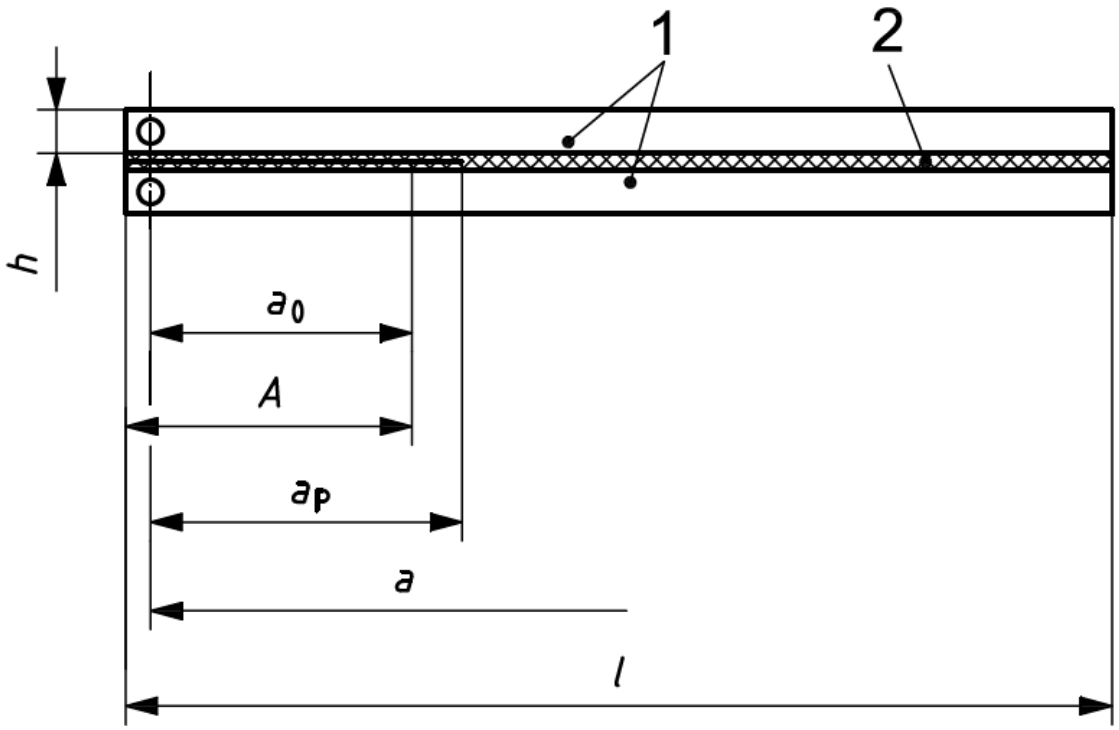

Figure 24. Specimen specifications according to ISO 25217:2009

4.2.3 Manufacturing

The substrates have been machined from C45 steel billets to design specifications. After machining, surface preparation has been performed before bonding, following the good practices shown in previous sections of this paper.

The bonding area has been delimited and masked, in order to act only on the wanted part of the substrate, then degreasing with acetone, manual sandblasting with a dedicated machine and a second degreasing with acetone have been performed.

Specimens have been carefully prepared by spreading the adhesive on both sides of the bonding surfaces, a crack has been realized by applying a folded aluminium foil up to 50 mm from the loading line as prescribed by the standard, and spacers have been used to provide the correct bonding thickness required for each specimen. A Teflon jig has been used to provide correct alignment of the substrates during the curing phase.

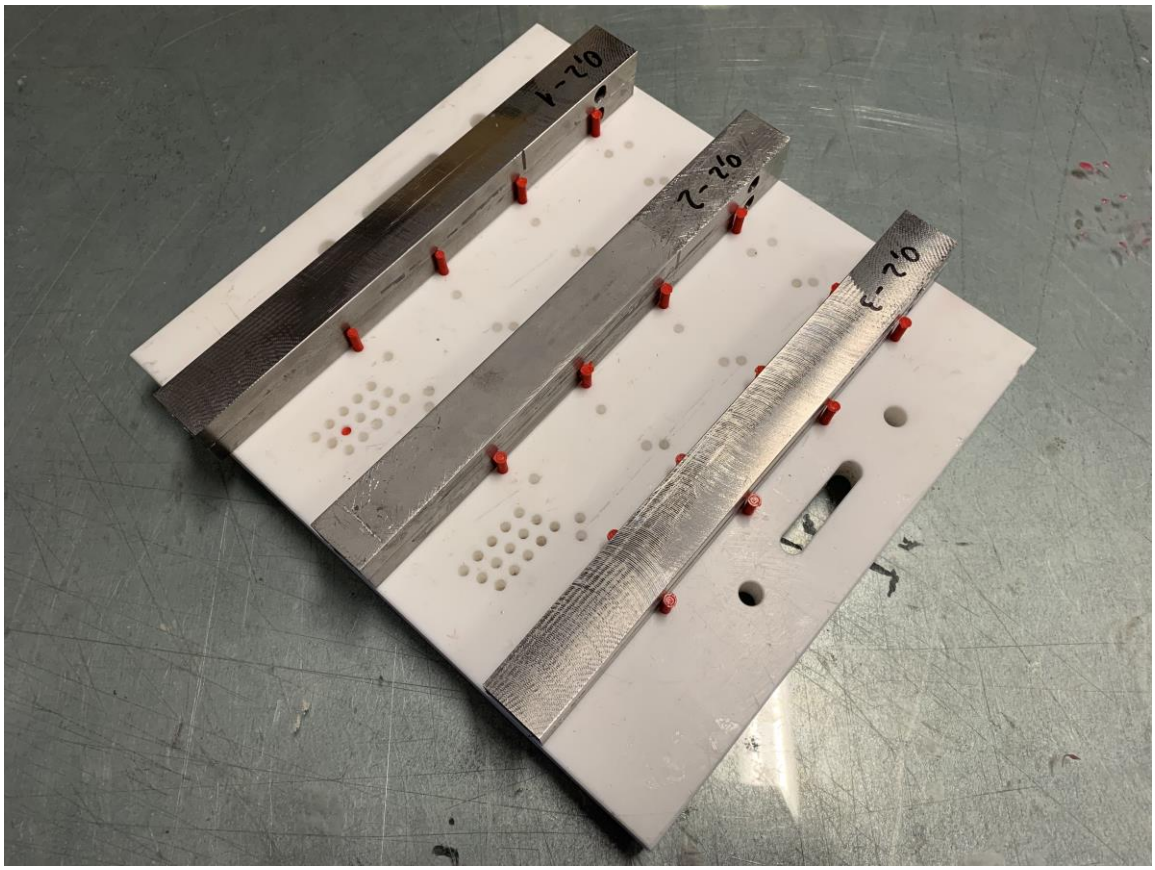

Figure 25. SLJ preparation Jig

These DCBs have been left to cure for 24 hours at room temperature, as it was designated as the standard curing cycle by the adhesive manufacturer.
As pointed out at the beginning of this section three different adhesive thicknesses have been studied on these joints (0.3mm – 0.8mm – 1.1mm).
For repeatability reasons, three samples for each configuration have been produced, for a total of 9 specimens.

4.2.4 Testing

Testing of the specimens was carried out with the Instron machine.
Specimens have been placed in the machine in a horizontal position, ensuring their centring on the grips of the machine. A Digital Image Correlation (DIC) camera has been used and set up before the test to record the specimens during the test and evaluate in postprocessing with a dedicated software the displacement of fixing points and the crack propagation parameters, which will be illustrated later in this chapter.
Then the test has been performed with the head of the machine moving at 2mm/min as prescribed by the standard procedure.

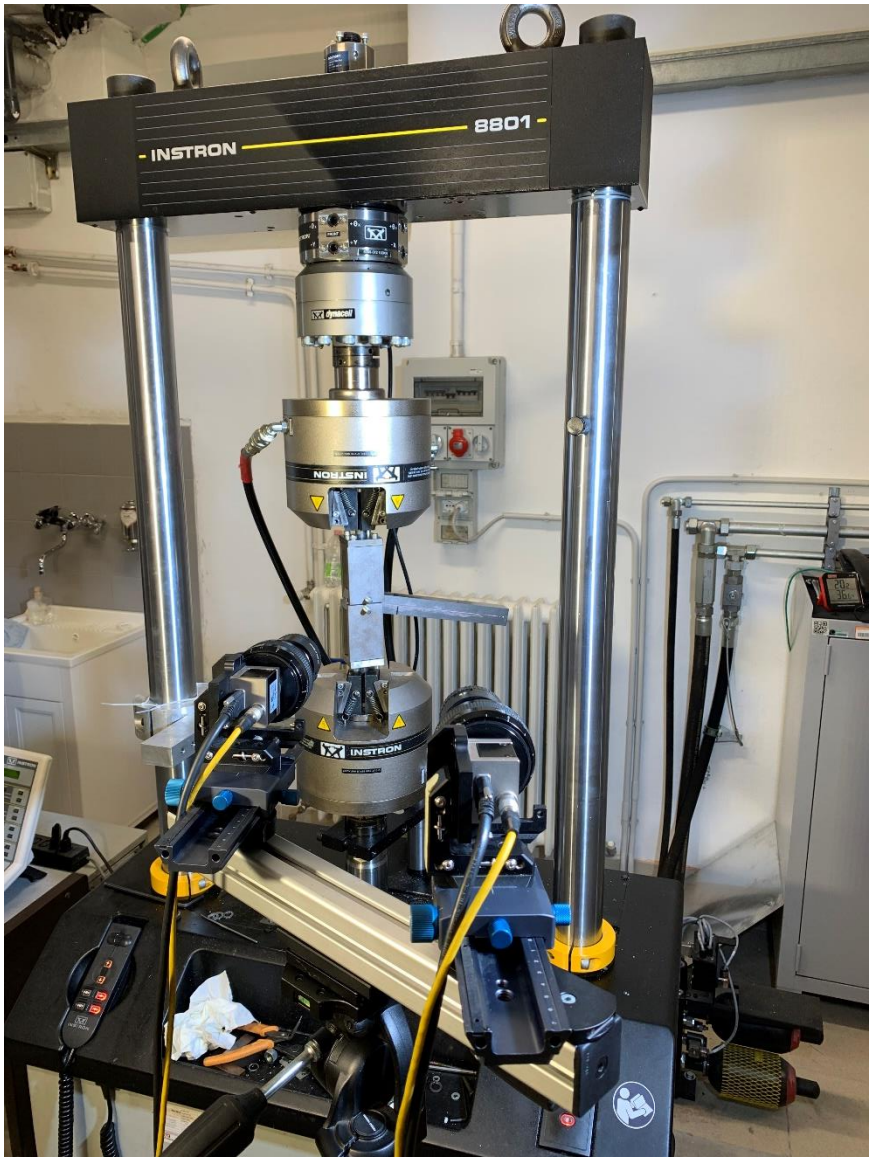

Figure 26. DCB tested specimen and DIC camera

4.2.5 Results and fracture analysis

In this section, the fracture surfaces of the broken specimens have been analyzed, as well as Load-Displacement curves for each sample.

In the following each thickness tested has been shown, with three samples each, that have been tested for repeatability reasons. Some codes have been assigned to individual specimens in order to distinguish them in terms of different parameters of study.

An example is given by: T0.3_A, which carries the information of adhesive thickness = 0.3mm and sample one of three = A.

- Thickness 0.3mm

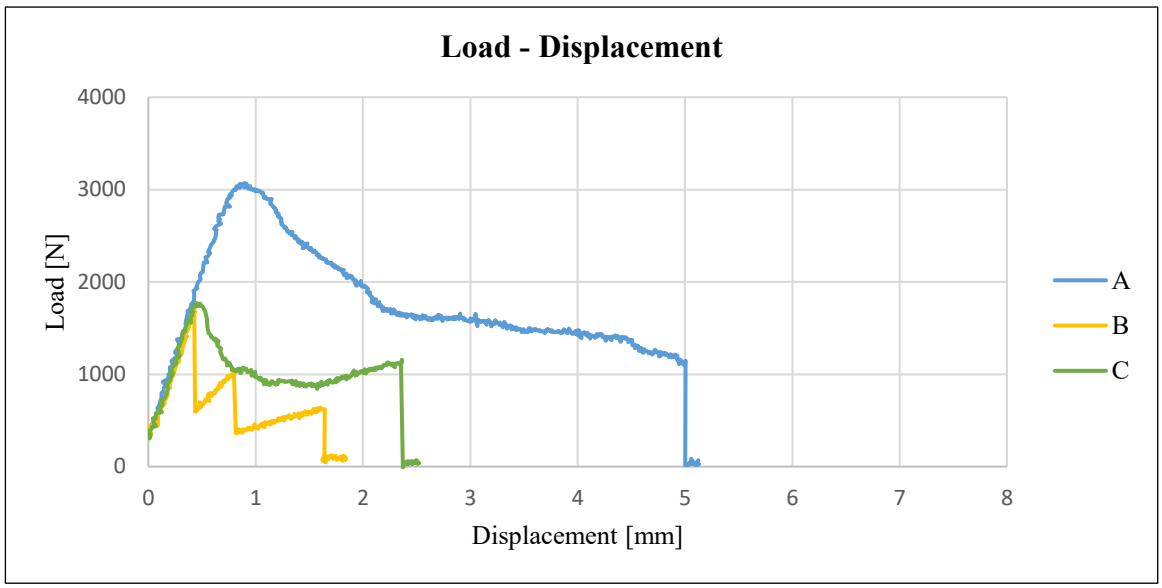

Figure 27. Load - Displacement chart T0.3

Figure 28. Fracture surfaces T0.3 (A – C – B)

In this configuration the three specimens behaved differently, with specimens B and C showing an early failure of the adhesive, resulting in a low peak load and different behaviour after rupture with decreasing/increasing load at higher displacements as the crack propagated into the adhesive. Specimen A instead was the only one that showed a constantly decreasing load after reaching the peak, which is the desired and expected condition. Specimen B showed a stick-slip type of crack propagation.

The made considerations can be supported by analyzing the fracture surfaces, in fat we can distinguish:

- Specimen A: cohesive throughout the whole surface of the adhesive.
- Specimen B: mainly cohesive, but many imperfections and voids were present, as well as adhesive failure in some areas.
- Specimen C: adhesive failure between the two halves, as if the two didn't bond together well.

After these considerations, specimen A will be the representative one for this thickness.

- Thickness 0.8mm

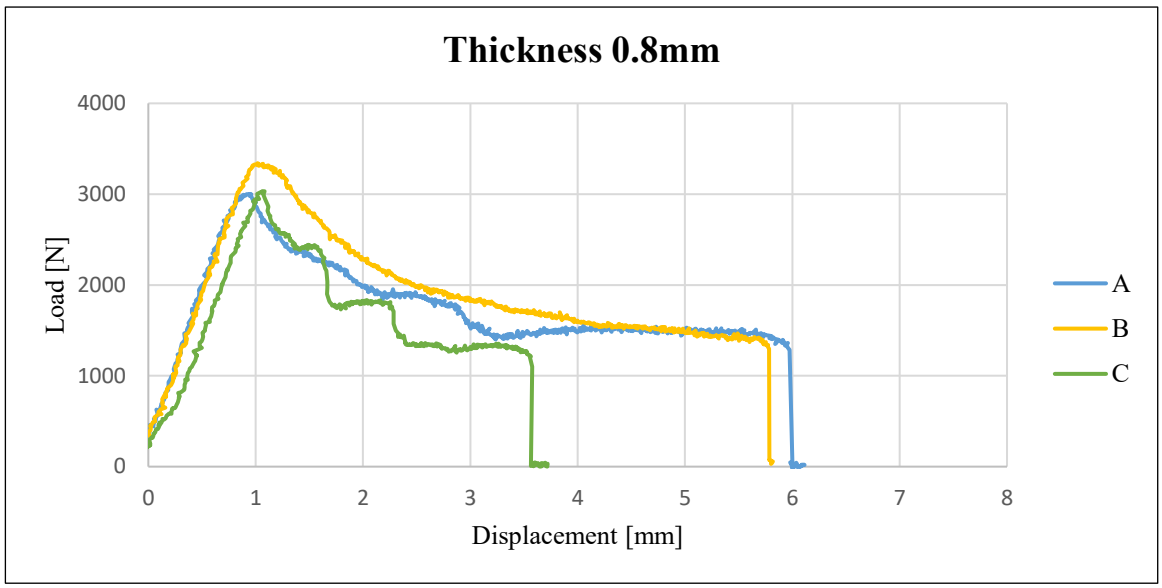

Figure 29. Load - Displacement chart T0.8

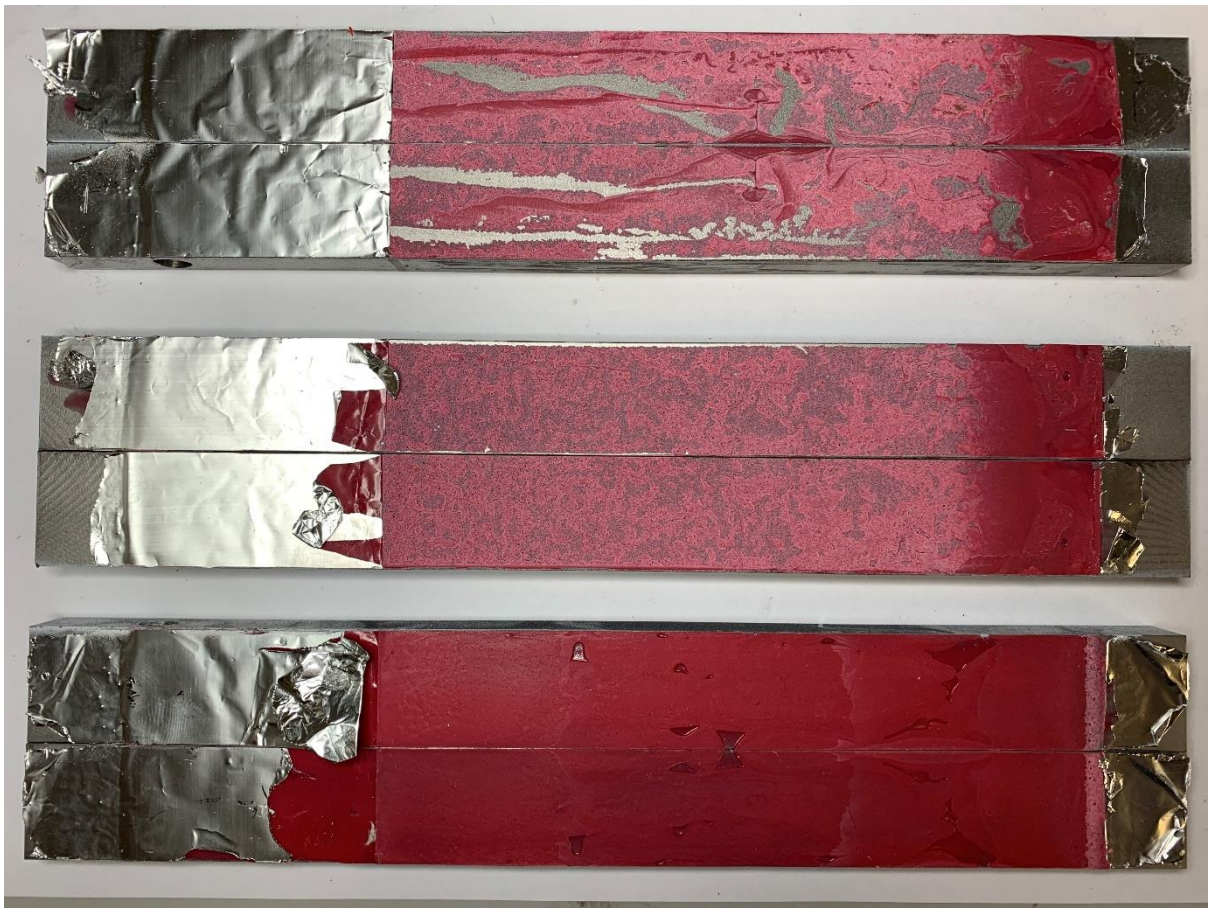

Figure 30. Fracture surfaces T0.8 (A – B – C)

In this configuration the three specimens behaved a bit differently, with the specimen A and C showing an early failure of the adhesive compared to B, resulting in a low peak load and unexpected behaviour after the rupture with decreasing/increasing load at higher displacements as the crack propagated into the adhesive. Specimen B instead was the only one that showed a constantly decreasing load after reaching the peak, which is the desired and expected condition. Specimen C showed a stick-slip type of crack propagation.

The made considerations can be supported by analyzing the fracture surfaces, in fat we can distinguish:

- Specimen A: mainly cohesive, but many imperfections and voids were present, as well as adhesive failure in some areas.
- Specimen B: cohesive throughout the whole surface of the adhesive.
- Specimen C: adhesive failure between the two halves, as if the two didn't bond together well.

After these considerations, specimen B will be the representative one for this thickness.

- Thickness 1.1mm

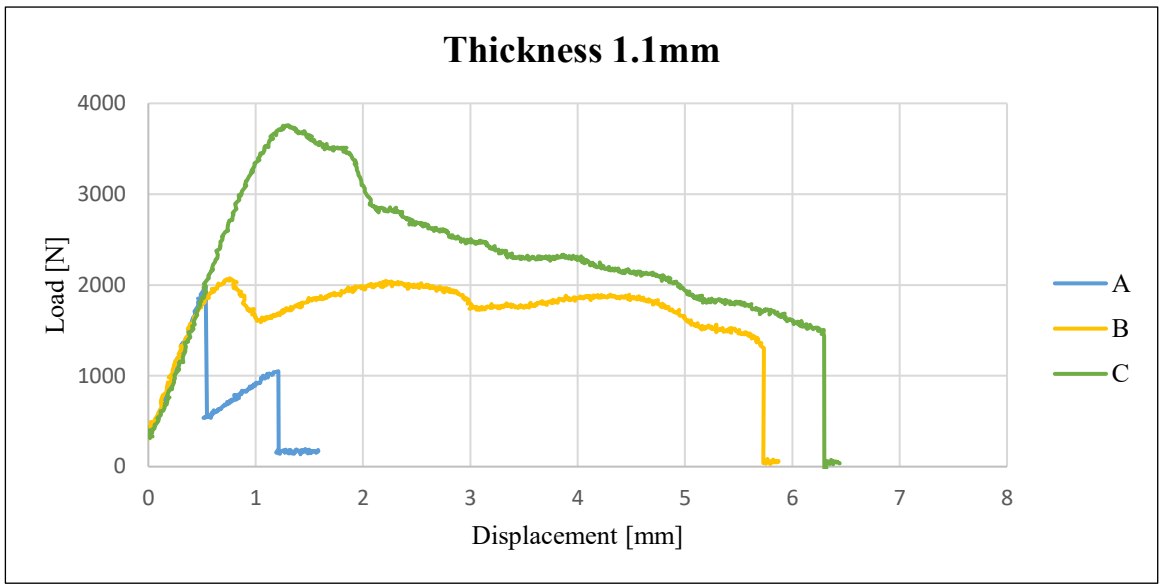

Figure 31. Load - Displacement chart T1.1

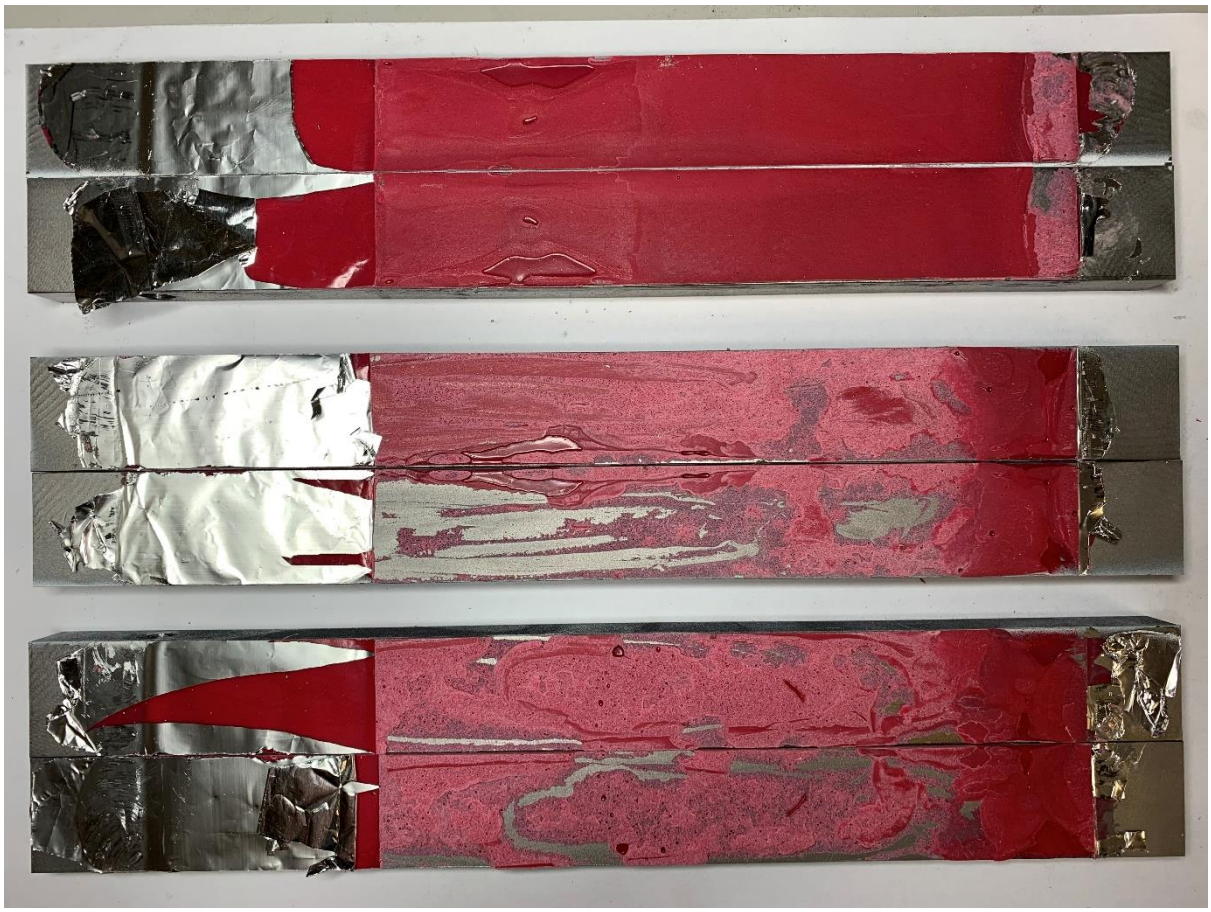

Figure 32. Fracture surfaces T1.1 (A – B – C)

In this configuration the three specimens behaved differently, with specimen A and B showing an early failure of the adhesive compared to C, resulting in a low peak load and a different behavior after the rupture with decreasing/increasing load at higher displacements as the crack propagated into the adhesive. Specimen C instead was the only one that showed a constantly decreasing load after reaching the peak, which is the desired and expected condition. Specimen A showed a stick-slip type of crack propagation.

The made considerations can be supported by analyzing the fracture surfaces, in fat we can distinguish:

- Specimen A: adhesive failure between the two halves, as if the two didn't bond together well.
- Specimen B: mainly cohesive, but many imperfections and voids were present, as well as adhesive failure in some areas.
- Specimen C: mainly cohesive, but some imperfections and voids were present, as well as adhesive failure in some areas, in a lower percentage with respect to B.

After these considerations, specimen C will be the representative one for this thickness.

Now a sensitivity analysis based on the actual Load-Displacement curves obtained from the test will be shown.
In the following diagrams, only one representative curve for each configuration will be displayed.

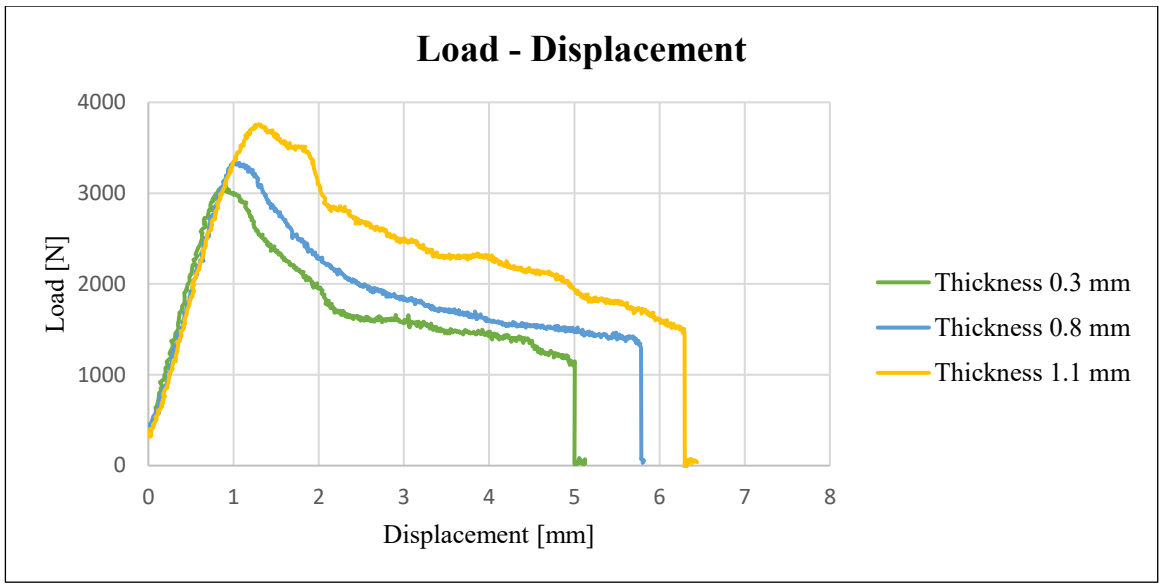

Figure 33. Load – Displacement DCB

From the Load – Displacement curve of the three thicknesses it is possible to distinguish some phases of the test, the first part of elastic behaviour where no damage of the adhesive is visible and very little difference can be seen among the different thicknesses, then load increases up to the peak load, which is the initiation of the damage in the adhesive and crack starts to propagate inside the adhesive, due to the two substrates that are separated by the pulling force of the machine. From the graph, it is clear how for higher thicknesses of the adhesive layer, higher peak loads are reached. Then a decreasing load phase is visible where propagation of the crack continues inside the adhesive encountering less resistance as it propagates, thus the load decreases. At last complete separation is visible with load approaching zero value.
Observing the area under the curves gives a measure of the ability of the specimen to absorb energy before complete failure and it's quite obvious that for higher thicknesses the adhesive is able to absorb more energy before reaching failure. This concept will be confirmed by the evaluation of the fracture energy parameter of the adhesive for the three studied thicknesses.

As introduced before the goal of DCB tests was to determine the internal fracture energy related to mode I also indicated as G_IC.

G_IC and $G_{II}C$ are the critical strain energy release rates or the G-values reached by crack propagation. This parameter can therefore be understood as the resistance that the material offers to counteract the crack propagation. G is related to the fracture toughness parameter of the fracture mechanics so that also G will depend on the size of the defect, the defect configuration and the stress conditions. The value of G_IC can be identified as the value of G at the moment the crack begins to propagate. In general, the crack propagates only if the value of G is greater than that of the resistance opposed by the material, and also how the crack propagates (stable/unstable propagation) depends on many different factors related to the bonding.
To determine the G_IC it is necessary to monitor the crack, and this requires additional effort and the availability of the necessary instrumentation. In addition, following the crack propagation can give rise to complications caused either by the possible instability of the propagation or simply by the fact that the crack apex cannot be clearly identified. In fact, for this research dedicated software able to capture and elaborate crack propagation from DIC camera images has been used.
The crack propagates in the bulk material in a way perpendicular to the maximum main tension, while in the thin layer, the crack propagates following the pattern of the adhesive layer, weaker and less rigid. As the adhesive layer thickness grows, G_IC grows to greater values than the bulk material and then decreases to a massive value. [1]

As described by the utilized standard there are three methods that have to be used to determine the internal fracture energy:

- Simple Beam Theory (SBT)
- Corrected Beam Theory (CBT)
- Experimental Compliance Method (ECM)

The crack present in the adhesive can be considered as a wedged beam, for this reason, the compliance of the sample system can be considered as the compliance of a beam embedded in the adhesive. Although compliance with the SBT method has been evaluated considering the bending and shear deformation, it does not take into account the rotation of the apex of the crack caused by the fact that the beam is not perfectly

wedged. Using the SBT method therefore underestimates the compliance of the system. This phenomenon actually makes a not negligible contribution to the compliance of the system, which has led to the development of a correct formulation of the previous CBT method, which considers the crack larger than the real value of the quantity Δ. This leads to an additional amount of deformability, which improves the estimation of system compliance.
The latest technique presented by the standard is ECM and is based on a mathematical correction of compliance.

In this section, the following symbols and abbreviated terms apply:

- a crack length (mm), i.e. the distance between the load-line (intersection of the plane through pin-hole centres or centers of the hinge axes and plane of crack) and the tip of the precrack or crack on the edge of the specimen
- B, width of the specimen (mm)
- C, compliance δ/P of the specimen (mm/N)
- Es, independently measured flexural or tensile modulus of the arms of the substrate beam (GPa)
- F, large-displacement correction
- G_IC, critical strain energy release rate, or adhesive fracture energy, for the applied mode I opening load (J/m2)
- h, thickness of the substrate beam at a crack length a (mm)
- m, specimen geometry factor
- n, slope of a plot of logC versus loga
- P, load-cell of the test machine (N)
- Δ, crack-length correction for a beam that is not perfectly built-in (mm)
- δ, displacement of the cross-head of the test machine (mm)

Here equations used in the three different methods will be shown.

- Simple Beam Theory: This method is the simplest one and is the only one that can be used in case of unstable crack propagation, which happened on some of the tested specimen (stick-slip failure).

$$G_I C = \frac{4P^2}{E_s B^2}\left(\frac{3a^2}{h^3} + \frac{1}{h}\right)$$

- Corrected Beam Theory: This method takes into consideration a slightly longer crack length, by accounting for Δ, which is found experimentally by plotting crack length vs compliance^1/3 and intersecting the linear regression curve with the horizontal axis to find its distance from the origin. Moreover, a large-displacement correction factor is also taken into consideration.

$$G_I C = \frac{3P\delta}{2B(a + |\Delta|)}F$$

where,

$$\mathrm{F} = 1 - \frac{3}{10}\left(\frac{\delta}{a}\right)^2$$

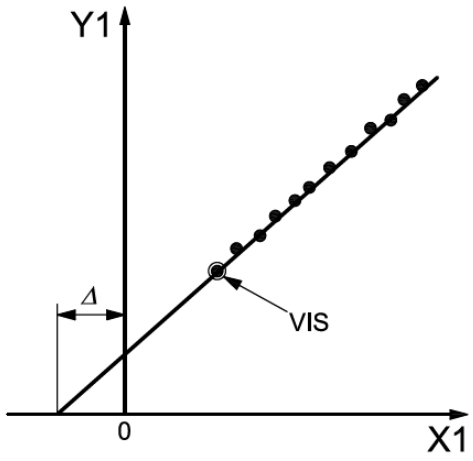

a) The correction for the corrected beam theory (CBT) method for the DCB test specimen

Figure 34. CBT - a vs c^1/3

- Experimental Compliance Method: This last method instead considers the slope of the linear regression of loga vs logC plot.

$$G_I C = \frac{nP\delta}{2Ba} F$$

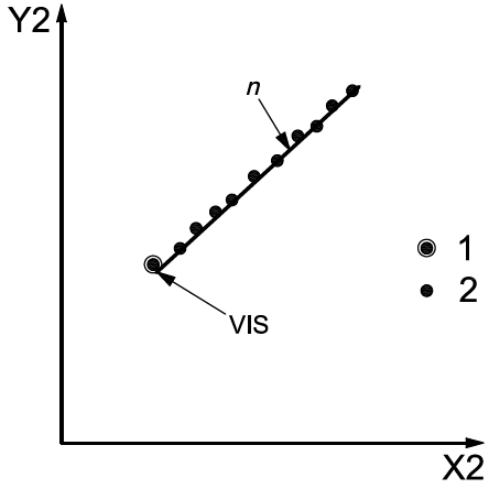

b) The slope n for the experimental compliance method (ECM) for the DCB test specimen

Figure 35. loga vs logC

In the following the obtained results will be displayed. The first method has been used for all the specimens, since it is valid in any condition, while the 2nd and 3rd have only been used to get the $G_I C$ value of one specimen for each thickness that didn't show a stick-slip crack propagation.

Table 3. $G_I C$ obtained from experimental data

Specimen	GIC from SBT [N/mm]	GIC from CBT [N/mm]	GIC from ECM [N/mm]
T0.3_A	1.434177	2.429672	2.430788
T0.3_B	0.508566	-	-
T0.3_C	0.526588	-	-
T0.8_A	1.461305	-	-
T0.8_B	1.643557	2.953565	3.097602
T0.8_C	1.688915	-	-
T1.1_A	0.674438	-	-
T1.1_B	0.698321	-	-
T1.1_C	2.220343	4.185459	4.285018

As expected the Simple Beam theory is underestimating the G_IC value with respect to the other two methods. Corrected beam theory and Experimental Compliance Method results are instead quite close to each other.

4.3 SLJ test

4.3.1 Requested properties

The following properties, related to the adhesive, have been evaluated through single-lap joint tests:

- Tensile lap shear strength on CFRP specimens

4.3.2 Test requirements and standards

The preparation and testing of these specimens have been done following the ASTM International standard D5868 – 01, which is a test method for lap shear adhesion for fiber-reinforced plastic (FRP) bonding.

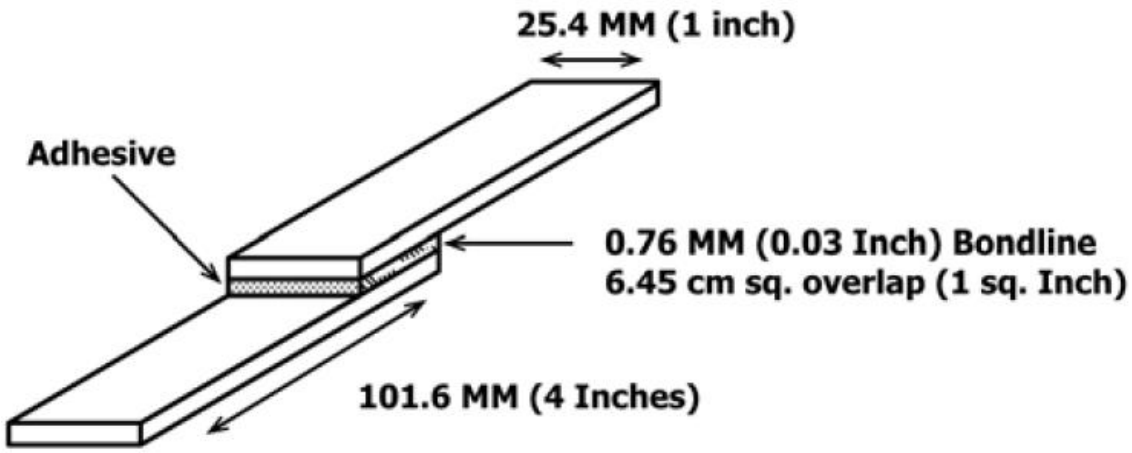

Figure 36. Specimen specifications according to ASTM D5868 - 01

4.3.3 Manufacturing

The substrates have been realized with a CFRP laminate made of prepreg Nano-lite N140L nano-engineered toughened epoxy prepreg and cured in an autoclave. The specimens then have been obtained with a water jet cutter to meet the dimension

specifications of the following standard. The machine used is an industrial caliber CNC waterjet cutter from Wazer.

Figure 37. Wazer waterjet cutter

After cutting, CFRP surface preparation has been performed prior to bonding, following the good practices pointed out in previous sections of this paper.

In fact bonding area has been delimited and masked, in order to act only on the wanted part of the substrate, then degreasing with acetone, mechanical abrasion with sandpaper 1000 grit and a second degreasing with acetone have been performed.

The choice of 1000 sandpaper grit has been made after several trials on pre-series samples devoted to the assessment of the most cohesive failure for the given configurations. The manufactured samples span between 180 and 1000 grit, with the latter showing the best results.

Between the second degreasing phase and adhesive application on the bonding area a minimum of 15 minutes have been waited to let the acetone fully evaporate from the surface.

With the help of a dedicated Teflon jig specimens have been carefully prepared by spreading the adhesive on both sides of the bonding surfaces. Spacers have been used to provide the correct bonding thickness required for each specimen.

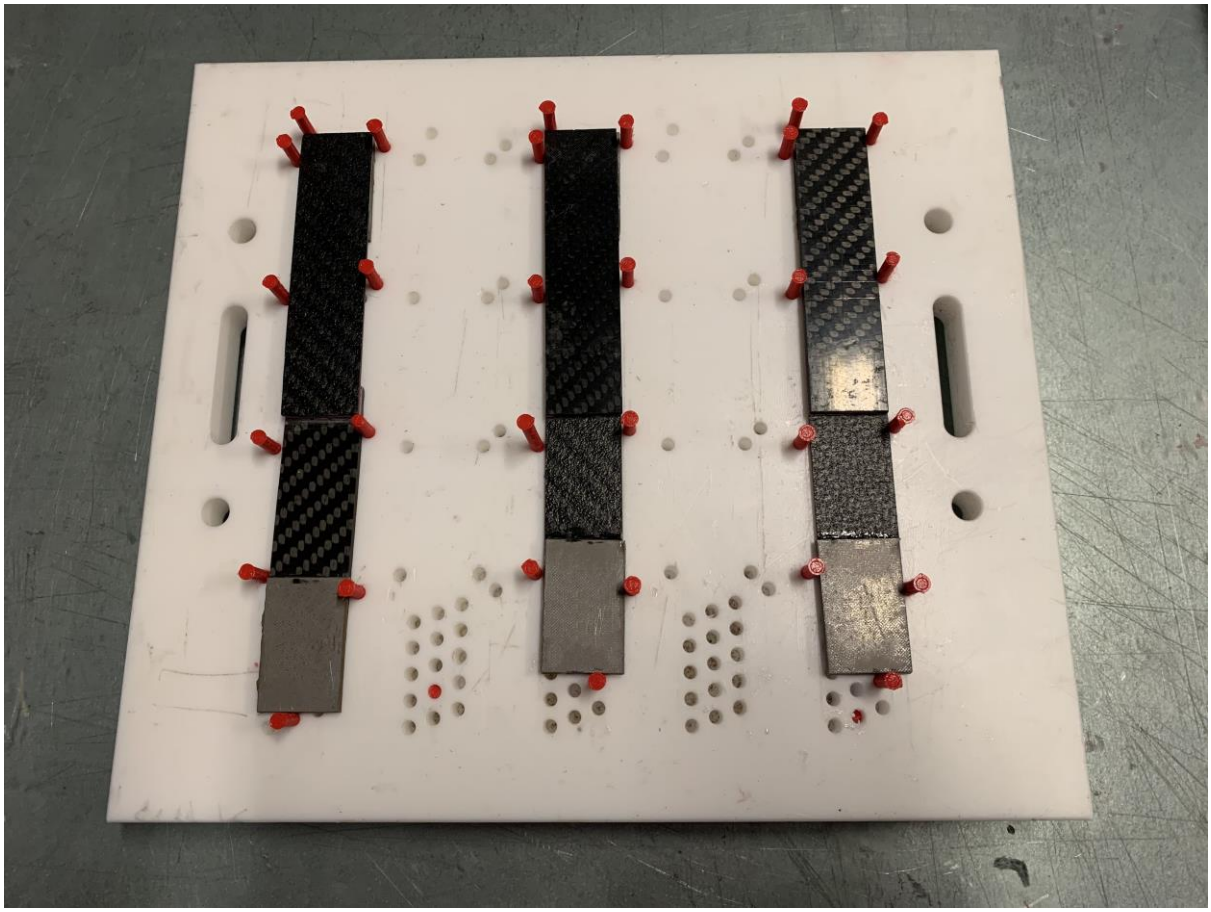

Figure 38. SLJ preparation Jig

These SLJ have been left to cure for 24 hours at room temperature, as it was designated as the standard curing cycle by the adhesive manufacturer.

As a last foresight, tabs have been added at the extremities of the substrates for the tensile test machine grips. These tabs have been realized with the same thickness of the substrate + bonding area in order to have a correct alignment of the specimen when subjected to the acting load during the test, to avoid excessive bending of the joint.

As pointed out in the beginning of this section three different adhesive thicknesses have been studied on these joints (0.3mm – 0.8mm – 1.1mm).

For each of these thicknesses three different overlap length have been studied in order to get enough values regarding the possible areas adopted during actual production of components.

The overlap lengths that have been chosen were:

- 10mm: minimum overlap that can be realized without having a big influence of border effect on the fracture of the adhesive, which can lead to a misinterpretation of the tests results.
- 20mm: average overlap length realized during production.
- 30mm: maximum overlap length, beyond which bonding area becomes too wide and adhesive is not exploited at its full potentialities.

To ensure similar testing condition of the different configurations, the tabs length has been adapted to each overlap in order to have the same 'free length', which is the distance between the end of the bonding area of study and the beginning of the bonding area of the tabs.
For repeatability reasons, three samples for each configuration have been produced, for a total of 27 specimens.

4.3.4 Testing

Testing of the specimens was carried out with the Instron machine.
Specimens have been placed in the machine in an upright position, ensuring the centering of the tabs on the grips of the machine. Then clamping on the extremities was done with 60 bar of pressure on the hydraulic circuit of the machine, this was done to ensure enough clamping force, to avoid slippage of the specimen during the test, but also to avoid a too-large pressure that could have caused damage by generating delamination issues in the composite laminate.
Then the test was performed with the head of the machine moving at 2mm/min and force–displacement data were acquired from the machine with a data acquisition frequency of 20 Hz.

Figure 39. SLJ tested specimen

4.3.5 Results and fracture analysis

In this section, the fracture surfaces of the broken specimens have been analyzed, as well as Load-Displacement curves for each sample.

Knowing the failure modes explained in the first chapter of this research, it has been possible to assign a particular mode of failure to all the specimens tested.

In the following, each overlap and thickness configuration has been shown, with three samples each, that have been tested for repeatability reasons. Some codes have been assigned to individual specimens to distinguish them in terms of different parameters of study.

An example is given by: O10_T0.3_A, which carries the information of overlap length = 10mm, adhesive thickness = 0.3mm and sample one of three = A.

- Overlap 10mm – Thickness 0.3mm

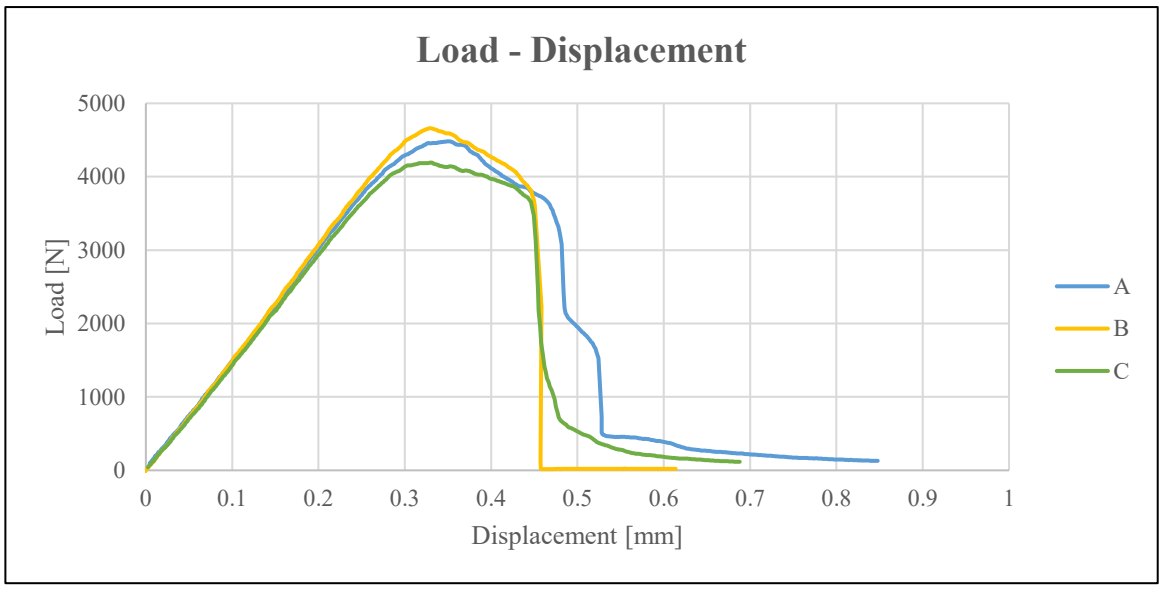

Figure 40. Load - Displacement chart O10_T0.3

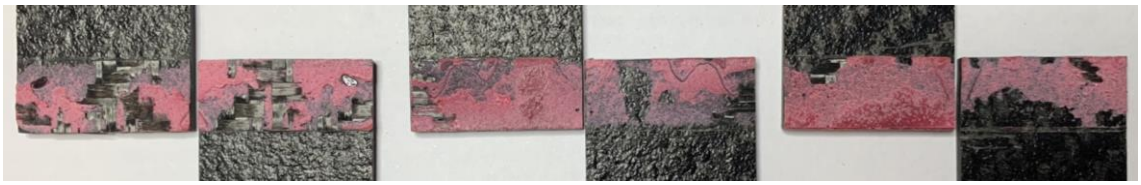

Figure 41. Fracture surface O10_T0.3 (A – B – C)

In this configuration by looking at the plot we can see a ductile behavior for all the specimens.

By analyzing the fracture surfaces we can distinguish:

- Specimen A: mainly cohesive and light fibre tear.
- Specimen B: mainly cohesive and thin layer cohesive failure in a restricted area.
- Specimen C: mainly cohesive and thin layer cohesive failure in a restricted area.

Despite having slightly different fracture surfaces, all the specimens showed a similar trend in the Force-Displacement curve and cohesive failure is said to be the predominant failure mode for this configuration.

- Overlap 10mm – Thickness 0.8mm

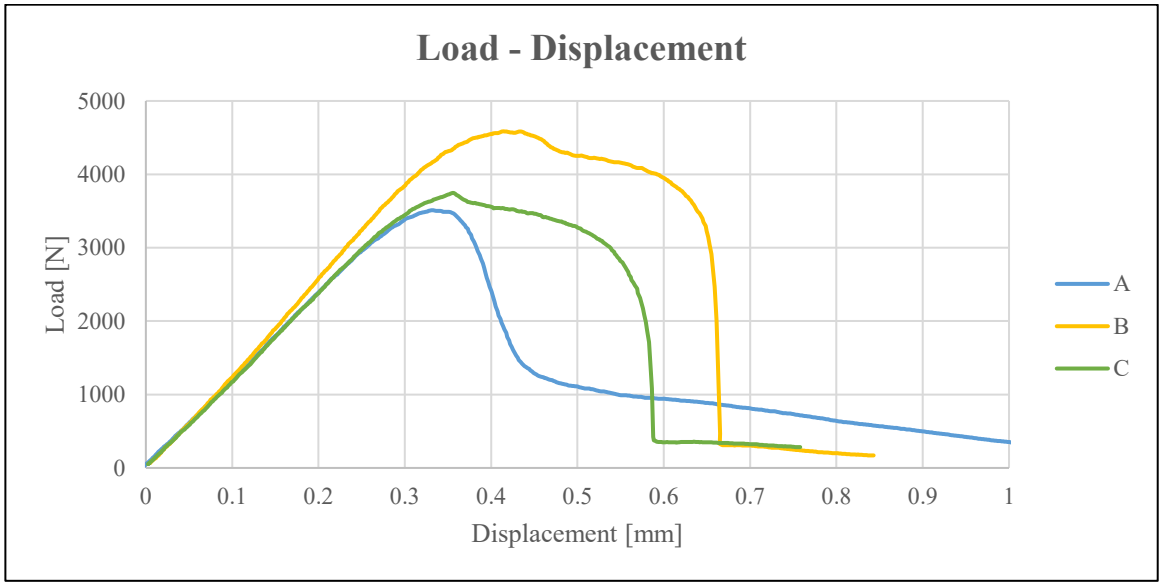

Figure 42. Load - Displacement chart O10_T0.8

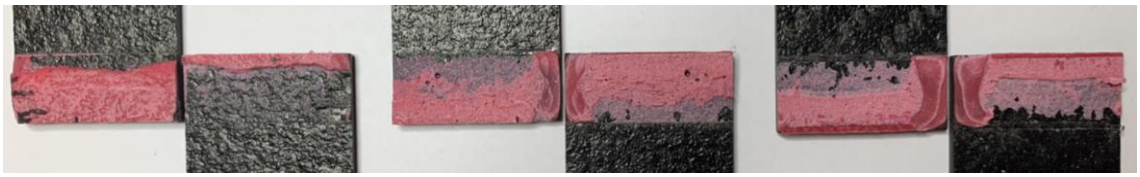

Figure 43. Fracture surface O10_T0.8 (A – B – C)

In this configuration, by looking at the plot we can see a ductile behavior for all the specimens.

By analyzing the fracture surfaces we can distinguish:

- Specimen A: thin layer cohesive failure.
- Specimen B: cohesive failure.
- Specimen C: mainly cohesive and adhesive failure in a restricted area.

The specimens showed a variable trend in the Force-Displacement curve after reaching the peak load with a wider area under the curve for specimen B, which had the most cohesive failure among the three samples. This high variability in the curves after peak load can be explained by the different failure surfaces obtained.

- Overlap 10mm – Thickness 1.1mm

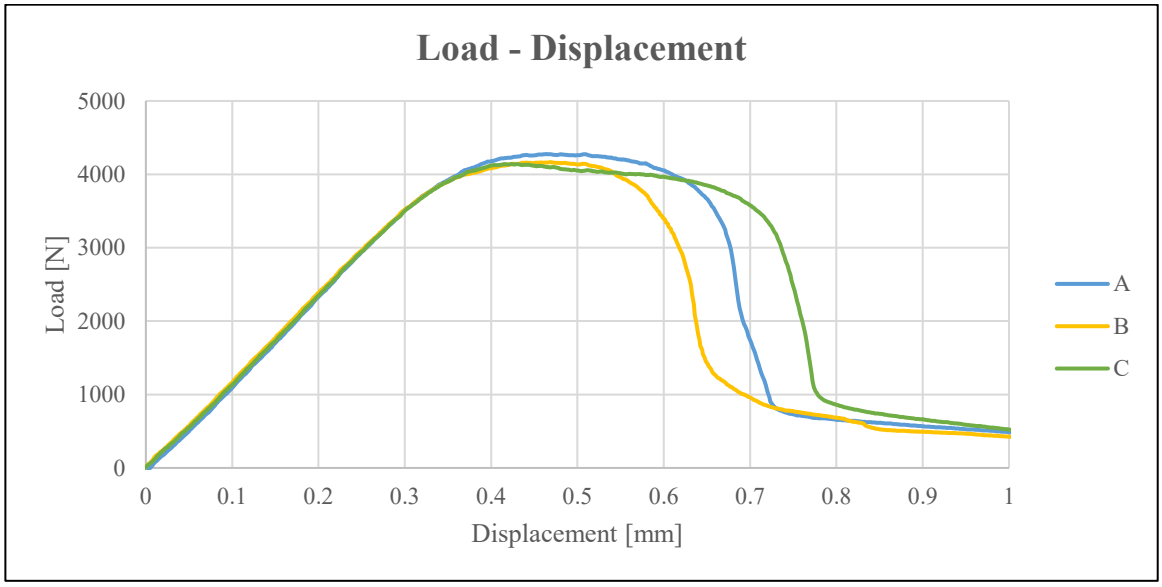

Figure 44. Load - Displacement chart O10_T1.1

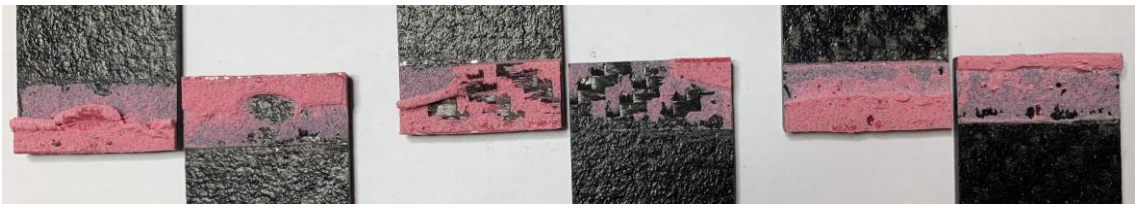

Figure 45. Fracture surface O10_T1.1 (A – B – C)

In this configuration, by looking at the plot we can see a ductile behavior for all the specimens.

By analyzing the fracture surfaces we can distinguish:

- Specimen A: cohesive failure.
- Specimen B: cohesive and light fibre tear failure.
- Specimen C: cohesive failure.

Despite having slightly different fracture surfaces, all the specimens showed a similar trend in the Force-Displacement curve and cohesive failure is said to be the predominant failure mode for this configuration. Samples B and C, which sowed a higher degree of cohesive failure, have been able to absorb more energy before complete failure.

- Overlap 20mm – Thickness 0.3mm

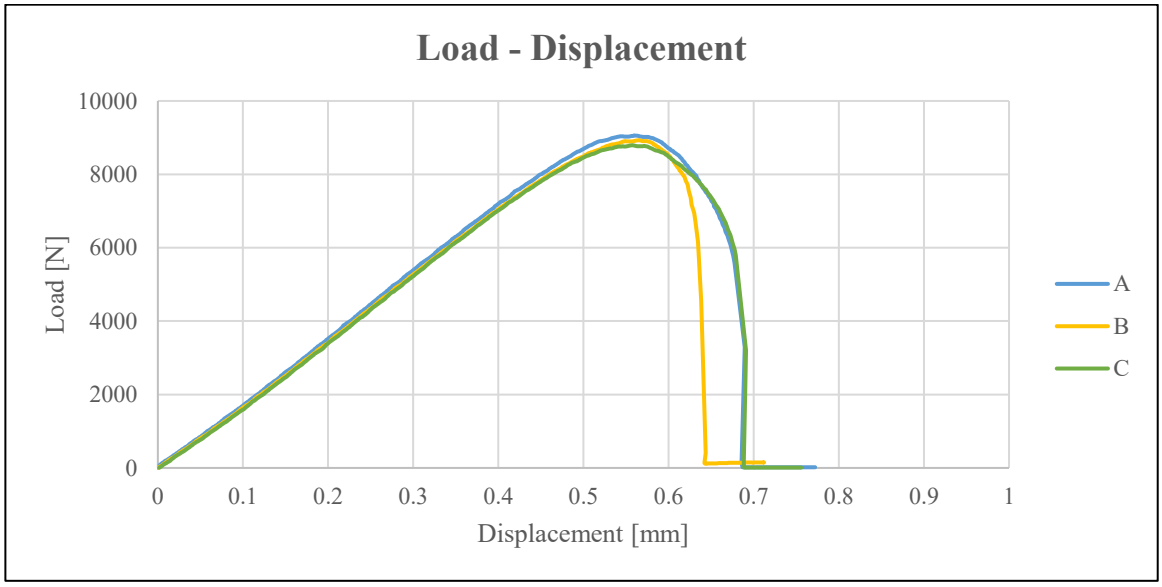

Figure 46. Load - Displacement chart O20_T0.3

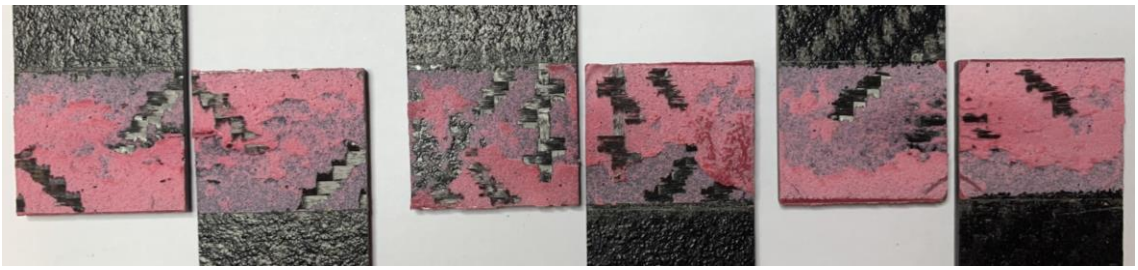

Figure 47. Fracture surface O20_T0.3 (A – B – C)

In this configuration, by looking at the plot we can see a ductile behavior for all the specimens.

By analyzing the fracture surfaces we can distinguish:

- Specimen A: cohesive failure.
- Specimen B: cohesive, light fiber tear and thin layer cohesive failure.
- Specimen C: cohesive failure.

Despite having slightly different fracture surfaces, all the specimens showed a similar trend in the Force-Displacement curve and cohesive failure is said to be the predominant failure mode for this configuration. Samples A and B, which sowed a higher degree of cohesive failure, have been able to absorb more energy before complete failure.

- Overlap 20mm – Thickness 0.8mm

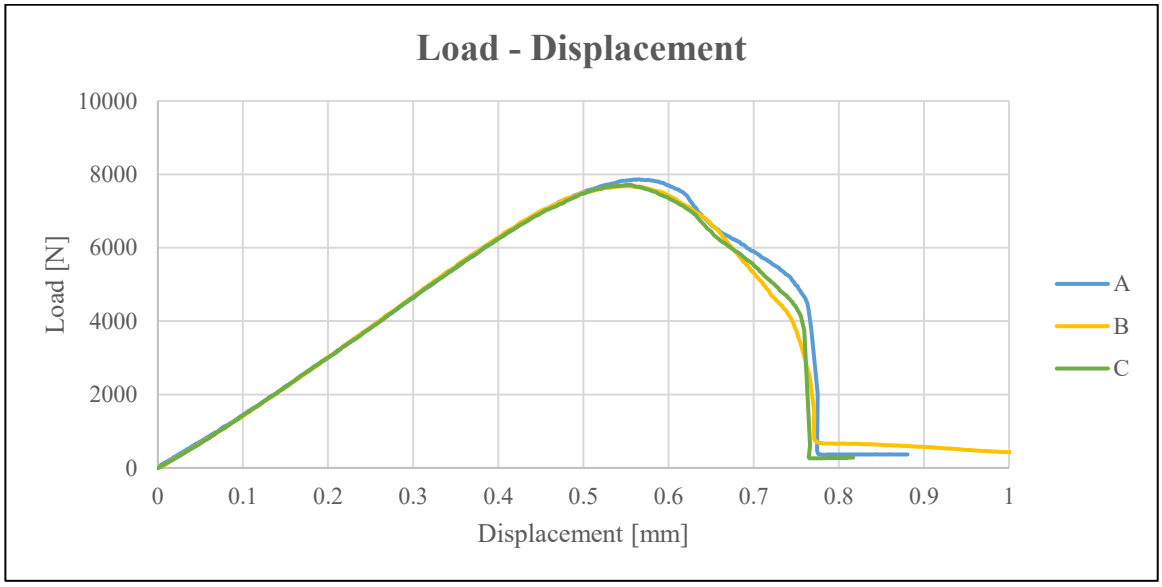

Figure 48. Load - Displacement chart O20_T0.8

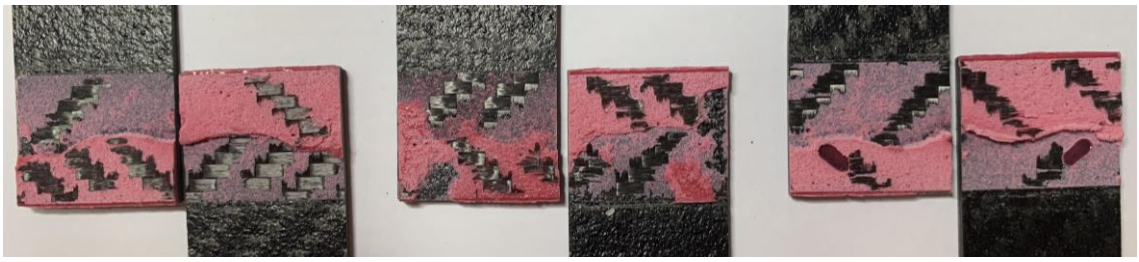

Figure 49. Fracture surface O20_T0.8 (A – B – C)

In this configuration, by looking at the plot we can see a ductile behavior for all the specimens.

By analyzing the fracture surfaces we can distinguish:

- Specimen A: cohesive and light fiber tear failure.
- Specimen B: cohesive, light fiber tear and thin layer cohesive failure.
- Specimen C: mainly cohesive and light fiber tear failure in a restricted area.

Despite having slightly different fracture surfaces, all the specimens showed a similar trend in the Force-Displacement curve, this small difference can be due to the proximity of the limit between cohesive failure and fiber tear failure. Cohesive failure is said to be the predominant failure mode for this configuration.

- Overlap 20mm – Thickness 1.1mm

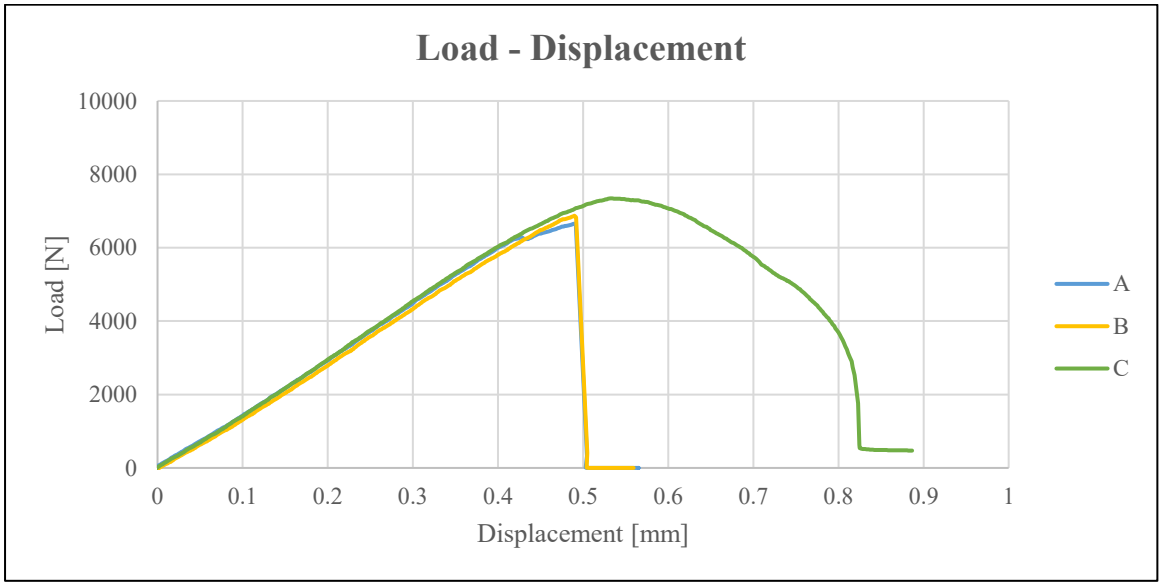

Figure 50. Load - Displacement chart O20_T1.1

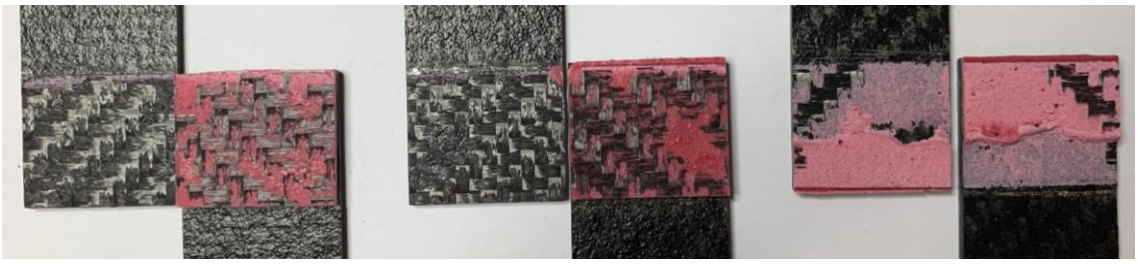

Figure 51. Fracture surface O20_T1.1 (A – B – C)

In this configuration, by looking at the plot we can see a fragile behavior for two specimens and ductile for one.

By analyzing the fracture surfaces we can distinguish:

- Specimen A: light fiber tear failure.
- Specimen B: light fiber tear failure.
- Specimen C: mainly cohesive and light fiber tear failure in a restricted area.

Specimens A e B showed a similar trend in Force-Displacement curve with immediate rupture once peak load has been reached, this has been caused by a complete premature failure of the substrate and rapture of the fibers. Specimen C instead had a cohesive failure, in fact its curve shows a ductile behaviour, which is the one wanted for this tests, so this is the representative specimen for this configuration.

- Overlap 30mm – Thickness 0.3mm

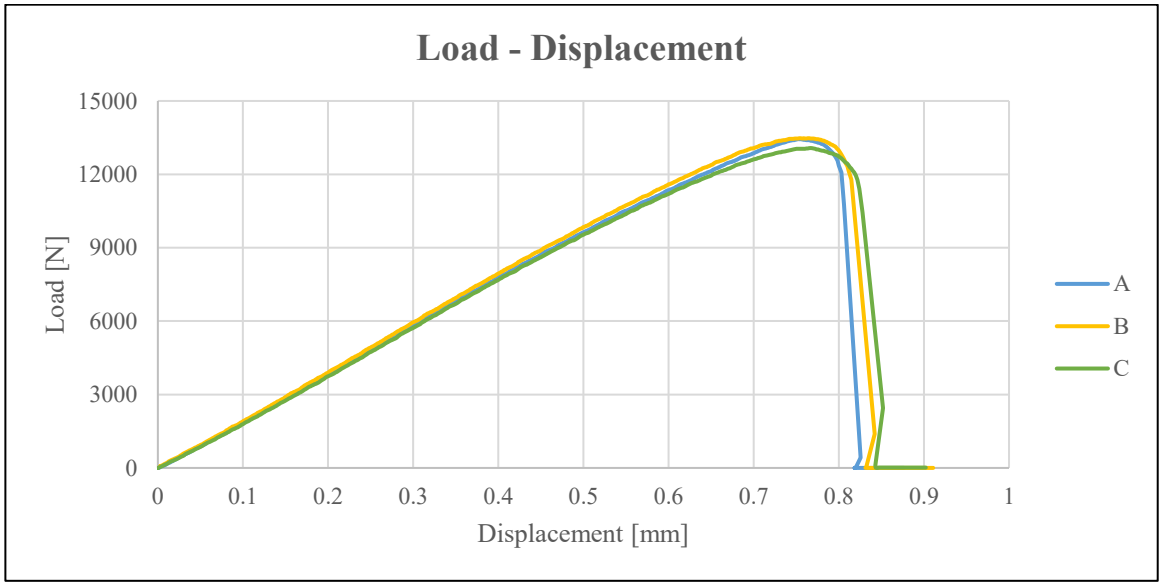

Figure 52. Load - Displacement chart O30_T0.3

Figure 53. Fracture surface O30_T0.3 (A – B – C)

In this configuration, by looking at the plot we can see a fragile/ductile behavior for all the specimens.

By analyzing the fracture surfaces we can distinguish:

- Specimen A: mostly light fiber tear and cohesive failure at the tips.
- Specimen B: mostly light fiber tear and cohesive failure at the tips.
- Specimen C: mostly light fiber tear and cohesive failure at the tips.

All the specimens showed a similar trend in the Force-Displacement curve with a combination of fragile and ductile behavior. This is confirmed by looking at the fracture surfaces since at the tips of the overlap, areas of cohesive failure are noticeable, which causes the knee part of the curve after peak load has been reached, that is not an

imminent rupture but gradually fails, up to a point where the fracture becomes mostly fiber tear and the brittle behavior of the fiber shows up.

- Overlap 30mm – Thickness 0.8mm

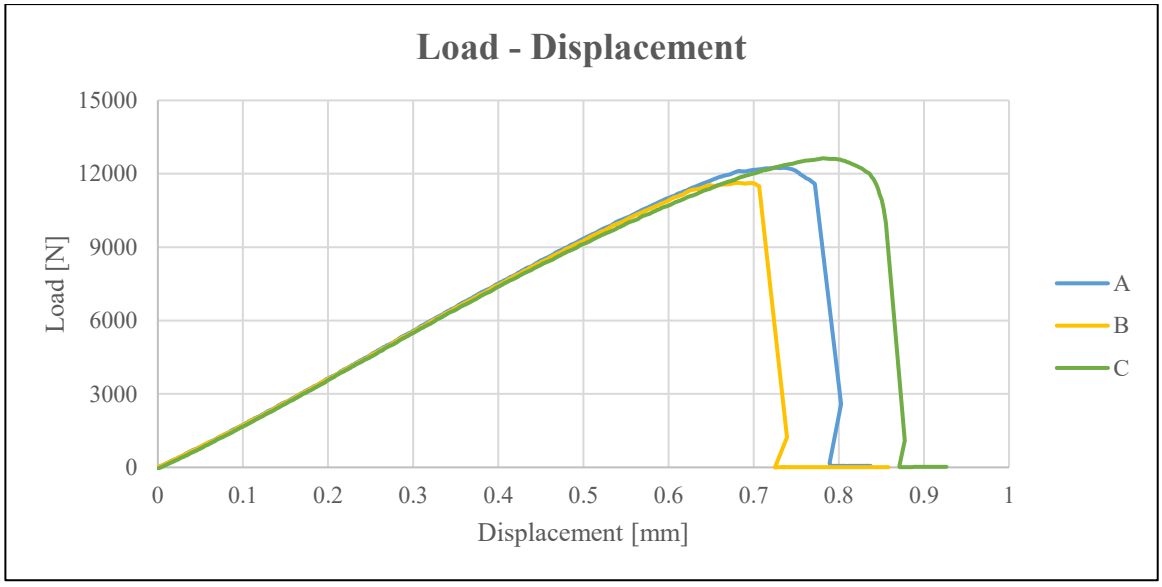

Figure 54. Load - Displacement chart O30_T0.8

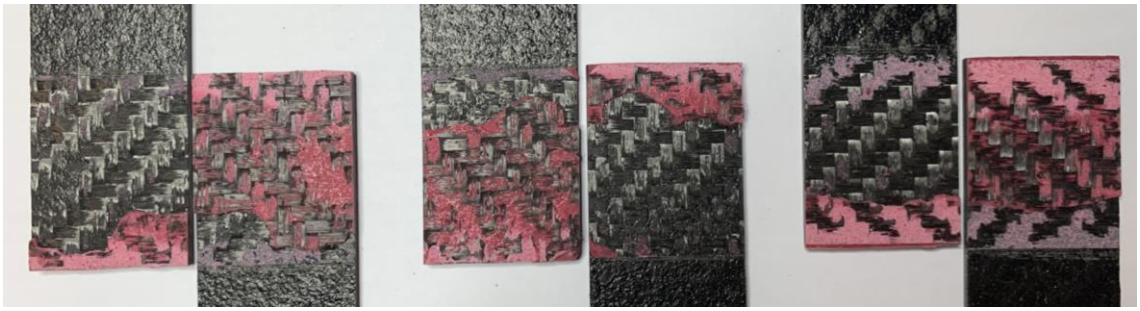

Figure 55. Fracture surface O30_T0.8 (A – B – C)

In this configuration, by looking at the plot we can see a fragile/ductile behavior for all the specimens.

By analyzing the fracture surfaces we can distinguish:

- Specimen A: mostly light fiber tear and cohesive failure at the tips.
- Specimen B: mostly light fiber tear and cohesive failure at the tips.
- Specimen C: mostly light fiber tear and cohesive failure at the tips.

All the specimens showed a similar trend in Force-Displacement curve with a combination of fragile and ductile behavior. This is confirmed by looking at the fracture surfaces since at the tips of the overlap areas of cohesive failure are noticeable, which causes the knee part of the curve after peak load has been reached, which is not an imminent rupture but gradually fails, up to a point where the fracture becomes mostly fiber tear and the brittle behavior of the fiber shows up.

- Overlap 30mm – Thickness 1.1mm

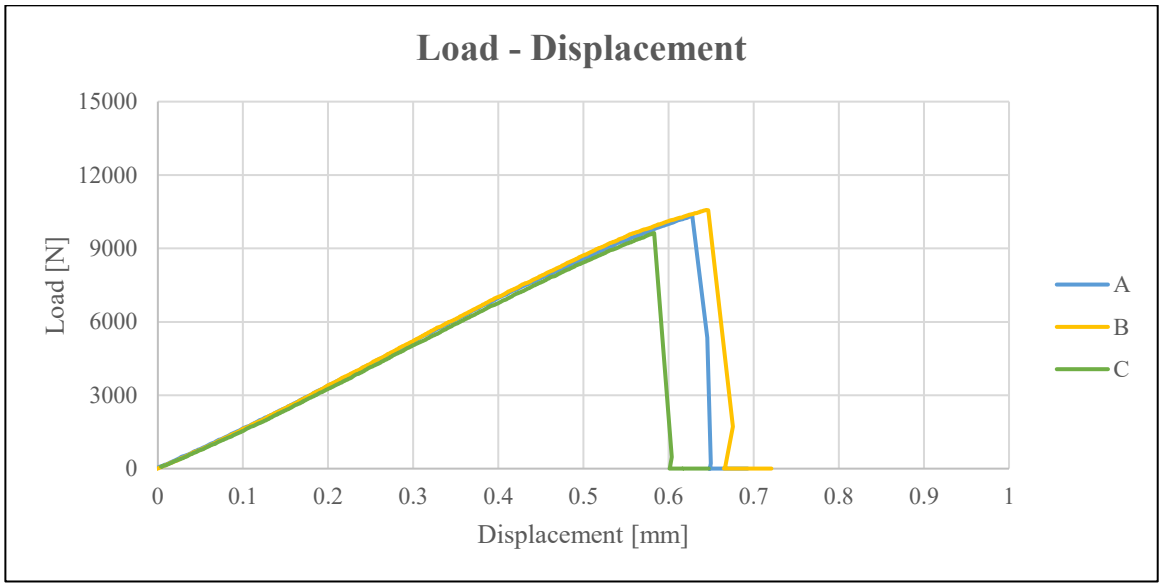

Figure 56. Load - Displacement chart O30_T1.1

Figure 57. Fracture surface O30_T1.1 (A – B – C)

In this configuration, by looking at the plot we can see a fragile behavior for all the specimens.

By analyzing the fracture surfaces we can distinguish:

- Specimen A: mostly light fiber tear and adhesive failure in restricted areas.

- Specimen B: adhesive and light fiber tear failure.
- Specimen C: adhesive and light fiber tear failure.

All specimens showed a similar trend in Force-Displacement curve with immediate rupture once peak load has been reached, this has been caused by a complete premature fail of the substrate and rapture of the fibers. In other areas where adhesive failure happened maybe some surface defects were present that caused incorrect adhesion.

Concentration of the stresses at the bonding area tips and fiber tear failure will be supported by additional theory models and explanations in the following chapter: 4.3.6 Theory models.

To better analyze the results and compare each tested condition, further data analysis has been done to obtain the maximum shear stress reached before failure, to compare the experimental data of all the configurations with the values listed in the datasheet.
A sensitivity analysis of all the parameters of the study has been carried out and will be shown after the shear stress display.

Table 4. Shear stress analysis O_10

Overlap 10mm						
Adhesive thickness [mm]	**Code**	**Max force [N]**	**Bonding area [mm^2]**	**Shear stress [MPa]**	**Standard deviation [MPa]**	**Average shear stress [MPa]**
0.3	O10_T0.3_A	4482.6	236.9	18.9	0.93	18.8
	O10_T0.3_B	4661.2	235.2	19.8		
	O10_T0.3_C	4194.1	238.8	17.6		
0.8	O10_T0.8_A	3510.9	233.8	15.0	1.61	17.1
	O10_T0.8_B	4586.4	242.1	18.9		
	O10_T0.8_C	3746.8	217.3	17.2		
1.1	O10_T1.1_A	4276.5	244.8	17.5	0.19	17.2
	O10_T1.1_B	4166.4	244.4	17.0		
	O10_T1.1_C	4141.5	242.8	17.1		

Table 5. Shear stress analysis O_20

Overlap 20mm						
Adhesive thickness [mm]	**Code**	**Max force [N]**	**Bonding area [mm²]**	**Shear stress [MPa]**	**Standard deviation [MPa]**	**Average shear stress [MPa]**
0.3	O20_T0.3_A	9060.7	484.4	18.7	0.37	18.8
	O20_T0.3_B	8929.3	484.6	18.4		
	O20_T0.3_C	8790.1	455.1	19.3		
0.8	O20_T0.8_A	7863.3	463.4	17.0	0.27	16.7
	O20_T0.8_B	7683.7	470.9	16.3		
	O20_T0.8_C	7714.9	460.8	16.7		
1.1	O20_T1.1_A	6661.5	483.0	13.8	0.87	14.6
	O20_T1.1_B	6872.2	484.7	14.2		
	O20_T1.1_C	7346.0	464.9	15.8		

Table 6. Shear stress analysis O_30

Overlap 30mm						
Adhesive thickness [mm]	**Code**	**Max force [N]**	**Bonding area [mm²]**	**Shear strength [MPa]**	**Standard deviation [MPa]**	**Average shear strength [MPa]**
0.3	O30_T0.3_A	13441.5	729.2	18.4	0.32	18.5
	O30_T0.3_B	13475.3	714.7	18.9		
	O30_T0.3_C	13075.2	723.2	18.1		
0.8	O30_T0.8_A	12245.6	718.1	17.1	0.60	17.0
	O30_T0.8_B	11627.5	716.4	16.2		
	O30_T0.8_C	12630.9	713.8	17.7		
1.1	O30_T1.1_A	10339.5	683.8	15.1	0.67	14.5
	O30_T1.1_B	10571.1	719.2	14.7		
	O30_T1.1_C	9629.7	711.1	13.5		

Now some sensitivity analysis on the effect of thickness and overlap on the shear stress obtained during the test will be shown.

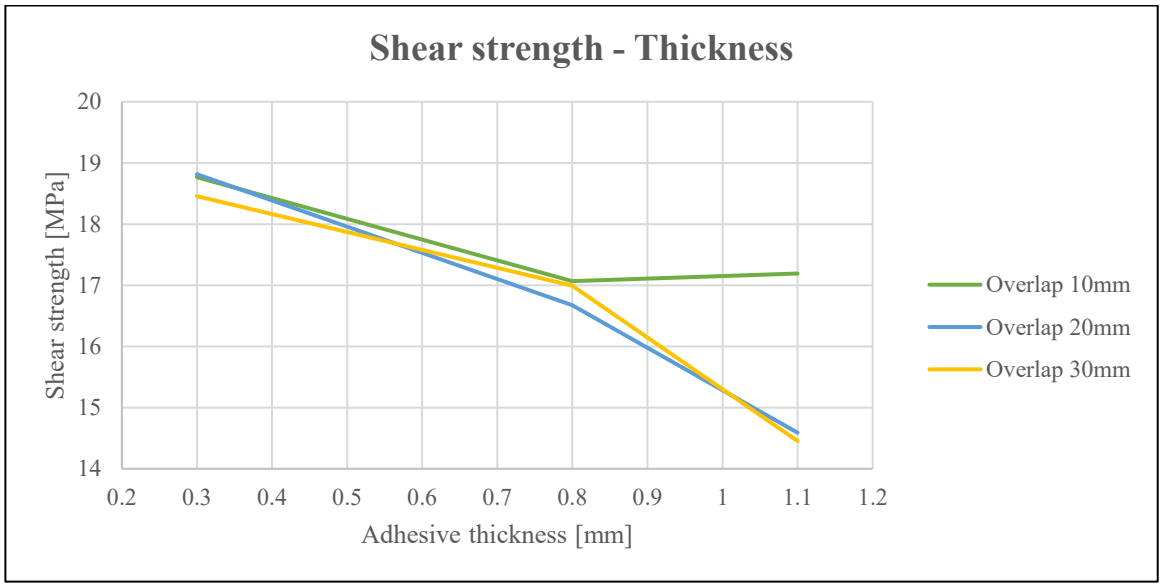

Figure 58. Shear strength - Thickness chart

It is clear from the graph that a general trend can be seen, that is a decrease in the shear strength of the adhesive as adhesive thickness increases. The configurations O20_T1.1 and O30_T1.1 showed a low degree of cohesive failure, so if we exclude those values we could see a pretty much constant curve from 0.8mm of adhesive thickness to 1.1mm as for the case at overlap 10mm.

These results are well related to theory concepts, in which for low thicknesses of the adhesive layer better performances are obtained since the adhesive is kind of forced between the two substrates and crack propagation has a preferred direction along the adhesive layer, while for higher thicknesses the adhesive itself acts more like a bulk material, in which crack propagation happens more in a perpendicular plane for the bonding area. This phenomenon was clearly visible on the failure surfaces of the tested specimens.

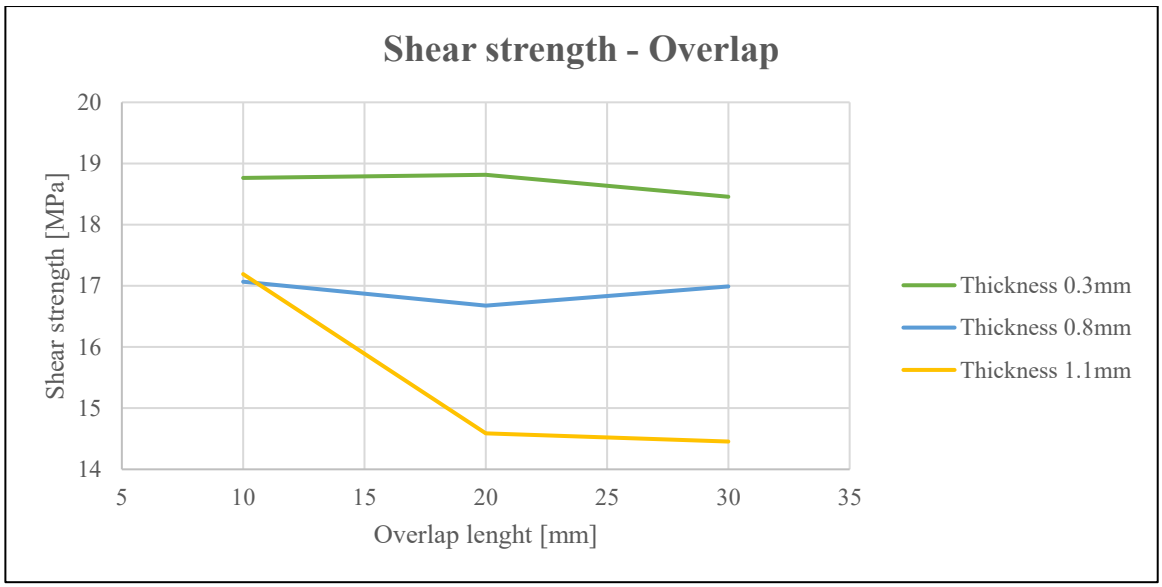

Figure 59. Shear strength - Overlap chart

By looking at the shear strength vs overlap diagram, the different overlap length do not influence a lot the shear strength, instead the adhesive thickness has a big influence on it. Same remarks can be done here with the exclusion of the values related to O20_T1.1 and O30_T1.1 due to their non-cohesive failures.

Now a sensitivity analysis based on the actual Load-Displacement curves obtained from the test will be shown.
In the following diagrams only one representative curve for each configuration will be displayed (usually the one with the highest degree of cohesive failure).

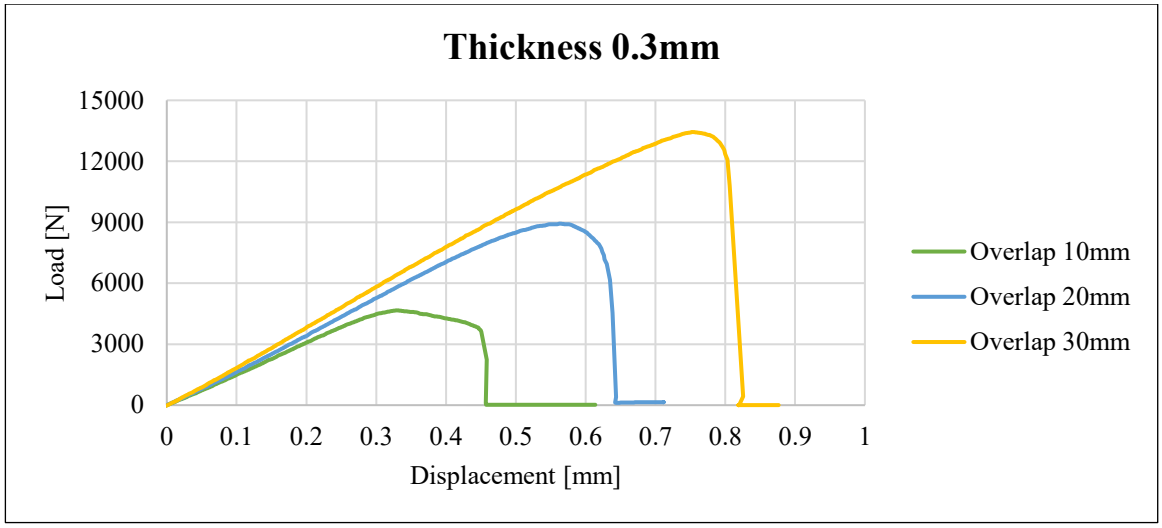

Figure 60. Load – Displacement T_0.3

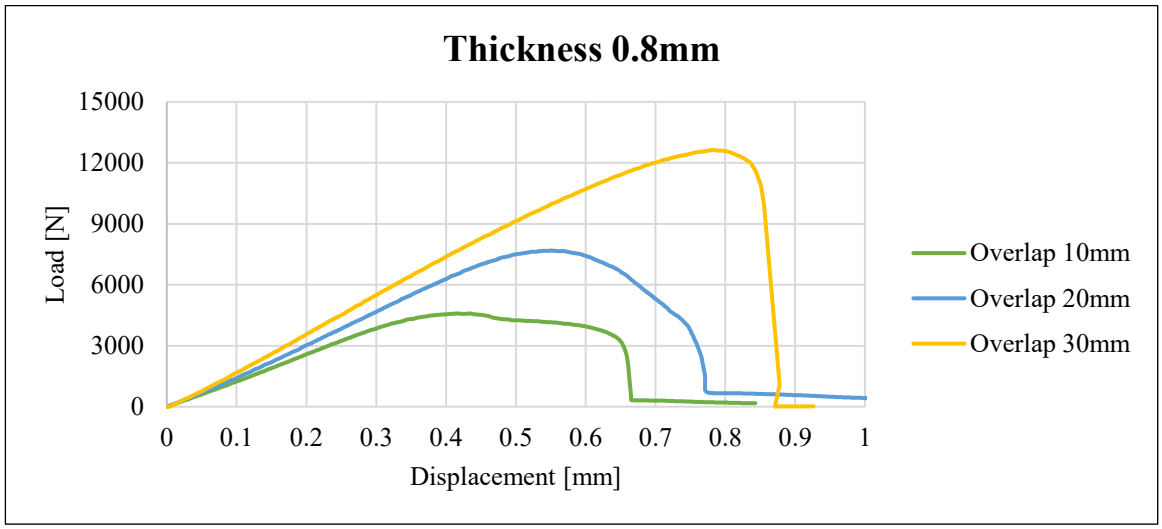

Figure 61. Load – Displacement T_0.8

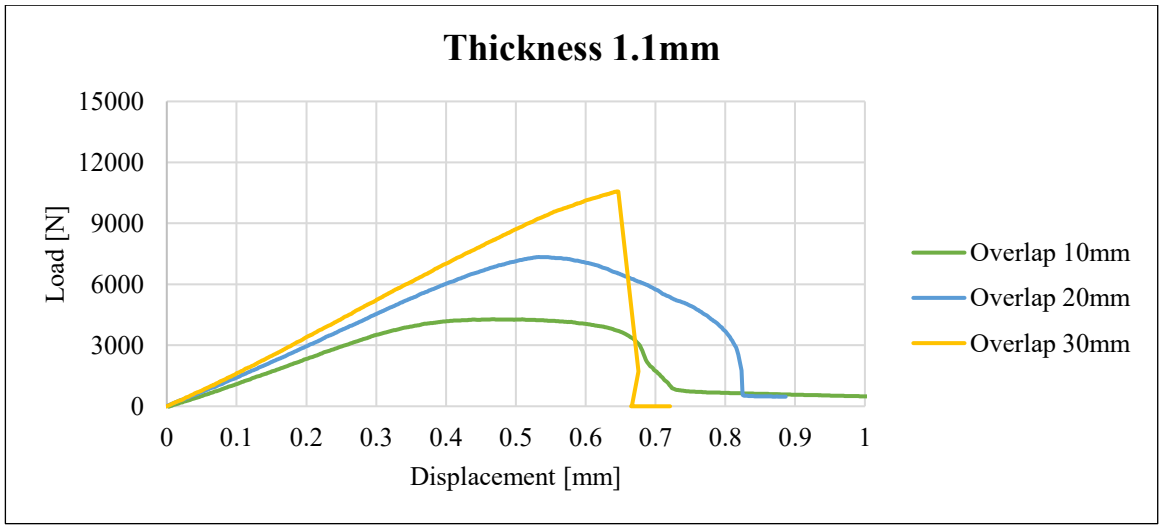

Figure 62. Load – Displacement T_1.1

General comments can be made on the three diagrams that are valid in the same way for all of them.

It is noticeable how by increasing the overlap, a slightly stiffer joint is realized in the first linear part, but also a visible higher displacement at failure can be seen. Load at failure is increasing with overlap length, but as we have seen in the previous diagrams the overall shear strength is not affected by this parameter, since the ratio force over area remains the same.

All these considerations applied to all the curves, apart from the O30_T1.1, that had a non-cohesive failure as seen before.

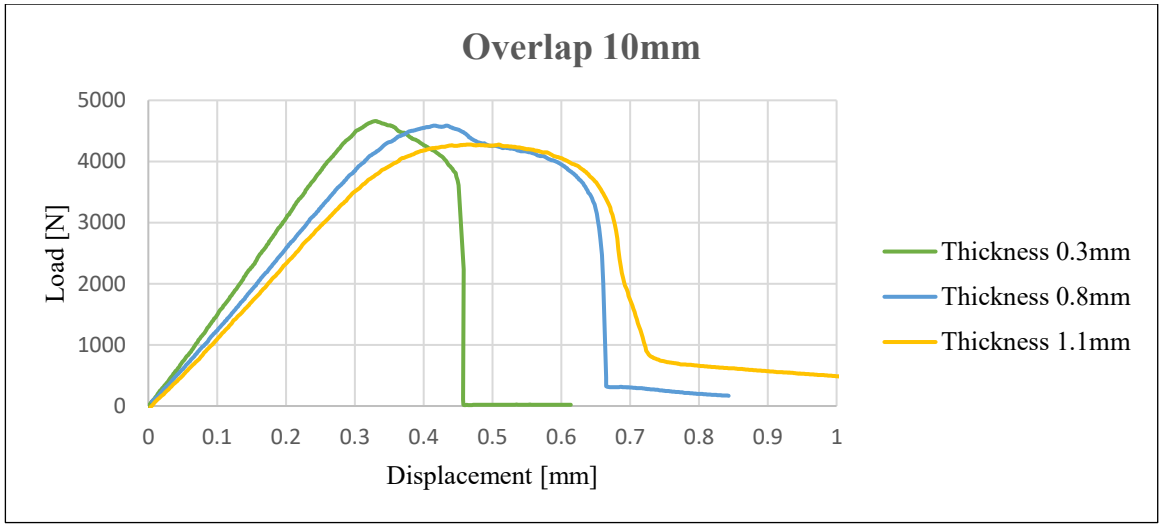

Figure 63. Load – Displacement O_10

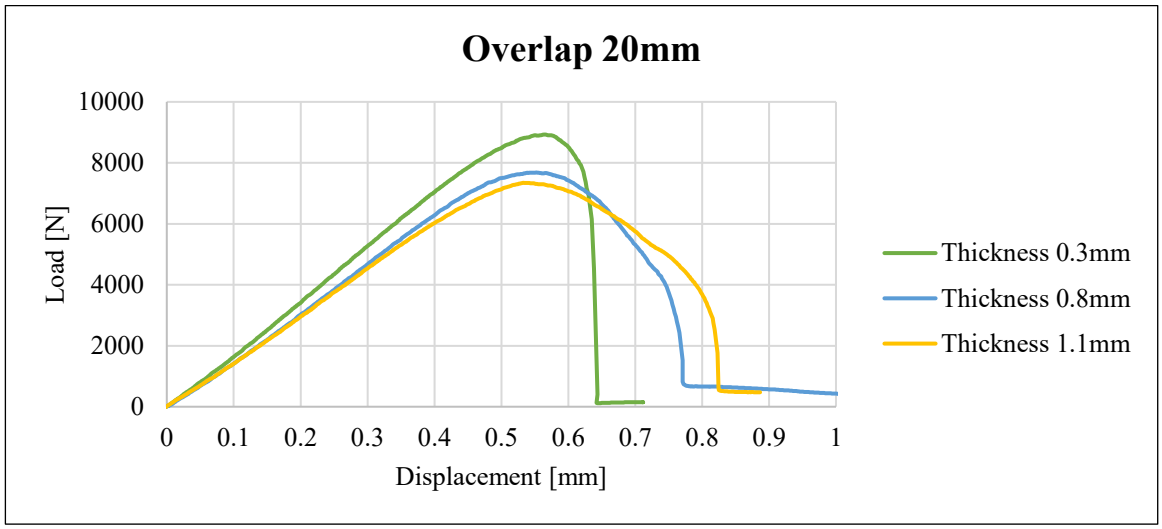

Figure 64. Load – Displacement O_20

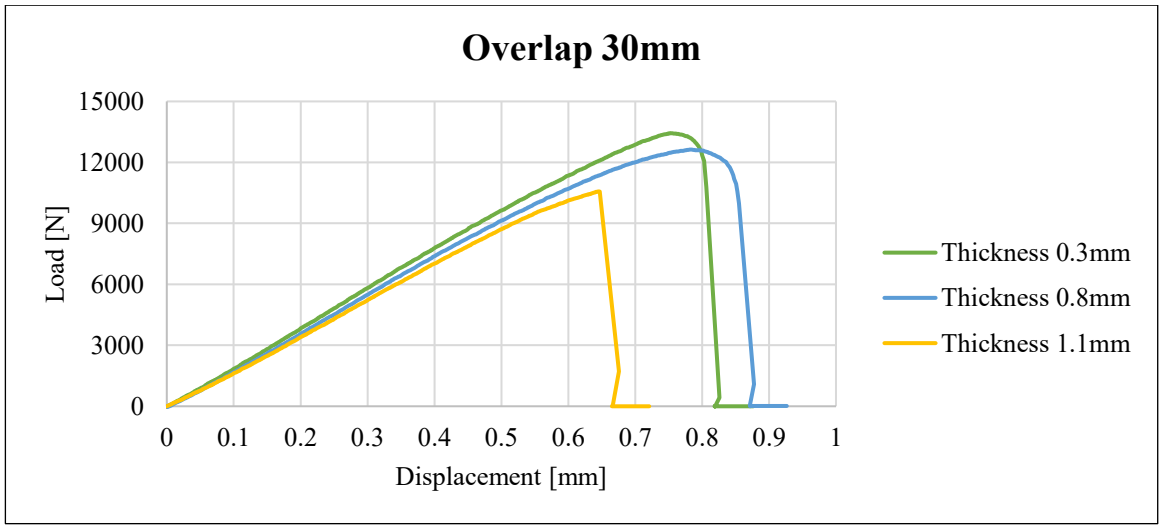

Figure 65. Load – Displacement O_30

General comments can be made on the three diagrams that are valid in the same way for all of them.

It is noticeable how by increasing the adhesive thickness, joint stiffness slightly decreases in the first linear part, but also a visible higher displacement at failure can be seen. This means that the adhesive is able to absorb more energy before failure, traceable to the higher adhesive quantity in the joint and to lower, more dispersed stresses.

All these considerations applied to all the curves, apart from the O30_T1.1, that had a non-cohesive failure as seen before.

4.3.6 Theory models

Many literature studies and models have been presented over the years to predict the tensional state inside the adhesive joint, actually, each model differs from the others and to this day there isn't a clear and fixed explanation of the actual phenomena. For sure for complex geometries nowadays FEM is used to predict and analyze the structure behavior, but many analytical models can explain quite well the stress distribution in a relatively simple single lap joint configuration.

A classic linear elastic theory proposed by Volkersen applied to SLJ with an applied shear force and non-deformable adherend can be representative of a simplified solution.

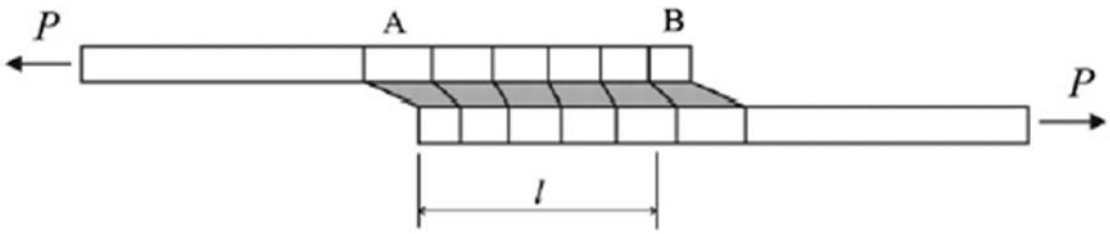

Figure 66.Adhesive elements deformation in Volkersen's model [9].

Shear stress in the upper substrate is maximum at point A and diminishes down to being null at point B. The same but opposite considerations are valid for the lower substrate. In the adhesive instead, the shear stress is maximum at the extremities of the overlap and minimum in the middle. This trend is extremized for small overlap length, where the stresses at the extremities are way higher than the ones in the middle, while for longer overlap the stress distribution is way more flat with lower peaks at the extremities.

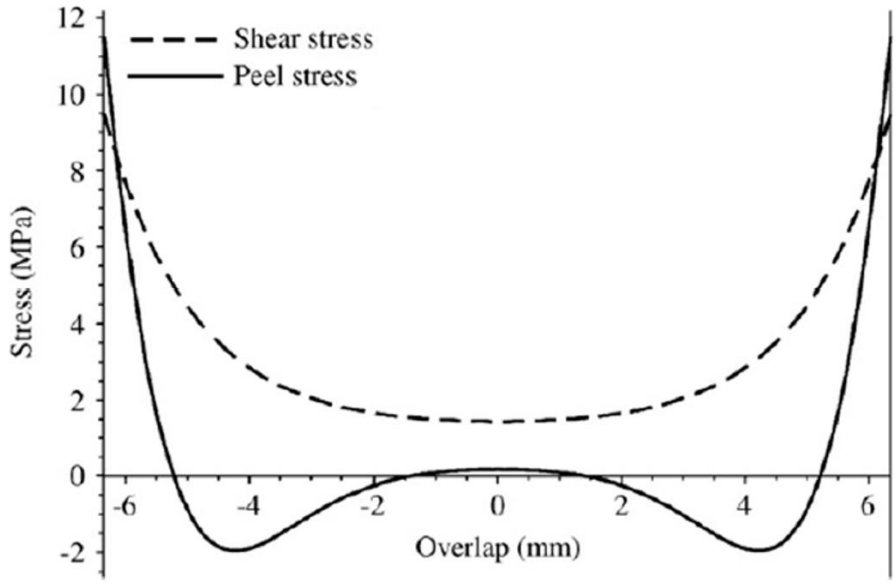

Figure 67. Shear and peel stress along the overlap in a SLJ configuration [9].

This relatively simple analytical model is able to catch quite well the trend of the stresses in the actual joint. In fact from FEM results the same trend is visible and will be discussed later in the chapter: 5.2 RADIOSS.

The fiber tear phenomena that happened on some of the joints can be explained by the concepts related to Hart-Smith theory that will be presented and used as an explanation of the facts that happened.

In a single lap joint configuration subjected to load application, in the substrate two different stresses arise, shear (τ) and normal (σ). Through analytical models they showed an omega (ω) trend of the normal stresses along the joint length, with peaks at the tips of the bonding area and a local maximum in the middle. These high concentrated

normal stresses cause the fibers of the composite material to deform and have high stresses in a direction that is perpendicular to the fiber causing out of-the-plane stress, which can cause premature failure, since the fibers are able to sustain high load only along their longitudinal direction. This effect combined with the high rotation caused by longer overlap used and stress concentrations due to geometric non linearities at the tip of the bonding area, could be a satisfying explanation of the failure that happened in some of the specimens tested in this research, like the fibre tear failure visible in figure 57. In fact, during the experimental test, high rotation of the bonding area was visible up to a sudden snap of the specimen at the moment of failure, this imminent rupture can be correlated to the high stress concentrations at the extremities of the bonding area, that combined with the high peel stress forced the fibres of the CFRP substrate to be subjected to an out-of-plane load that led to imminent fibre failure.

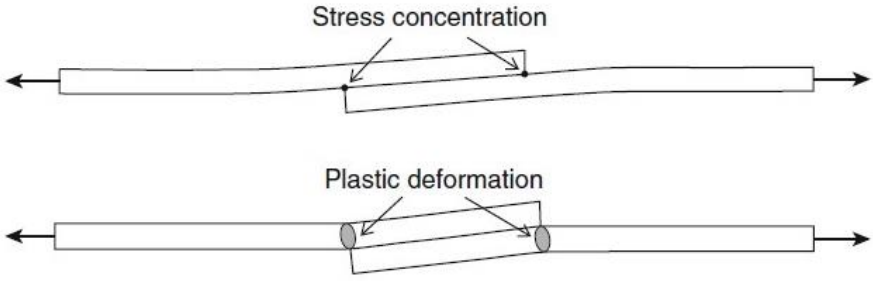

Figure 68. Specimen rotation and stress concentration [10].

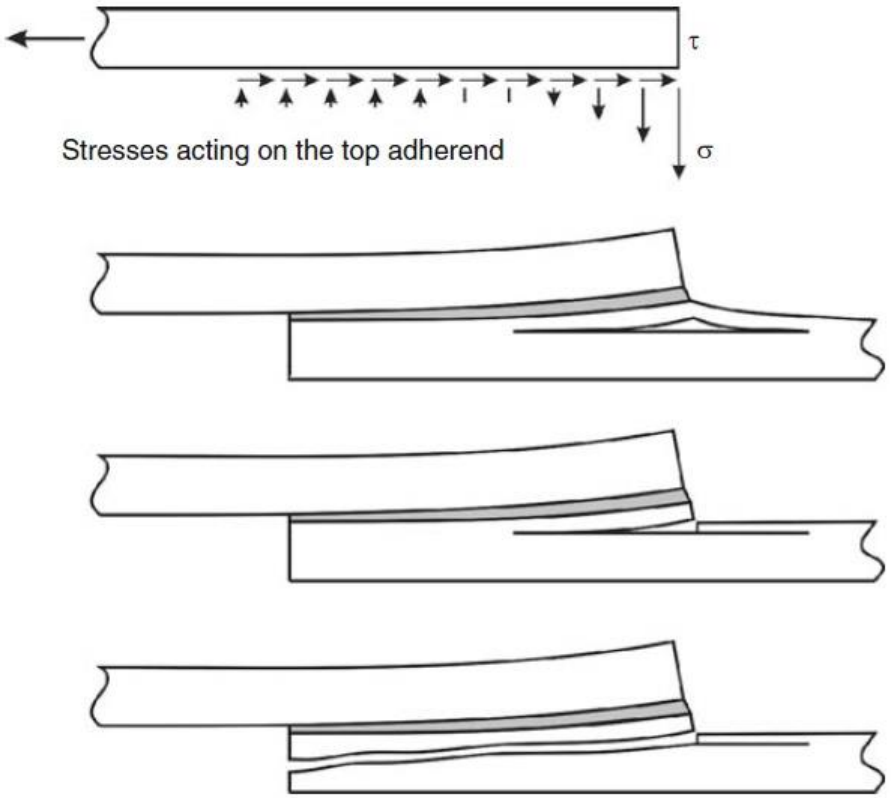

Figure 69. Fiber tear visualization according to Hart-Smith [11].

4 Numerical simulation

One of the targets of this research was the correlation between experimental and numerical data obtained from the previously listed tests; so in this chapter only a general presentation on the basic concepts of numerical simulations will be reported, without getting in to detail on the theory behind this modelling technique, which is out of the scope of this study.

Finite element analysis (FEA) is a widely used computer-based numerical calculation method able to solve a wide variety of problems. The method involves splitting an entire system into multiple well-defined elements connected at nodes, this process is called discretization. Parameters of study are identified at the nodes and the values between nodes are determined by polynomial interpolation. The values are determined by computationally solving a series of simultaneous equations, the accuracy of matrix methods and results depends on discretization.
The method's current popularity is due to its ability to model many classes of problems regardless of geometry, boundary conditions and loads. Modelling the behavior of adhesive joints is complicated by several factors, including the complex geometry, the complex material behavior, and the environmental sensitivity. FEA is currently the only technique that can comprehensively address the challenges of modelling bonded joints under realistic operating conditions. However, a reliable and robust method of using FEA to model failure in bonded joints is still to be developed [1].

In general, the finite element method (FEM), has been used to solve boundary value problems in many fields. The initial applications of the finite element method were in aircraft structures but it is now widely applied to the solution of many other engineering problems. These include the stress and thermal analysis of components, crash analysis of vehicles, seismic analysis of civil engineering structures, nuclear engineering, fluid flow analysis, soil structure interaction, steady state and transient behavior of electronic devices, and electromagnetics.

Thanks to its wide variety of applications, FEM has grown a lot of interest in the last decades, from any kind of company to increase the virtual simulation phase during the design process of any product, in order to limit physical testing which is way more expensive, in terms of money but also time. Since Physical testing requires, initial planning of the production testing phase, some sort of rapid prototyping technique to produce the required product, use of testing equipment, rigs and places, data acquisition machines, and so on; it is easily noticeable the amount of time, energy and money saved by the use of FEA.
As announced before the use of composites is increasing in modern structures and FEA provides a convenient method to determine the performance and durability of composites. The fabrication of different types of composite lay-up can be explored at design stage to avoid problems during manufacturing. FEA can also be used in the optimization of structural components, full vehicle body noise and vibration analysis are performed to improve the performance of modern vehicles. Nowadays basically any component of a vehicle has been subjected to some sort of FEA analysis before being produced, being it a structural, thermal, electromagnetic, computational fluid dynamic or other type of analysis [11].

In this research, FEM applied to structural problems has been involved, to replicate the experimental tests in virtual simulations, with the goal of getting results as close as possible to the actual tests performed.
In particular, two different software have been used:

- RADIOSS, which is a multidisciplinary finite element solver developed by Altair Engineering.
- LS-DYNA, which is an advanced general-purpose Multiphysics simulation software package owned by Ansys.

Regardless of the used software, in general the complete simulation can be divided in three phases: [1]

- Pre-processing: during which all the geometries defined in the model are meshed into 1D, 2D or 3D elements depending on the type of structure that is simulated

and on the degree of accuracy wanted. Loads and boundary conditions are set, as well as material properties and other information to describe the model.
As a general rule, valid for any parameter and condition, the more accurate and detailed a simulation is, the longer it will take to solve the problem, so a tradeoff between computational time and detailed simulation has to be found. Without getting in to much detail, simulation time can be heavily affected by element size, element order, non-linearities, type of contact, etc.

- Processing: the solver solves the problem and creates output files with the results of the analysis process such as nodal deflections, element stresses, etc. This normally involves the solution of many thousands of equations and can involve the creation of large temporary files. This is generally controlled by the software package.

- Post-processing: the output from the processor enables the user to analyze the results from the analysis in text and/or graphical form. The user can view an analysis log giving details of the analysis process and search for status messages created by the software to indicate possible errors in the analysis. With the tendency toward larger models, shifting through large text files can be laborious and it is now more common to view results in graphical mode. However, some output in text format is often required and this can usually be controlled via the graphical interface. Graphic postprocessors are capable of presenting results in many different formats. One of the most useful plots to look at initially is the deformed mesh, any major errors should be obvious from the deformed shape. Contour plots can then be used to show the distribution of stresses, strains, displacements, or other parameters through the structure analyzed.
  Results in various directions can usually be viewed as well as a number of calculated parameters such as principal and von-Mises equivalent stresses and strain energy density. These should be viewed ‘‘unsmoothed’’ in the first instance in order to identify areas where further mesh refinement is required.

Since the focus of this study is understanding the mechanical behavior of the adhesive joint, a brief description of the model set-up regarding composites, metals and boundary conditions will be made. While modelling of the adhesive will be deeply discussed, starting from the type of elements used, which are called cohesive elements and as their name suggests, they have been developed to catch the cohesive failure of such material. These element types were available in both software used, although with different cards and use of different parameters for the description of the element.

5.1 Cohesive zone modelling

As anticipated before, various methods for the analysis of glued joints have been developed over time, in order to predict the distribution of the stresses in the adhesive and resistance provided by the connection.

Analytical or numerical analyses can be performed on such joints, the former have been developed to find solutions in closed form to very simple systems with relative boundary conditions. An example of a system analyzed with an analytical approach is the single lap joint, which presents a linear geometry and simple model. By increasing the model complexity, material or geometrical non linearities can be introduced along with non-homogeneous systems of equations to be solved, in such cases the use of numerical analyses is preferred. The numerical approach instead allows to solve in an approximate way the problem, regardless of its complexity, consequently any kind of bonded assembly can be simulated with a dedicated model.

As a result of engineering development in the field of adhesive linkages, several techniques have been developed and used for modelling such systems, referring to continuous mechanics, fracture mechanics, cohesive zone modelling and extended finite element method.

Traditional modelling schemes use failure criteria based on continuous or fracture mechanics, but these methods have some limitations in their use. Continuous mechanics criteria use stresses and strains that depend on mesh size in critical areas. The use of fracture mechanics criteria, which relate to stress concentration factor or energy parameters, was limited to the mechanics of elastic linear fracture, so they could be used in systems connected by adhesives that had a small amount of plastic deformation at the apex of the crack. Moreover, this approach required a system already damaged at the beginning of the simulation, forcing configuration and size of the crack [12].

Cohesive zone modelling is a very useful technique in the analysis of bonded joints, but also for modelling the interface between two different materials or for delamination between plies of composite laminate. This technique is a combination of continuous and fracture mechanics and allows for modelling of material damage through the use of

cohesive elements or elements defined by the definition of cohesive law, traction-separation relationships between two coupled nodes of the same element.
Cohesive zone modelling is based on the concept of introducing into the traditional finite element model an interface where a crack can nucleate and propagate. This modelling strategy allows to simulation of the crack propagation along the failure path of the joint and has the advantage of predicting with high accuracy the behavior of the joint, which allows to increase the diffusion of this technology. Of course, the model prepared by using cohesive modelling, usually, does not take into consideration defects or other impurities, thus, they present defect-free behaviour with the crack that propagates symmetrically from both edges of the SLJ.
In the case of adhesive bonding in the simulation, a layer of cohesive elements is interposed between the substrates.
The cohesive law takes into account the stiffness degradation of the cohesive element, which represents the actual degradation of the adhesive's properties when is subjected to damage or when a certain value of tension is reached, therefore a relative displacement between the faces of the crack.
Cohesive zone modelling allows a continuous or local type of approach.
In the continuous approach, a layer of cohesive elements represents a layer of thick adhesive material interposed between the two substrates. The stiffness of the cohesive elements corresponds to the stiffness of the adhesive layer.
In the local approach instead, two coupled nodes of the cohesive elements, which belong to the two sides of the crack, represent overlapping nodes of the two substrates, so a zero-thickness interface is realized [13] [14] [15].

5.1.1 Cohesive law

Cohesive law can have different forms: triangular, trapezoidal, exponential and so on.

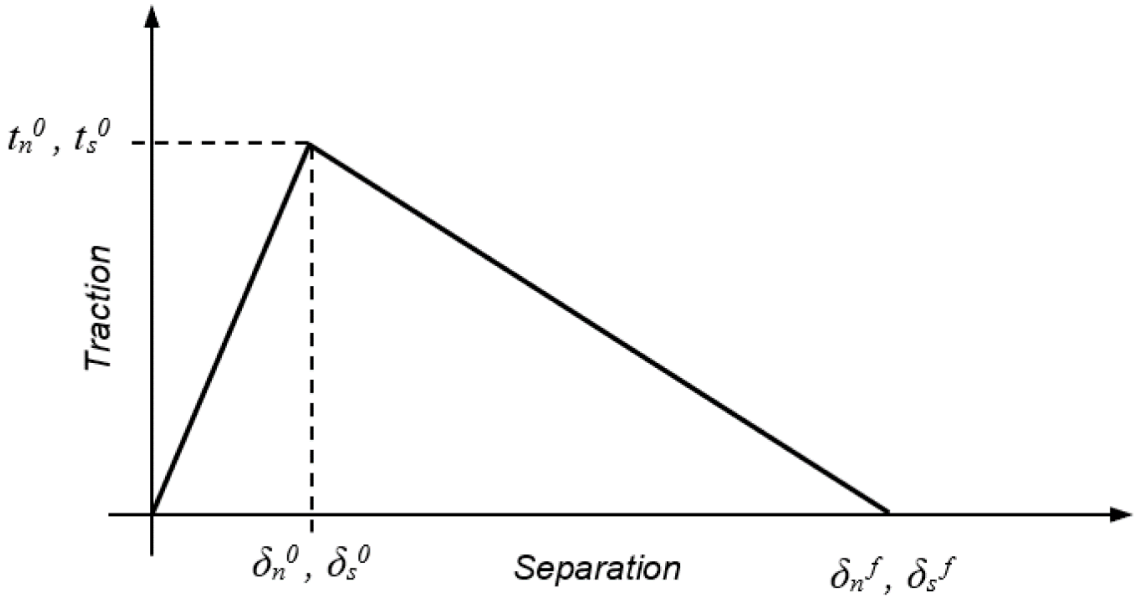

Figure 70. Triangular cohesive law [16].

By looking at the triangular one, which is the most used for structural adhesives, since they show a rapid decay of the properties during damage propagation we can notice that the first stretch of the curve represents the linear elastic behavior of the adhesive and the inclination corresponds to the stiffness of the adhesive layer. In the case of pure mode (tension or shear only), this trend remains linear until the peak tension for mode I t_n^0 or the peak shear for mode II t_s^0 is reached when damage begins. δ_n^0 and δ_s^0 are mode I and mode II separations at peak tension and shear respectively. Once the peak is reached a degradation of the properties happens and damage in the elements develops, this loss in stiffness continues until complete subsidence, which is reached at separation δ_n^f and δ_s^f for mode I and mode II respectively. This second part of the curve is also called softening for obvious reasons.
The damage law evolution is defined by the user specifying the form of the law of softening and the entity of the rate of energy release in the different modes $G_I c$ and $G_{II} c$. In the case of trapezoidal law, there is a constant traction stretch after the peak tension or shear at the start of the damage.

In the case of mixed mode loading a combination of the two pure modes is used according to different models. Tensional or energetic criteria usually combine the pure

mode laws. For the criteria regarding the beginning of the damage, the mechanics of the continuous is used, while for the propagation of the damage energy criteria related to fracture mechanics are usually used.

Criteria used to define the initiation of the damage in the case of mixed mode can be various and regard both stresses and deformations.

The damage evolution law describes the modality of stiffness degradation of the element after reaching the damage initiation criteria.

A damaging variable D is defined in a range between 0 and 1. This variable assumes value 0 at damage initiation and value 1 when complete failure of the element happens. The damage is considering all the active damaging mechanisms and the degradation caused by the different loading modes.

The damage evolution criteria are defined by the softening, the energy parameters G_ic or relative separation at failure.

Usually, for the prediction of the separation at failure in the case of mixed mode, energy criteria are used, this is done to combine cohesive laws in pure modes. These criteria use energy release rates in the different modes G_Ic, $G_{II}c$ and $G_{III}c$ [17] [18].

An example of this method is the complete failure of the elements when the following condition is achieved:

$$\left\{\frac{G_I}{G_{Ic}}\right\}^2 + \left\{\frac{G_{II}}{G_{IIc}}\right\}^2 + \left\{\frac{G_{III}}{G_{IIIc}}\right\}^2 = 1$$

When the stiffness of the element is completely degraded, the nodes corresponding to the element are separated and the crack propagates to the next pair of nodes.

Modelling of the cohesive zone was introduced by Dugale and Barenblatt [19] [20].

They associated the fracture process with the development of a fracture process zone around the tip of the crack in metals. When the size of this zone reaches a critical value, which depends on the fracture energy G_ic, the crack propagates. This theory is extendable to adhesive materials with the difference that the extension of the fracture process zone is limited to expand only through the adhesive layer because of the presence of adherends. This formulation explains the G_ic's dependence on the degree

of constraint of the adhesive layer, so on the thickness of it and on the thickness of the substrates in case of plastic deformation.
The advantage of this modelling strategy is that the results obtained in terms of tension distribution and peak resistance prediction are accurate thanks to the fact that different laws depending on the material or interface type can be used.
In order to use this law it is necessary to define the following parameters:

- The form of the cohesive law represents the behavior of the adhesive and the evolution of it with the development and growth of the entity of the damage.
- The cohesive tensile and shear strength t_n^0 and t_s^0, so the stress reached at the end of the elastic field of the material, which coincides with damage initiation.
- The values of deformation energy release rate in mode I and II achieved during the simulation and their critical values G_{Ic} and G_{IIc}, which represent the area under the traction – separation curve.

To identify the cohesive resistances and all the other parameters that define the law, different methodologies can be applied: [21]

- Parameter identification method allows to derive one property at a time from specific tests.
- Inverse method allows to obtain the parameters following an iterative activity and by comparing results obtained from FEM simulations with the experimental curves.
- Direct method instead allows to obtain the cohesive curve of a material or interface by differentiating the value of G with the crack opening for each of the two principal modes.

The method for identifying the parameters derives each one for the definition of the cohesive law with an appropriate test. A preliminary definition of the law of the material is necessary and it must be taken into account that the test must include the use of joints with small adhesive thickness, this is because the physical and mechanical properties of the bulk adhesive vary from those of a thin layer, due to the fact that the thin layer is constrained in the direction of adhesive thickness due to the presence of the substrates,

in this case the propagation of the damage occurs along the pattern of the adhesive layer because it is weaker and less rigid than the substrates, usually causing a fracture along the adhesive of the cohesive type.
In the case of bulk adhesive like in the Dog Bone samples of pure adhesive, the fracture propagation occurs perpendicular to the direction of maximum main stress, which is the direction of loading when a tensile test is performed.
The inverse method consists of an iterative fitting analysis aimed at identifying the cohesive parameters so as to have a good match between the experimental curves and the ones obtained from numerical simulation.
The direct method is the one that allows a more accurate representation of the cohesive zone modelling curve since it doesn't require estimating the curve and allows to identify it with precision.

5.1.2 Cohesive law choice

Cohesive laws can have different trends: triangular, trapezoidal, exponential or polynomial.
The previous paragraphs describe the triangular cohesive law and the parameters that characterize it.
The most important parameter for the choice of the cohesive law to be used is the behavior of the adhesive material of concern, as a rule of thumb, highly fragile adhesives are modeled with exponential laws, adhesives that show a fragile or little ductile behavior are modeled with triangular laws, while for ductile adhesives trapezoidal trends are usually used. The adhesive material is the most important characteristic for the choice of the law, but is not the only one, usually the choice depends also on the convergence of numerical solutions, which might be harder for complex trapezoidal or polynomial laws sometimes. A risk of simulating a ductile adhesive with a triangular law is that as soon as the damage starts an immediate decrease of the element resistance is appreciated due to the steeper softening portion of the curve, this can underestimate the properties of the joint.

Similarly for fragile adhesives simulated with a trapezoidal curve an increase in its resistance is seen so an overestimation of the properties may happen, which is even less safe than the previous case.

5.1.3 Cohesive parameters estimation

In order to identify the cohesive law, the parameters that characterize it are estimated by reproducing in the experimental tests the same constraint conditions and thicknesses adopted in the structures on which the study is focused on. The cohesive parameters to be determined for a linear law are G_{Ic} and G_{IIc}, t_n^0 and t_s^0. There aren't any standards for the definition of these parameters, but there are some techniques that have been established over time, the most used are those illustrated in the previous section: identification of the individual parameters, direct method and inverse method.
Usually the experimental tests performed to get the G_{Ic} are the Double Cantilever Beam (DCB) and the End Notched Flexure (ENF) to get the G_{IIc}. These parameters are valid for the pure mode I and II, but with the criteria mentioned before it is possible to get the wanted properties also for mixed mode. Single Lap Joints are characterized by a mixed mode loading since both shear and peel are present, so it's usually used as a test to validate the previous ones in mixed mode.
An important factor to take into account is that the cohesive laws are only valid for a defined thickness of the adhesive, because varying it will vary the properties of the joint. As long as the substrates work in the elastic field, their properties do not affect the adhesive properties of course.

5.2 RADIOSS

Preprocessing phase has been done by importing all the needed geometries into the software HyperMesh, then meshing all the wanted surfaces with 2D elements for shells and 3D for solids. Adhesives have been modelled with brick elements since the material and failure cards support this type of element only [22].

Adhesive property card has been defined by /PROP/TYPE43, which is designed for spotweld, welding line or glue-type connections.

The adhesive material card has been defined by /MAT/LAW69, which defines a hyper elastic and incompressible material specified using the Ogden, Mooney-Rivlin material models. It is generally used to model incompressible rubbers, polymers, foams, and elastomers. Material parameters are computed from engineering stress/strain curves from uniaxial tension and compression tests. It is used with shell and solid elements.

The adhesive failure card has been defined by /FAIL/CONNECT, which describes the failure model for connection material with elongation criteria and/or energy criteria.

Boundary conditions and loads have been applied replicating experimental test conditions to simulate the load applied by the tensile testing machine moving at a desired constant speed.

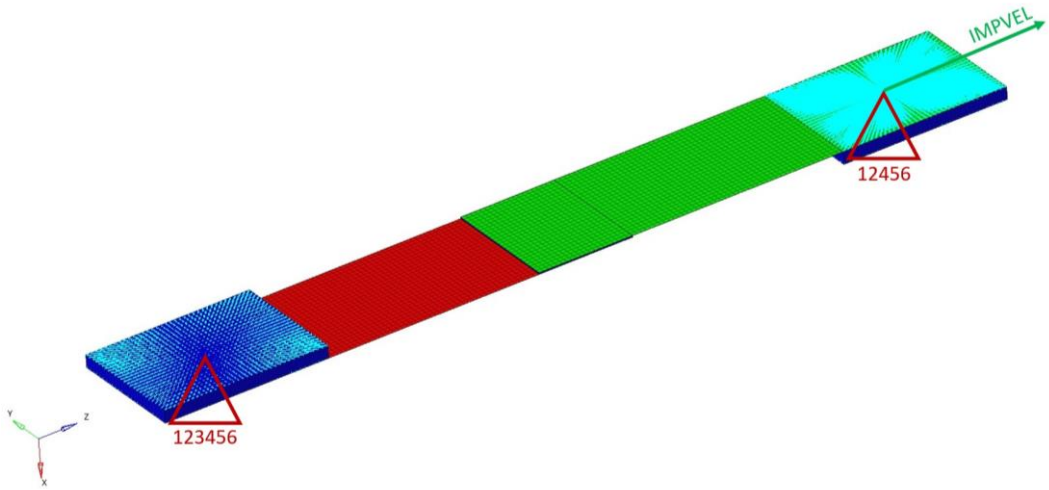

Figure 71. Example of a SLJ HyperMesh model

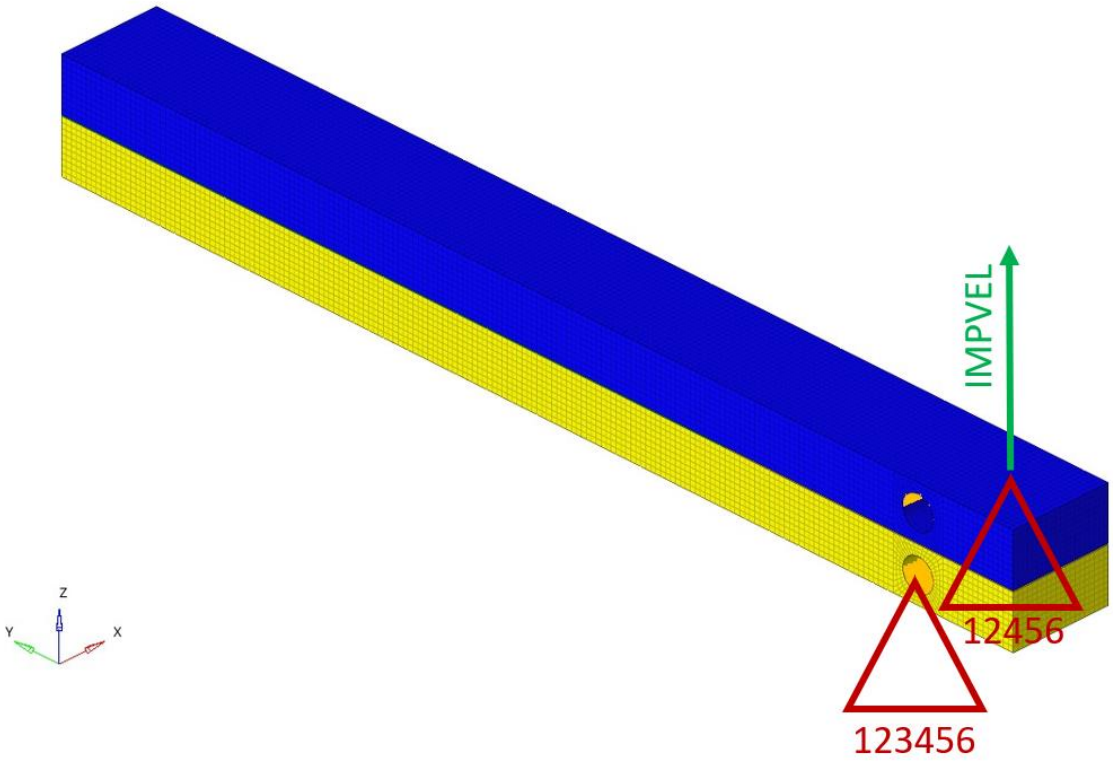

Figure 72. Example of a DCB HyperMesh model

Various trials have been done in order to get a fine enough mesh to catch all the details wanted for the results, the definition of specific time steps to get the results in a limited amount of time while still getting accurate results.

Since on SLJ the adhesive is subjected to a mixed mode loading, this test is used to validate the model of the adhesive. To confirm this in the post processing phase, carried out in the software HyperView, it was possible to check the contribution of mode I and mode II on the single elements, thanks to some specific output variables.

/ANIM/BRICK/USR1 - where, *EI* is the inter energy.

$$c1 = \frac{E(t)}{EI_{\max}}$$

/ANIM/BRICK/USR2

$$c2 = \left(\frac{En}{EN_{\max}}\right)^{N_n} + \left(\frac{Et}{ET_{\max}}\right)^{N_t}$$

/ANIM/BRICK/USR3

$$c3 = f_N\left(\dot{\varepsilon}_N\right) \cdot \frac{\varepsilon_N}{\varepsilon_{\max N}}$$

/ANIM/BRICK/USR4

$$c4 = f_T\left(\dot{\varepsilon}_T\right) \cdot \frac{\varepsilon_T}{\varepsilon_{\max T}}$$

/ANIM/BRICK/USR5

$$c5 = \left|\frac{\varepsilon_N}{\varepsilon_{\max N}} * \alpha_N * f_N\left(\dot{\varepsilon}_N\right)\right|^{\exp_N} + \left|\frac{\varepsilon_T}{\varepsilon_{\max_T}} * \alpha_T * f_T\left(\dot{\varepsilon}_T\right)\right|^{\exp_T} > 1$$

Figure 73. HyperView output variables [22].

USR1: is a variable used when a single general energy criteria is used for the element, without taking into account the single contribution of Mode I and II.

E(t), is the instantaneous internal energy of the element.

EI_{max}, is the maximum internal energy reachable by the element.

USR2: is a variable used when both energy contribution of Mode I and II are considered and it represents the sum of the two contributions.

En, is the instantaneous internal energy of the element for Mode I.

EN_{max}, is the maximum internal energy reachable by the element for Mode I.

N_n is the exponent for normal energy failure criteria.

Et, is the instantaneous internal energy of the element for Mode II.

ET_{max}, is the maximum internal energy reachable by the element for Mode II.

N_t is the exponent for tangential energy failure criteria.

USR3: is a variable used to visualize the single contribution of element relative displacement (elongation) caused by mode I.

$f_N(\dot{\varepsilon}N)$, is a function representing failure scale factor in normal direction vs elongation rate.

εN, is the instantaneous relative displacement of the element in Mode I.

$\varepsilon_{max}N$, is the maximum relative displacement of the element in Mode I.

USR4: is a variable used to visualize the single contribution of element relative displacement (elongation) caused by mode II.

$f_T(\dot{\varepsilon}T)$, is a function representing failure scale factor in tangential direction vs elongation rate.

εT, is the instantaneous relative displacement of the element in Mode II.

$\varepsilon_{max}T$, is the maximum relative displacement of the element in Mode II.

USR5: is a variable used to visualize the combined element relative displacement (elongation) caused mode I and II.

$f_N(\dot{\varepsilon}N)$, is a function representing failure scale factor in normal direction vs elongation rate.

εN, is the instantaneous relative displacement of the element in Mode I.

$\varepsilon_{max}N$, is the maximum relative displacement of the element in Mode I.

α_N is the normal direction scale factor.

exp_N is the failure exponent parameter in normal direction.

$f_T(\dot{\varepsilon}T)$, is a function representing failure scale factor in tangential direction vs elongation rate.

εT, is the instantaneous relative displacement of the element in Mode II.

$\varepsilon_{max}T$, is the maximum relative displacement of the element in Mode II.

α_T is the tangential direction scale factor.

exp_T is the failure exponent parameter in tangential direction.

5.2.1 Results and validation process

In this section, the validation process actuated for the adhesive card will be explained.

First of all some of the parameters related to adhesive material and failure card were estimated by references found in literature or previous experience. Then with SLJ experimental results correlation between numerical and experimental data was done. SLJ tests are useful to validate a virtual model since both contributions of peel and shear are present, so the mixed mode failure prevails, thus accurate properties of Mode I and II are required with adequate failure criteria accounting for the two modes.
In the following, the main parameter sensitivity analysis will be shown.
To better comprehend the effect of each parameter a graphic description will be given, with the arrow showing the direction of increment of the given parameter.

EN,ET: By increasing the failure internal energy the area under the curve increased with a later failure of the elements. So overall the joint is able to absorb more energy before failure. This is valid for both mode I (N - Normal) and II (T - Tangential)

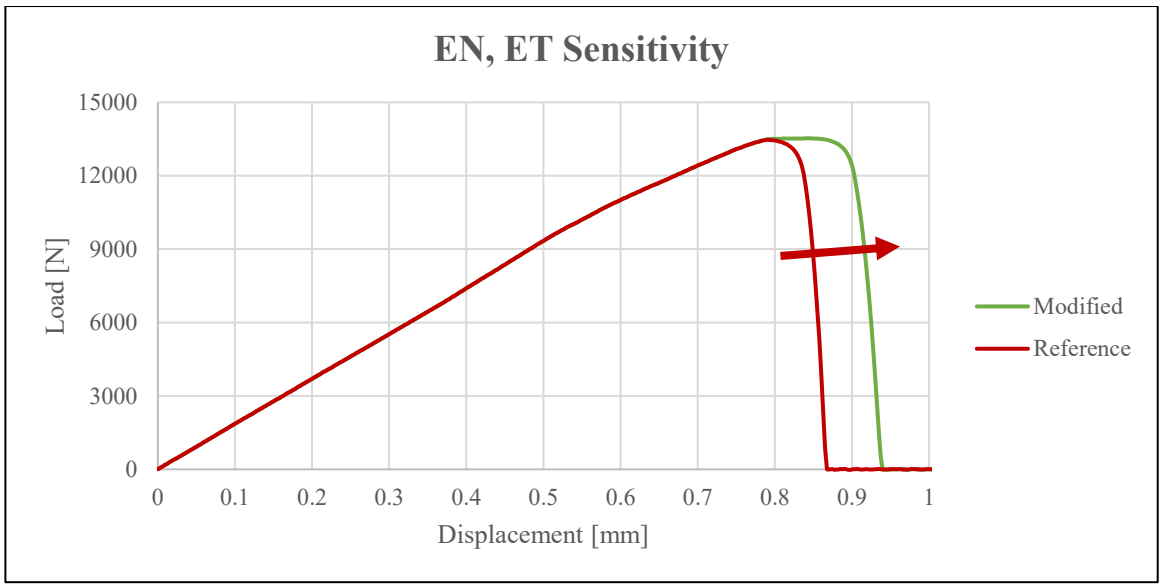

Figure 74. Internal energy parameter sensitivity

Tmax: By increasing the duration parameter for energy failure criteria again the area under the curve increased with a later failure of the elements, in particular by increasing Tmax a lower softening has been noticed with a more gradual failure of the elements. So overall the joint is able to absorb more energy before failure.

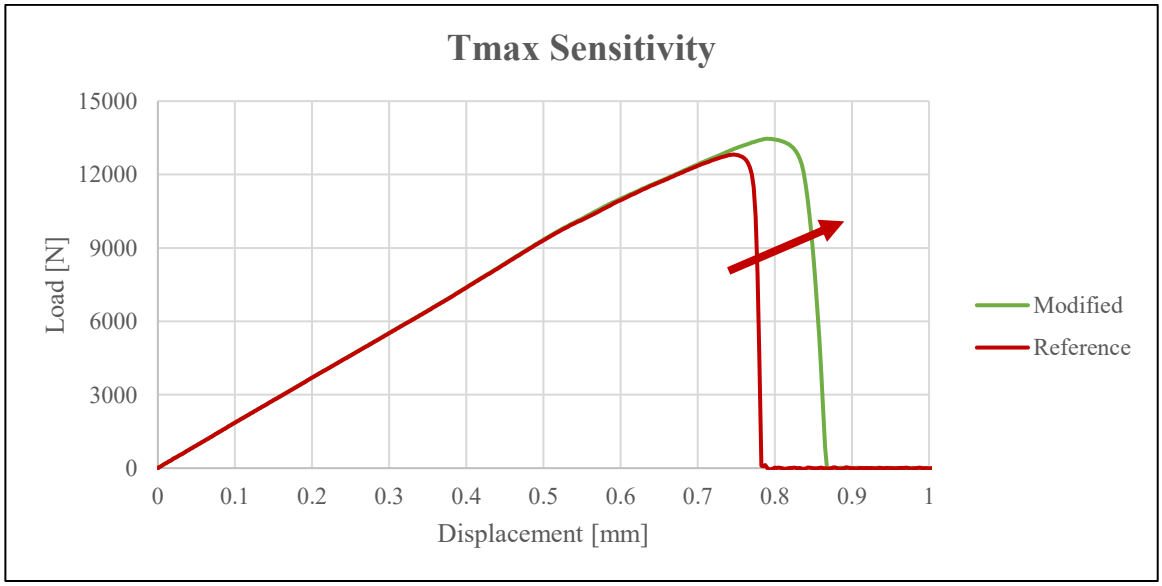

Figure 75. Duration parameter sensitivity

Nsoft: By increasing the softening exponent for failure parameter the area under the curve decreased with a sooner failure of the elements, in particular by increasing Nsoft a steeper softening has been noticed with a more sudden failure of the elements. So overall the joint is able to absorb less energy before failure.

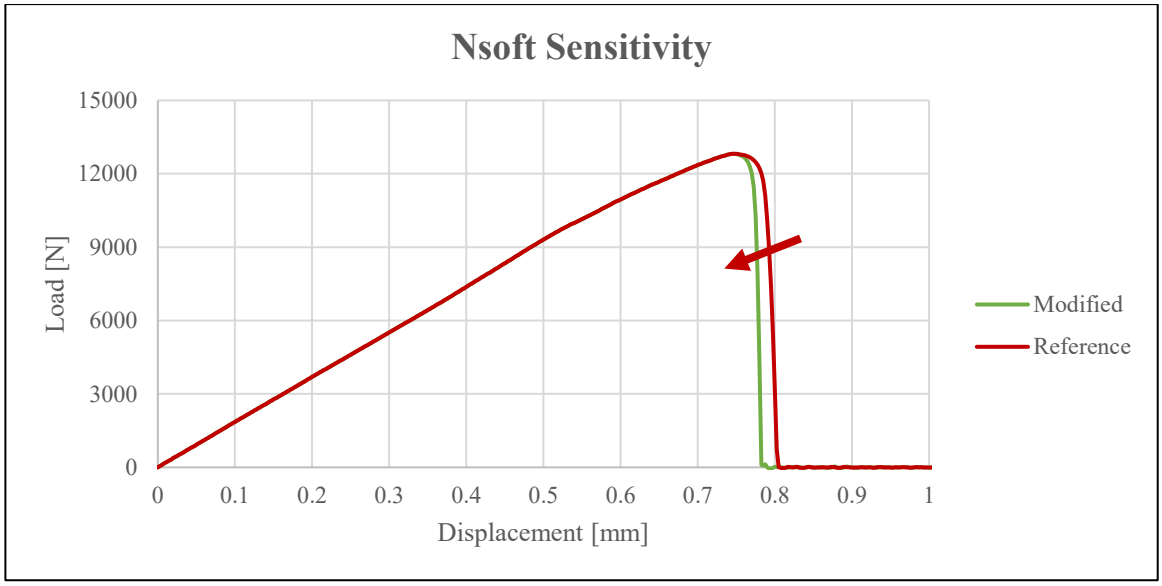

Figure 76.Softening exponent parameter sensitivity

Plastic stress: By increasing the plastic stress curve, the peak load reached before failure increased. The elements were able to sustain higher loads before failure.

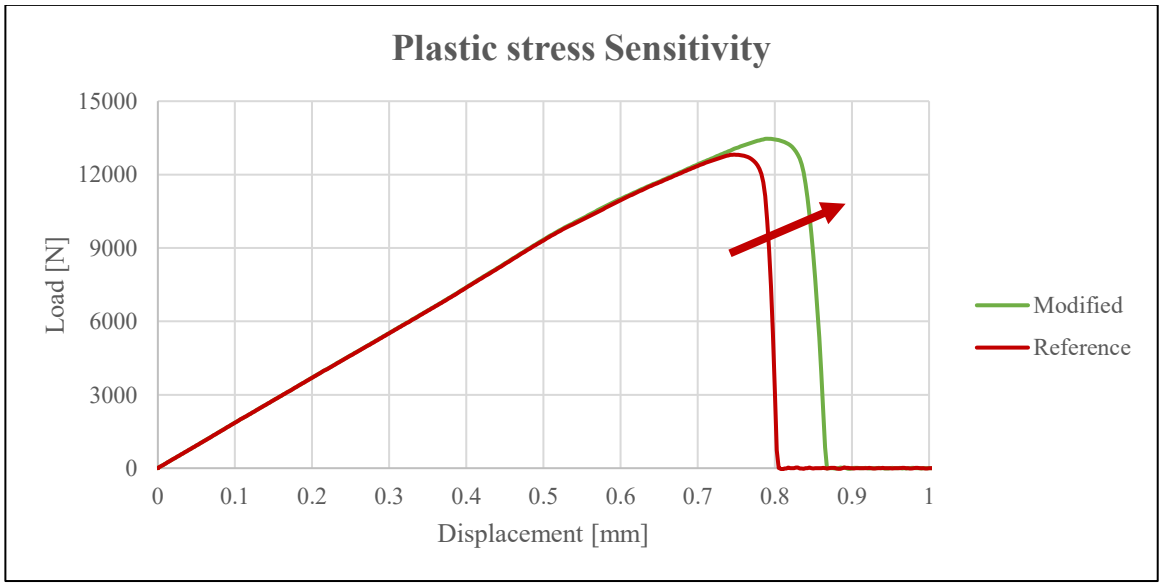

Figure 77. Plastic stress parameter sensitivity

The listed properties have been to most effective ones in the tuning of the card to obtain a proper behavior of the adhesive, trying to well represent the experimental data obtained in the lab tests.

In the following experimental vs numerical comparison will be shown for the various adhesive thicknesses and overlap length tested. The numerical results have been obtained with the tuned card with the values that most represented the experimental curve.

To correctly analyze the obtained results, the Load – Displacement curve can be divided in to three main phases: linear part of the curve up to the start of damage of the adhesive elements, initial damage of the adhesive elements and peak load, completion of damaging and max displacement at the break.

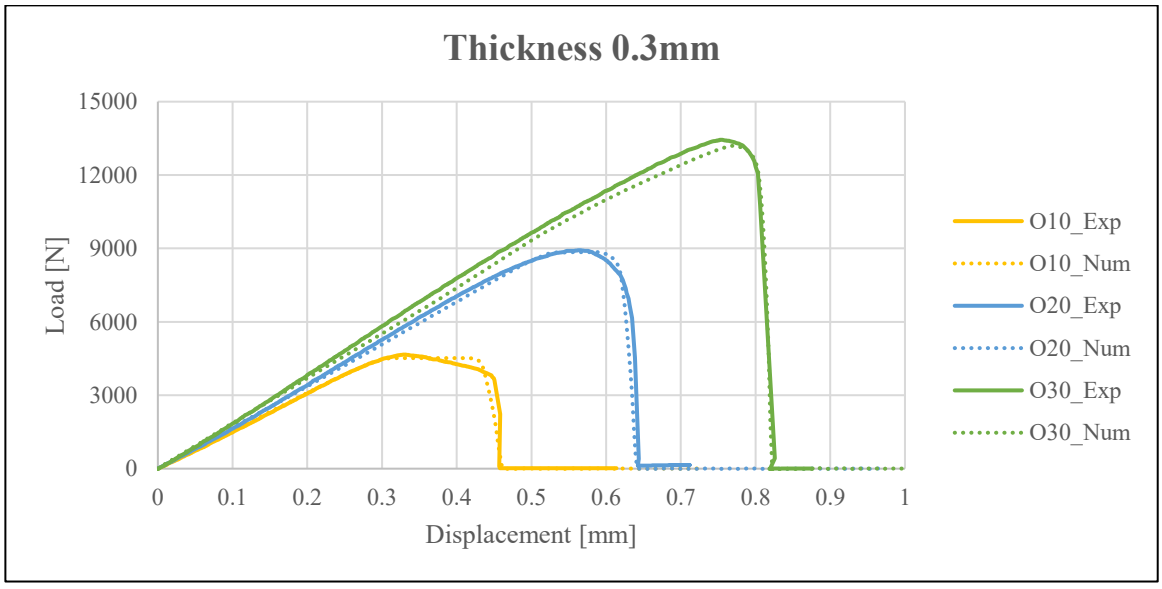

Figure 78. Experimental vs Numerical - SLJ - Thickness 0.3mm

For the 0.3mm adhesive thickness by looking at the curves, it was clear how for the linear part the stiffness was very well aligned with the experimental curves, especially for lower overlap lengths. Then for the peak load, all the cases showed a very similar value with respect to the experimental data, as well as a good representation of the damaging phase of the adhesive. In the last phase of the damaging also the softening

was quite well represented with accurate displacement at break values. Overall for this case numerical simulation curves copied quite well the experimental data, in particular the area under the curve, representing the energy absorbed during the test, was either the same or a bit lower for the virtual simulation, showing a conservative side which is preferred in the design phase, instead of an over estimation of the adhesive properties.

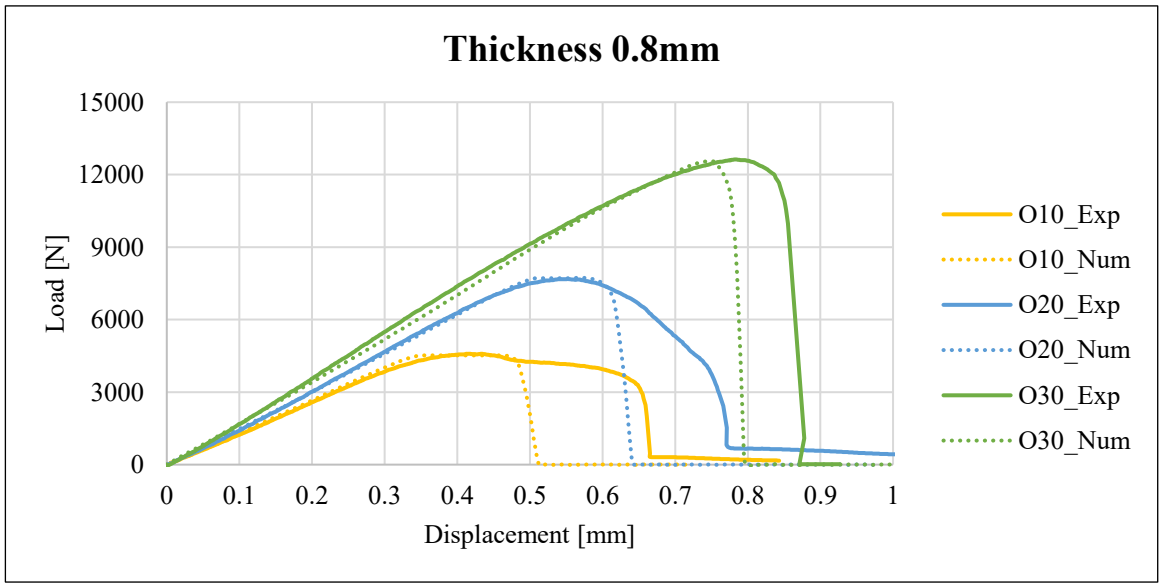

Figure 79. Experimental vs Numerical - SLJ - Thickness 0.8mm

Similar considerations can be made for the 0.8mm adhesive thickness, where the linear part was quite well represented in all cases. Peak load was again very similar between experimental and numerical curves. Then damage initiation and early propagation were represented well. Instead for the last phase, the numerical results showed an earlier failure of the adhesive, which was not able to absorb as much energy as for the experimental results. Acting on the internal energy parameter of the card could solve this early failure for this case, but would get worse in other ones.

Anyway, the early failure represents an under-estimation of the adhesive properties, which is on the safe side for the design phase.

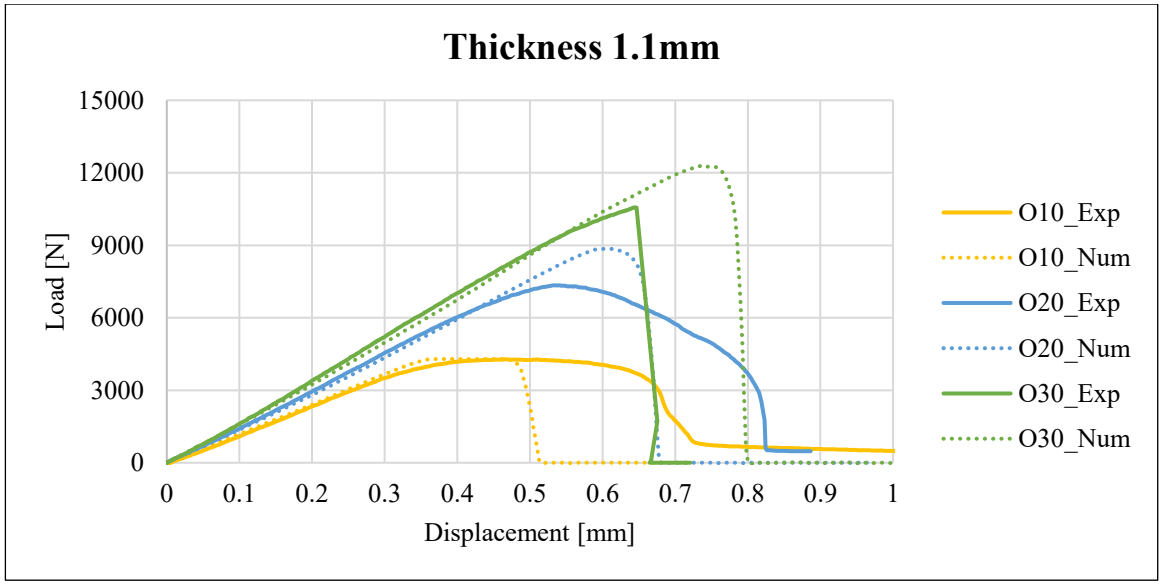

Figure 80. Experimental vs Numerical - SLJ - Thickness 1.1mm

For the 1.1mm adhesive thickness same considerations of the 0.8mm can be done for the 10mm overlap length. While for the 20mm and 30mm, since in the experimental results fiber tear failure happened, the simulation did not catch the particular CFRP failure, but showed a perfectly cohesive failure, which led to similar curves as for the previous cases, so the imminent fragile failure obtained in the lab tests was not caught. This condition showed an overestimation of the peak load in the 20mm and 30mm overlap length since in the simulation the fiber was still able to carry load without reaching premature failure. This lead also to an over estimation of the area under the curve for the 30mm case.

The adhesive card has been tuned for the 0.3mm adhesive thickness and used also for the other ones. This is not ideal since the adhesive behaves a bit differently in case of different thickness, in fact this inaccuracy was shown in the presented results. This choice has been taken to have a single card in the design phase, without having to perform different analyses for the same case. Since for higher adhesive thicknesses the numerical results showed a conservative trend, this allowed us to stick with the single card option.

It is possible to say that excluding the fiber tear cases obtained for higher overlap lengths and thicknesses, which the simulation was not able to represent, all the other cases were quite well represented by the numerical analysis, showing accurate results even for a single tuned card used for all the configurations.

In the post processing phase carried out in Altair Hyperview all the user variables given by the software have been used to visualize the behavior of the adhesive elements. Among all of them, USR3 and USR4 were the most useful ones, representing respectively the peel and shear contribution on each element of the adhesive. Through their display, it was possible to understand the overall trend of the relative displacement along the overlap lengths and correlate it to the analytical models presented in the previous chapter.

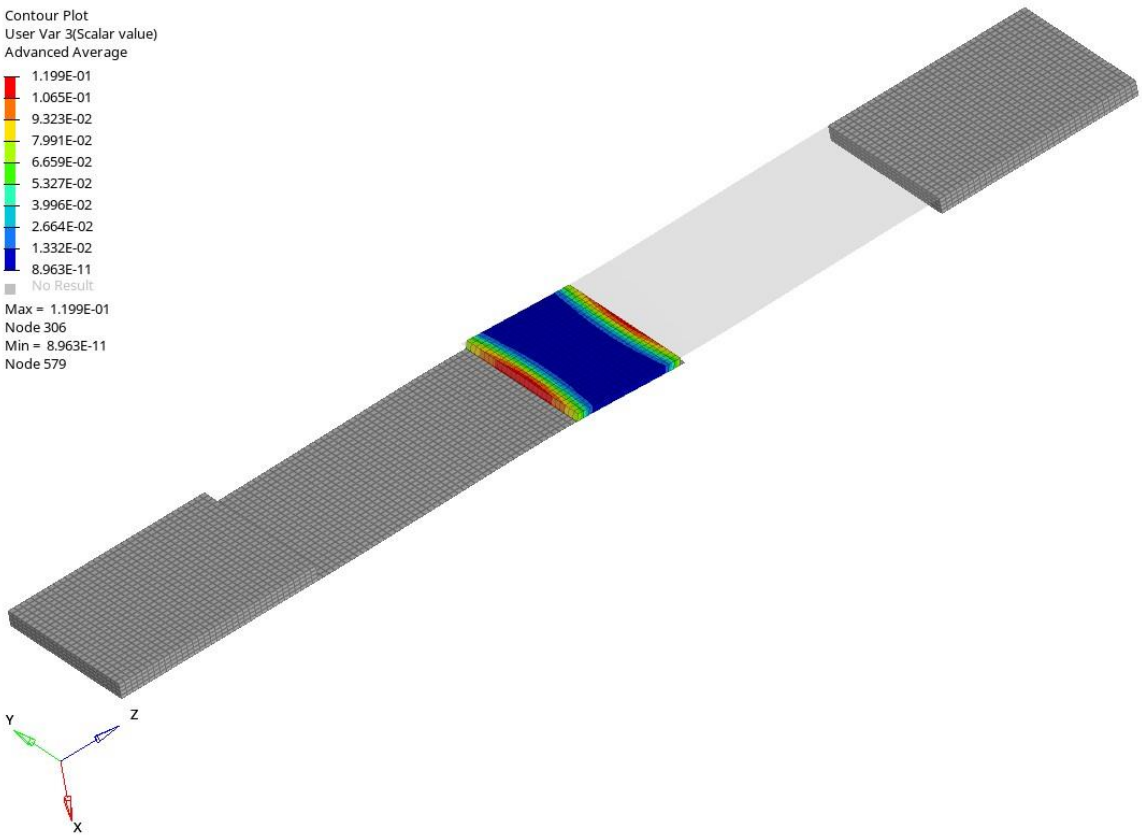

Figure 81. USR3 - SLJ Peel contribution

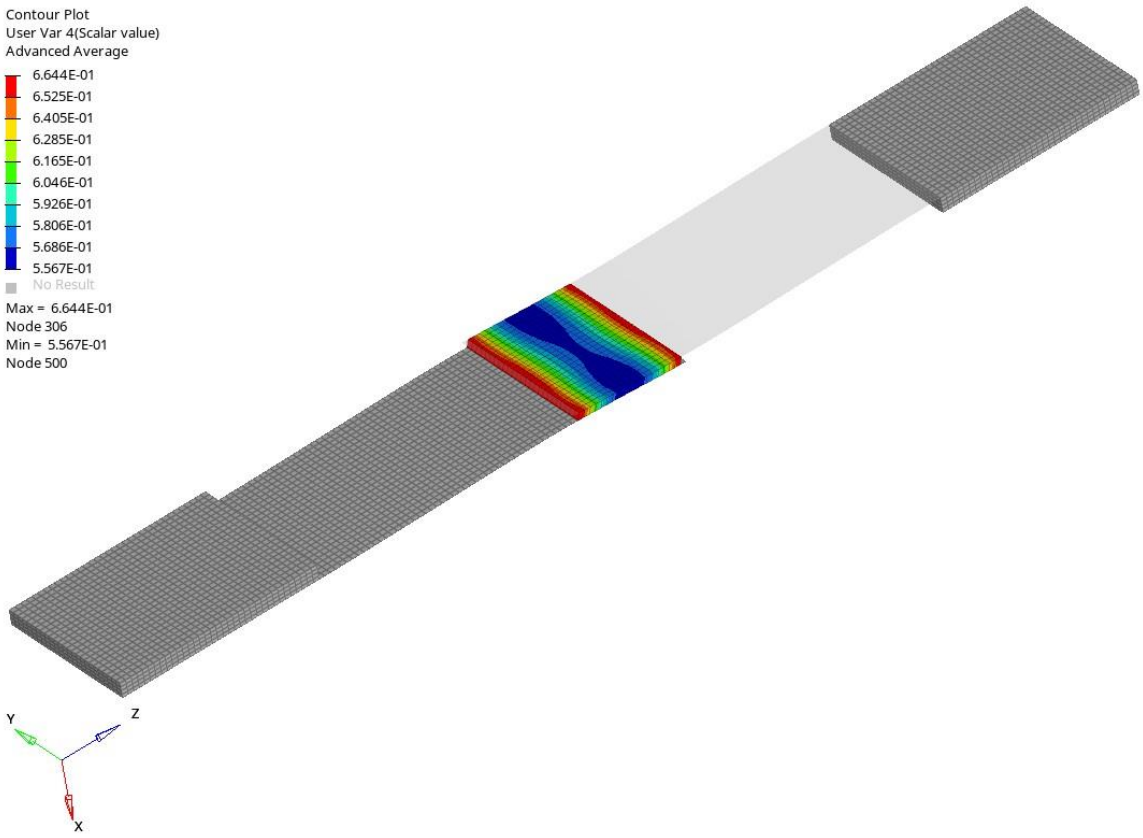

Figure 82. USR4 – SLJ Shear contribution

On top of the graphical display of the contours, a diagram showing the relative displacement contribution as a function of the overlap lengths can be useful to comprehend the actual trend in more detail. In the following graph, the USR3 and USR4 displayed were taken on the centerline of the joint with the zero centered in the middle of the bonding area. Being a relative displacement the values can range from 0 to 1 for both peel and shear.

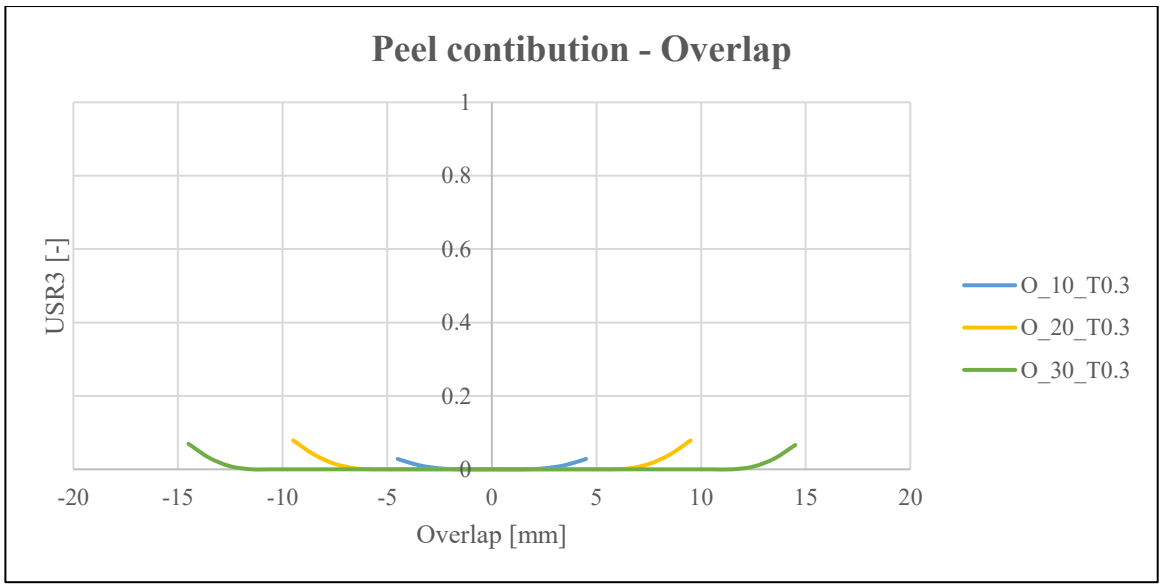

Figure 83. Peel contribution

In the SLJ configuration a little peel contribution can be seen, but still not negligible, in fact for higher overlap lengths its contribution is higher and it is responsible for the fibre tear failure described previously. As predicted from theory a higher contribution is present in the bonding area edges, with the maximum values reached at the tips.

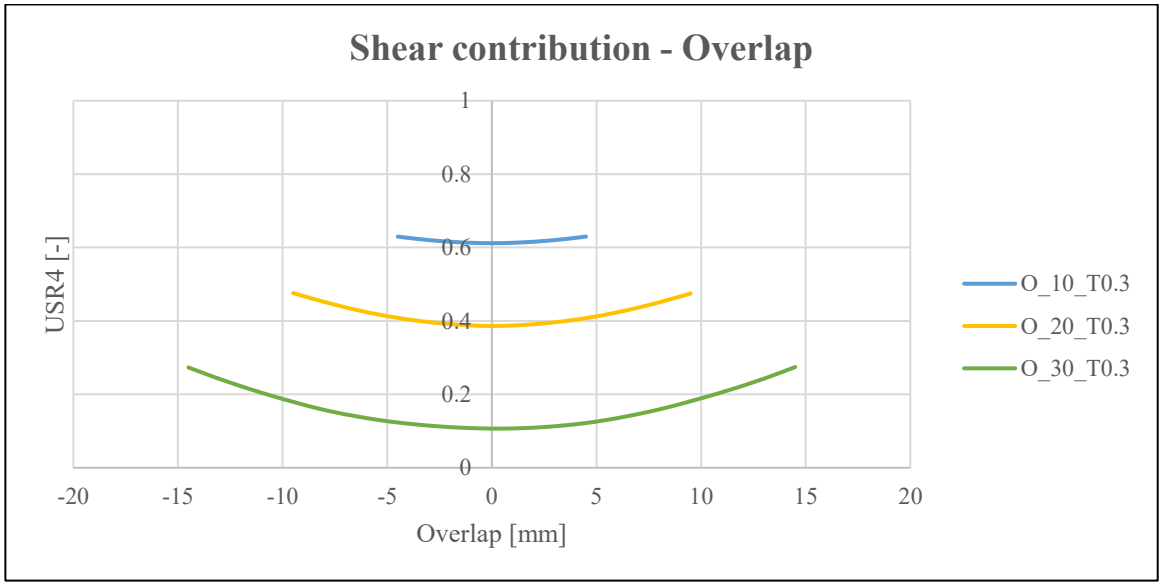

Figure 84. Shear contribution

From the shear contribution graph instead, as predicted from theory models, for smaller overlap lengths the shear is higher and more uniform along the bonding area, while for bigger overlap lengths the maximum is still at the tips, but the shear contribution diminishes significantly in the middle near the zero mark. This causes the adhesive present in the bonding area to not be fully exploited since it is highly loaded at the extremities and not in the middle. From the graph it is also possible to see a lower overall shear contribution for higher overlap lengths.

Now a more detailed diagram for the 10mm overlap length will be shown to compare it with the theory models.

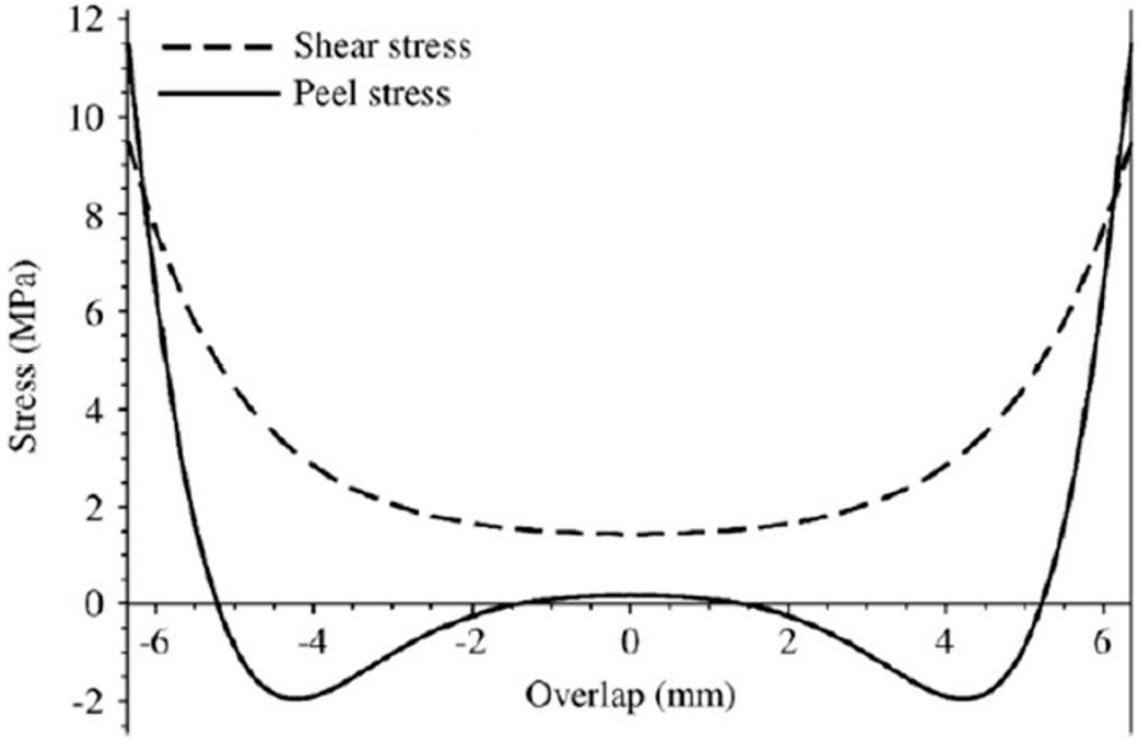

Figure 85. Theory model recall

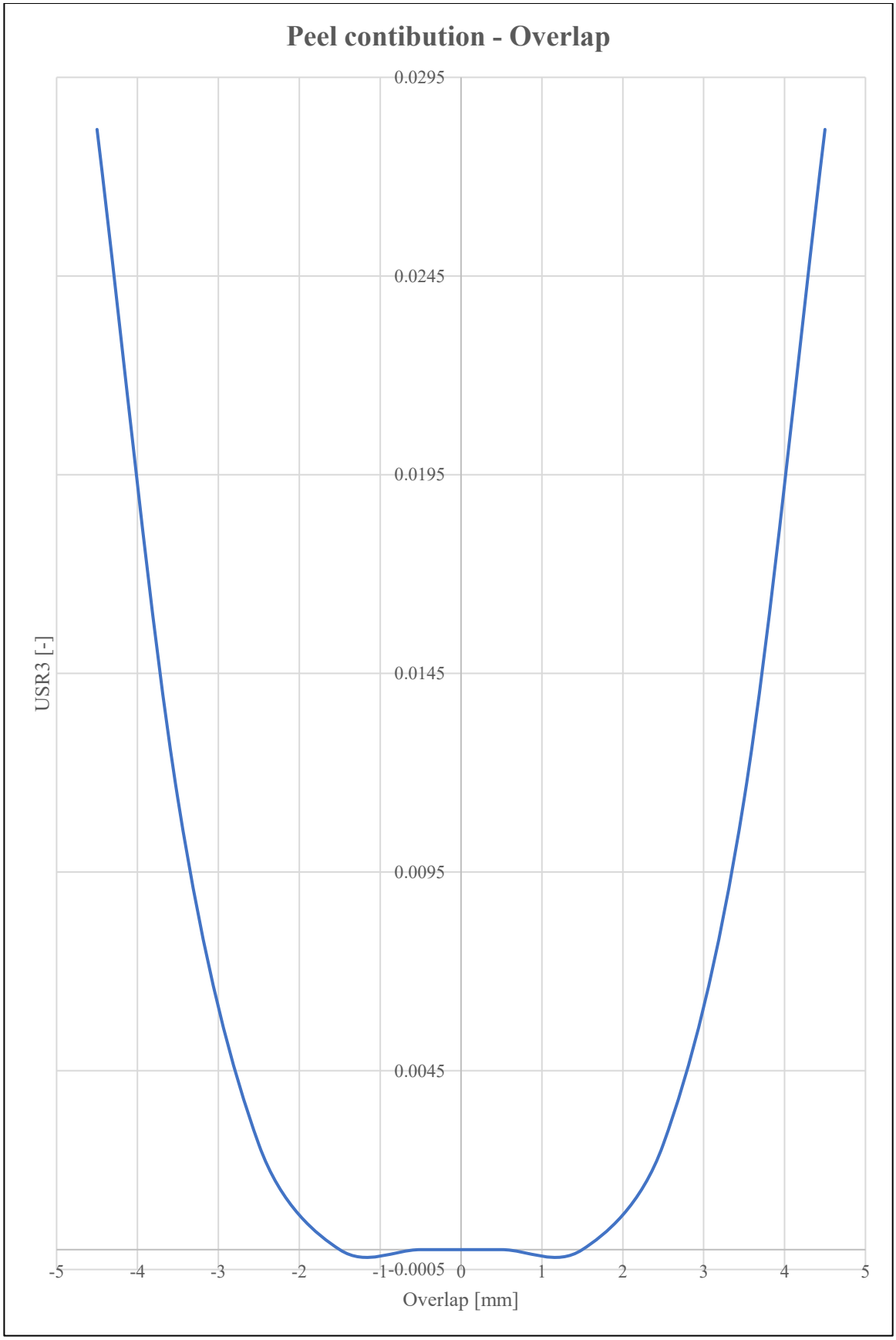

Figure 86. Peel contribution - 10mm overlap

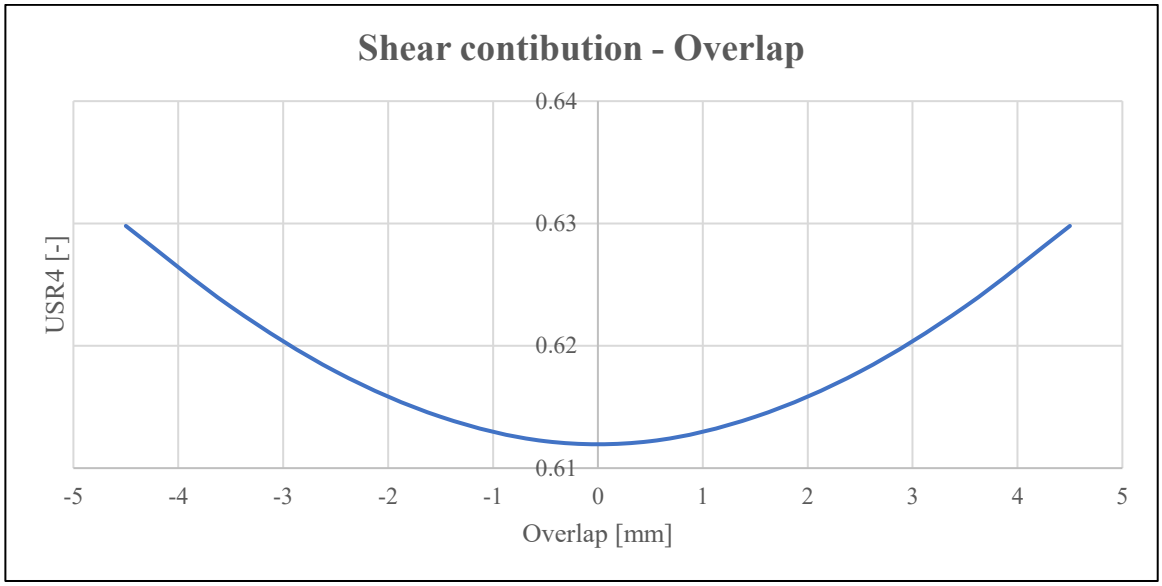

Figure 87. Shear contribution - 10mm overlap

By looking at the peel contribution it is visible the omega shape of the curve, which represents an inversion of the trend in the middle of the bonding area. The high contribution at the joint tips is also appreciable.
A wide parabolic trend is instead visible in the shear contribution, where maximum shear happens at the extremities and minimum one in the middle with a monotonic increasing trend.
In general both peel and shear numerical results showed a very similar trend with respect to the analytical model.

In the virtual simulation a desired timestep has been chosen to catch element deletion in an accurate way, in fact as can be seen in the next picture, elements are deleted step by step as adhesive degradation happens and even in the same row elements lose rigidity and reach failure one by one. This was a crucial step to include in the simulation to achieve accurate results and overlap experimental vs numerical curves.

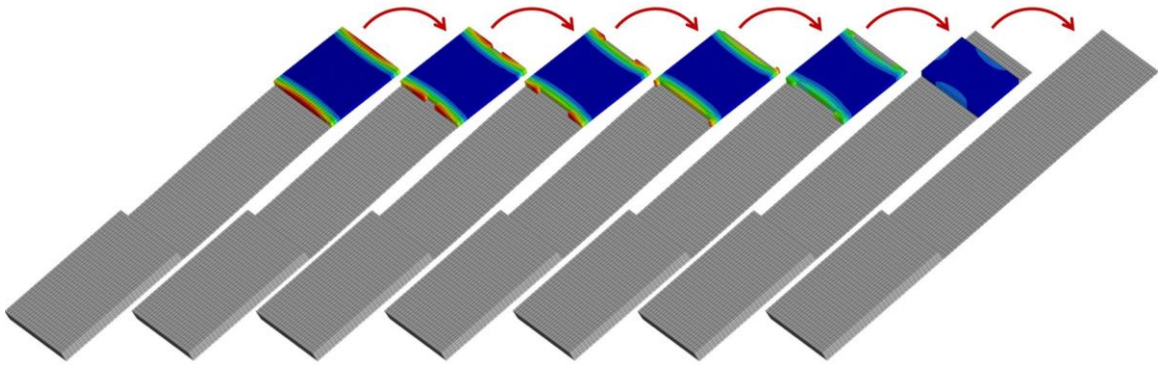

Figure 88. Adhesive element deletion

As a last study to achieve more accurate results a comparison between the use of 1 element on adhesive thickness and 3 elements has been carried out, with the latter showing a higher degree of freedom in the failure of the elements, representing better the non-perfect cohesive failure obtained in the real specimens. This showed also a higher capability to absorb energy before failure on the 3-element case, which could be beneficial in the representation of the cases at higher adhesive thickness, where the standard card was not able to predict the failure in such an accurate way.

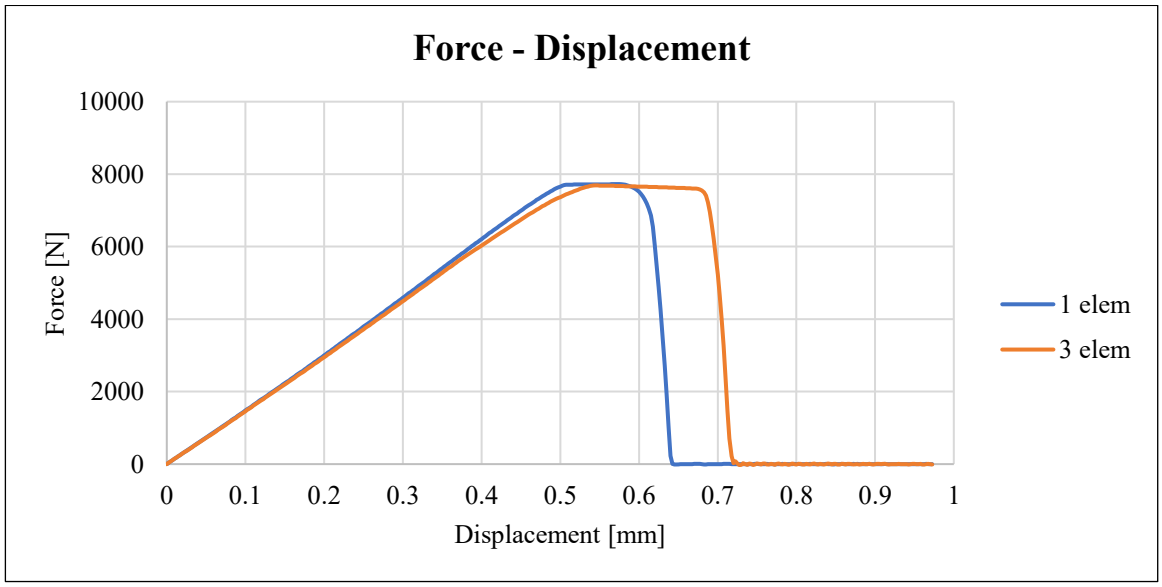

Figure 89. Load – Displacement, 1 element vs 3 element

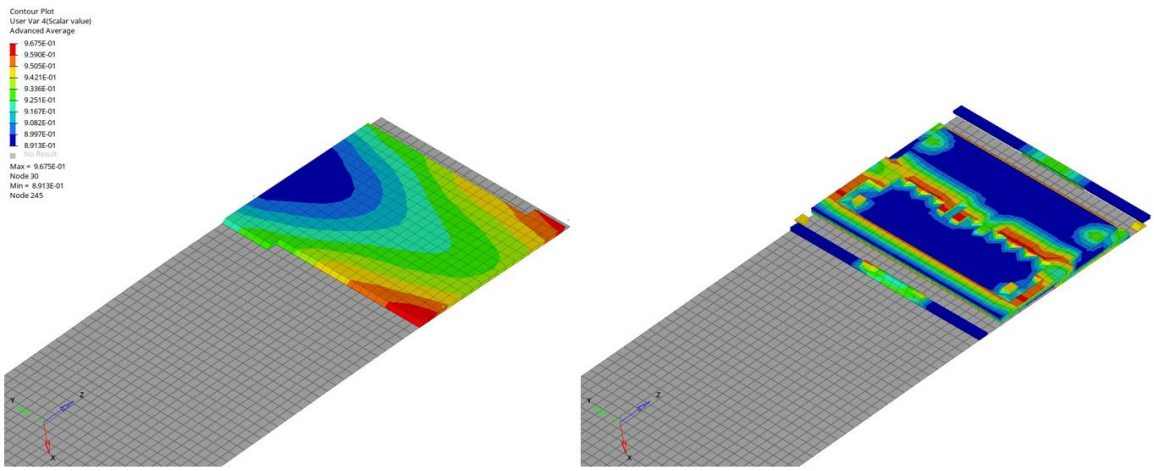

Figure 90. USR4, 1 element (left) vs 3 element (right)

On top of the SLJ models and their validations also DCB models have been developed for the three studied thicknesses. This allowed to simulate another experimental test in which pure mode I is the failure mode of the adhesive. The same parameters explained previously to describe the adhesive card in the SLJ section were used to develop the adhesive card to work also for this condition of loading and represent quite well the experimental curves.

In the following diagram the obtained results will be shown.

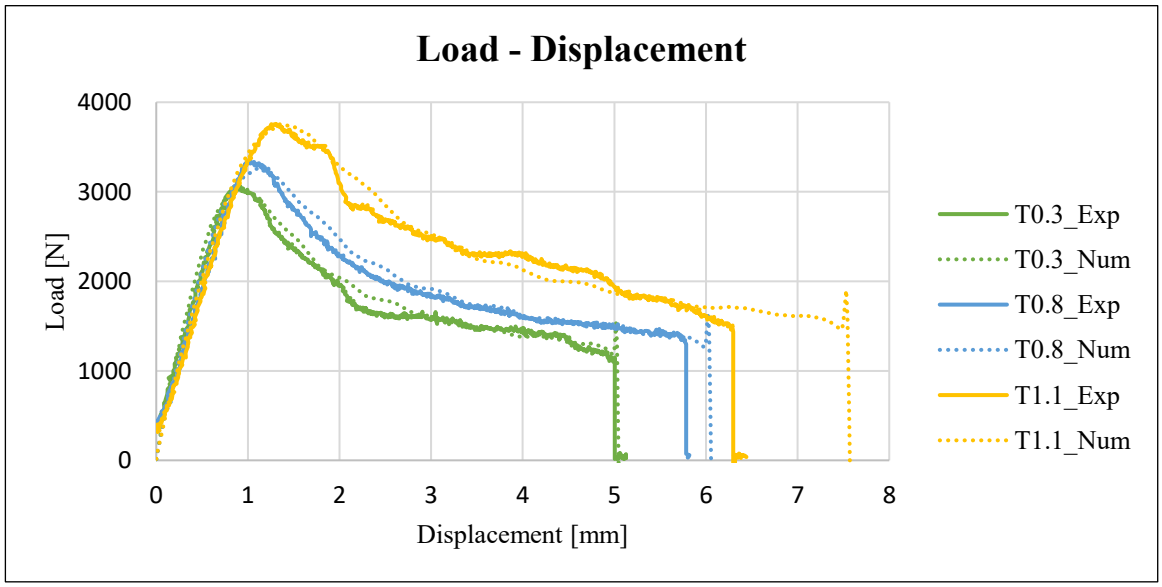

Figure 91. Experimental vs Numerical - DCB

As can be seen in the graph, all the numerical simulation curves represent very closely the experimental ones. In particular, it is possible to distinguish different phases of the specimen loading. The first part is related to the increment of load while everything remains in the elastic field and no damage has happened in the adhesive, this lasts up to peak load, which represents the start of the damaging phase of the adhesive up to the rupture of the first elements, after which load starts to decrease constantly and crack propagates in the adhesive layer, this condition lasts until the two substrates are separated. It is clear how the FEM results can copy well the experimental data, especially in the first part of the test up to around 5 mm of aperture which is the part of the test with the main focus, after which very large displacement and strong non-linearities arise, making for a simulation out of the scope of this research.

It's interesting to see from USR3 the peel contribution of this test, which as expected is dominant, being 99.9%.

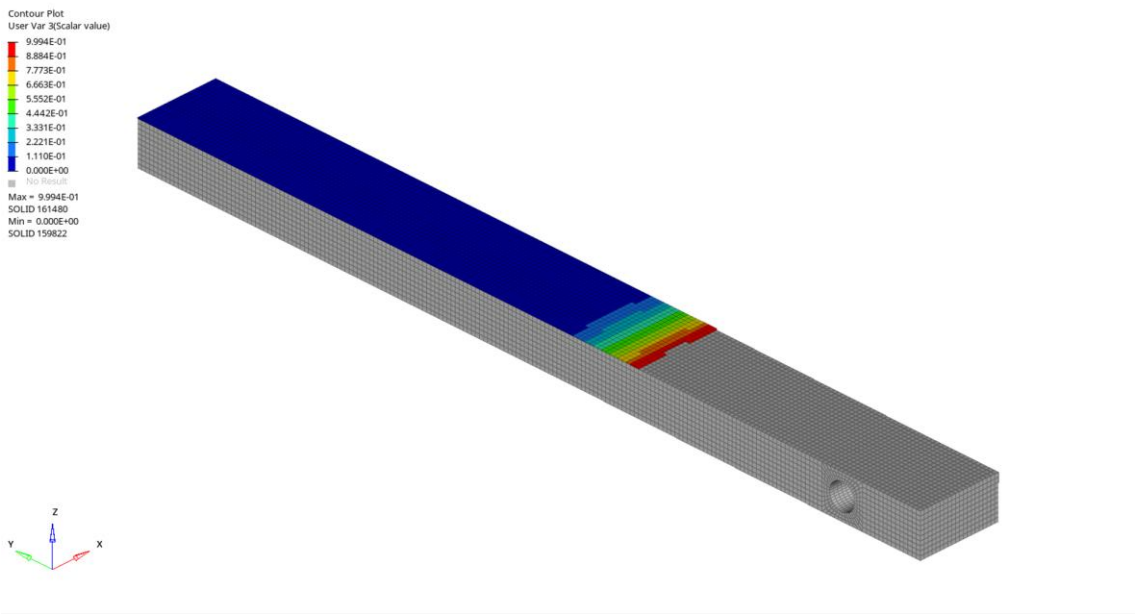

Figure 92. USR3 – DCB Peel contribution

5.3 LS-DYNA

Another target of this work was to compare the numerical results using two different software, so in this section, the results related to LS-DYNA solver will be shown.

In this case preprocessing phase has been done by importing all the needed geometries into the software LS-PrePost, then meshing all the wanted surfaces with 2D elements for shells and 3D for solids. Adhesives have been modelled with brick elements as for RADIOSS. To fully compare the results the models have been created in the same way in both software to replicate the same conditions. Some differences in the definition of some parameters and cards were necessary since the two solutions adopt different ways to replicate similar elements or components.

The adhesive card has been defined by MAT 138-COHESIVE_MIXED_MODE, which is a simplification of *MAT_COHESIVE_GENERAL restricted to linear softening. It includes a bilinear traction-separation law with a quadratic mixed-mode delamination criterion and a damage formulation. This material model can be used only with cohesive element formulations. [23]

Boundary conditions and loads have been applied replicating experimental test conditions to simulate the load applied by the tensile testing machine moving at a desired constant speed.

Also in LS-DYNA card tuning has been performed to obtain a small difference between experimental and numerical data. In this case, the adhesive card was much more straightforward, with way fewer inputs to define the card, since only the triangular law main parameters had to be inserted. This led to a faster and easier approach to the setting up of the model, but as the results will show, probably a less accurate solution for some of the tested configurations.

Basically, 6 main parameters were only needed to describe the card, so as done previously in the following the main parameters sensitivity analysis will be shown.
To better comprehend the effect of each parameter a graphic description will be given, with the arrow showing the direction of increment of the given parameter.

G_IC, $G_{II}C$: By increasing the energy release rate the area under the curve increased with a later failure of the elements. So overall the joint is able to absorb more energy before failure. This is valid for both modes I and II.

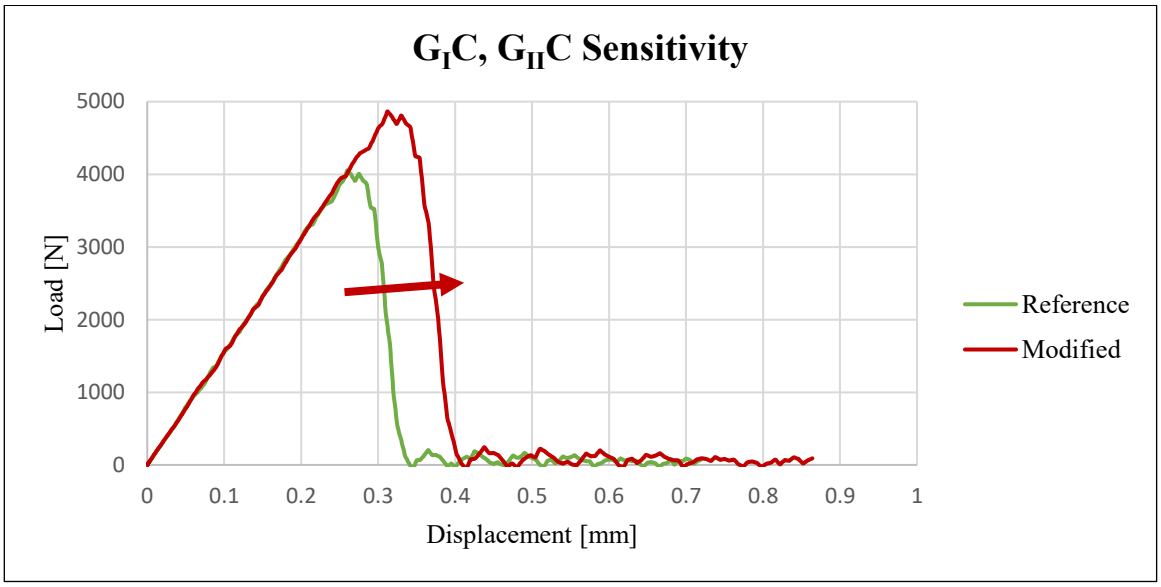

Figure 93. Energy release rate parameter sensitivity

EN, ET: By increasing the stiffness of the element the curve inclination in the first elastic part varied according to the element stiffness. This is valid for both normal and tangential stiffnesses.

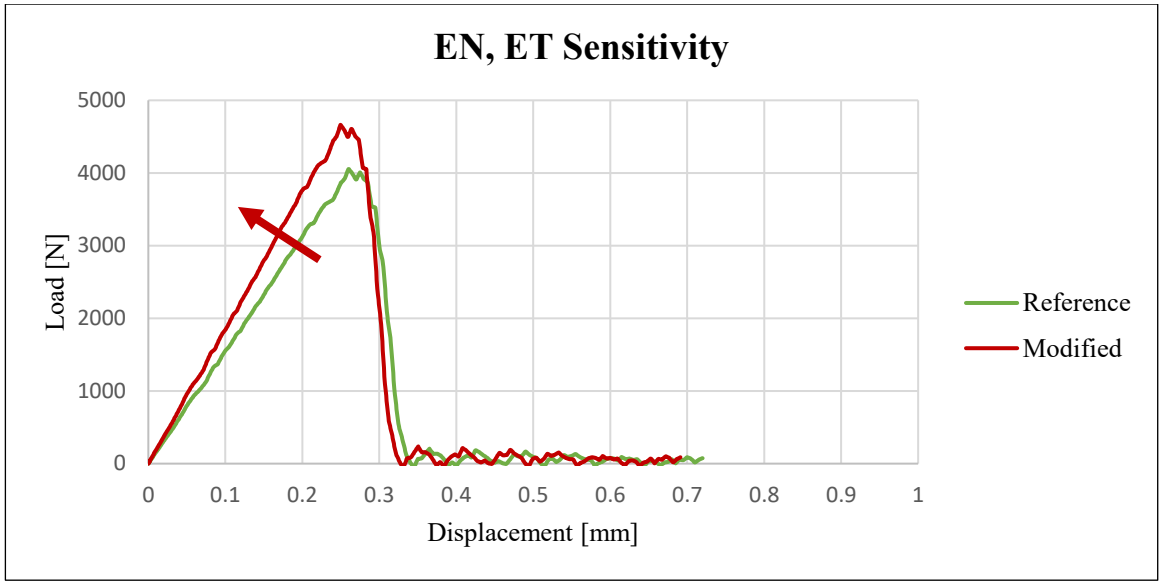

Figure 94. Element stiffness parameter sensitivity

T, S: Increasing peak traction of the adhesive elements led to an increase in loading capability of the adhesive as expected so the elements failed later at a higher load. Again this was valid both for normal and tangential direction.

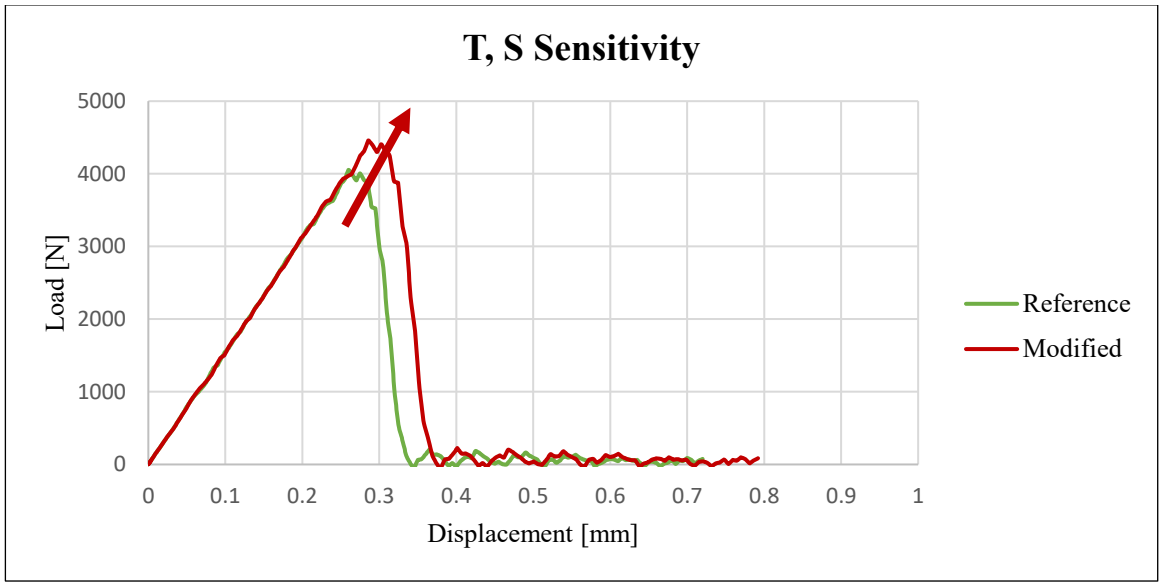

Figure 95. Peak traction parameter sensitivity

In the following, experimental vs numerical comparison will be shown for the various adhesive thicknesses and overlap length tested. The numerical results have been

obtained with the tuned card with the values that most represented the experimental curve.

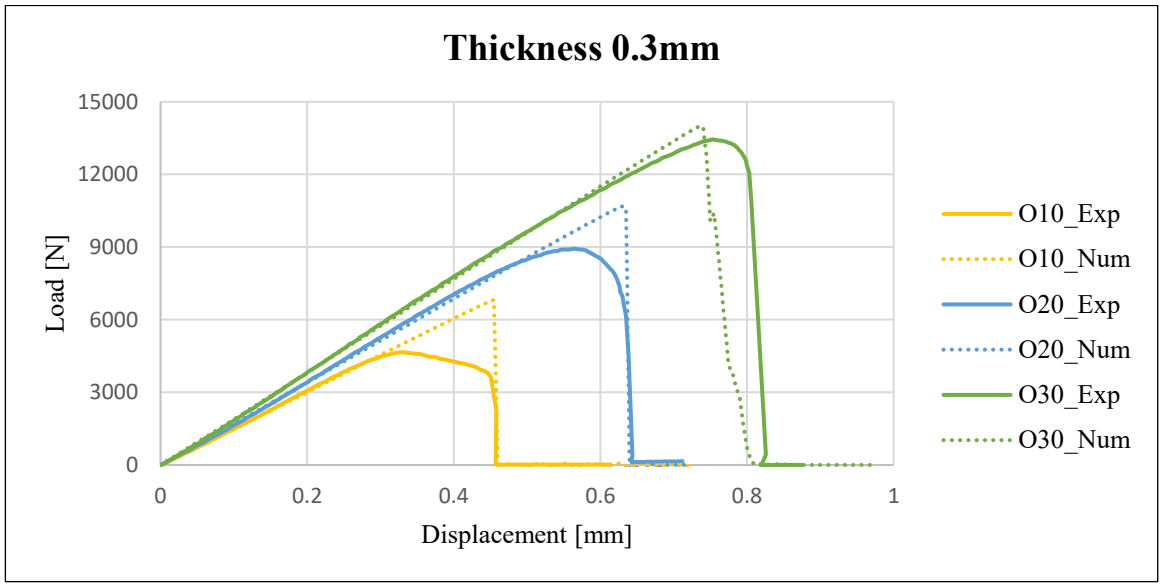

Figure 96. Experimental vs Numerical - SLJ - Thickness 0.3mm

For the 0.3mm adhesive thickness by looking at the curves, it was clear how for the linear part the stiffness was very well aligned with the experimental curves, especially for lower overlap lengths. Then regarding the peak load, numerical simulations were not able to catch the gradual degradation of the elements after the start of damage and propagation of it, while the rupture was imminent, coinciding with the final degradation and softening of the real tests, but carrying an over estimation of the peak load able to sustain by the specimen. This is not a desired condition since the simulation is not on the conservative side of the design with respect to the actual tests. This trend is more evident for lower overlap lengths, while the 30mm case showed a bit less imminent failure and a longer softening phase, representing better the experimental curve, but still not being quite close to the actual behavior of the adhesive.

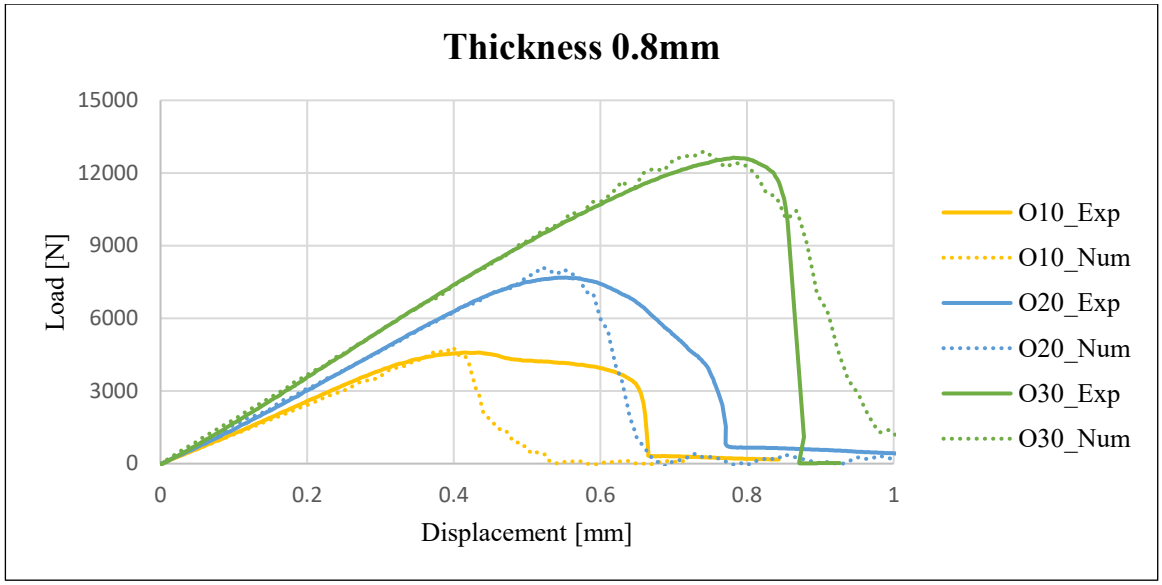

Figure 97. Experimental vs Numerical - SLJ - Thickness 0.8mm

For the 0.8mm adhesive thickness, where the linear part was quite well represented in all cases, the peak load was very similar between experimental and numerical curves. Here damage initiation and early propagation were represented better than in the 0.3mm case since a rounded knee is visible instead of the imminent rupture seen before. Instead for the last phase, the numerical results showed an earlier failure of the adhesive, which was not able to absorb as much energy as for the experimental results. Acting on the internal energy parameter of the card was not enough to copy well the experimental results since then overshoot of the peak load happened, so these results were a right trade-off. Anyway, the early failure represents an underestimation of the adhesive properties, which is on the safe side for the design phase in this case. These considerations were mainly applicable to the 10mm and 20mm overlap lengths, while the 30mm had a longer softening phase with respect to the actual data obtained from physical tests.

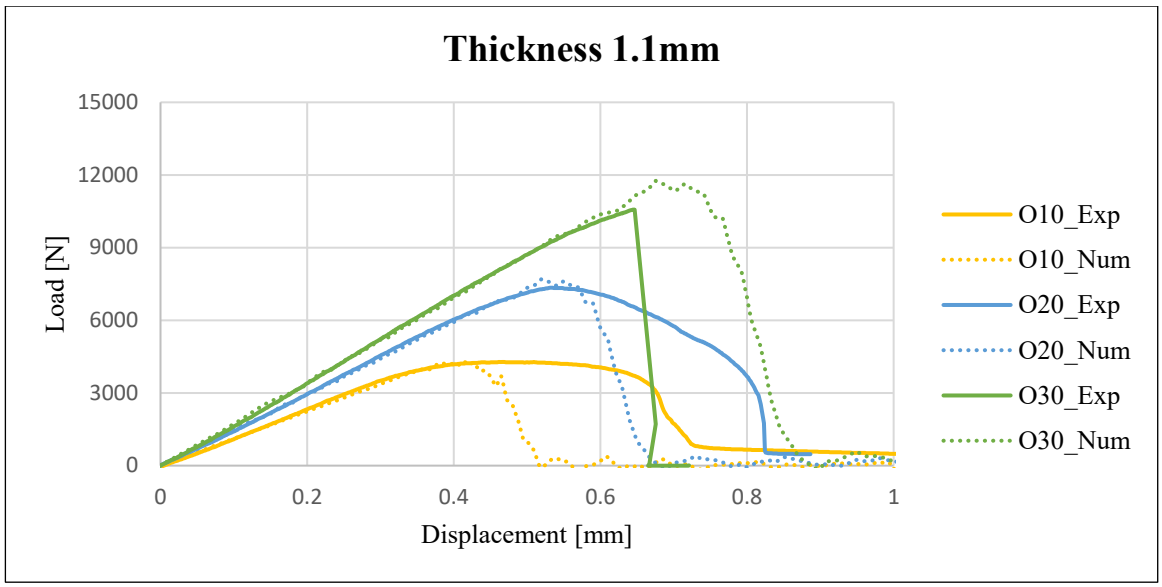

For the 1.1mm adhesive thickness same considerations of the 0.8mm can be done for the 10mm overlap length. While for the 20mm and 30mm, since in the experimental results fiber tear failure happened, the simulation did not catch the particular CFRP failure, but showed a perfectly cohesive failure, which led to similar curves as for the previous cases, so the imminent fragile failure obtained in the lab tests was not caught.

By looking at all the obtained results it is possible to say that general trends were quite closely caught by the simulations in some of the tried configurations, but some errors were also present in other ones. This again could be explained by the used card, which has very few input parameters, which is easy to use but less predictable in the results. Further studies could use a different card definition to obtain results closer to the experimental curves as well as try to represent the failure law of the card with a trapezoidal shape instead of the triangular one, which might help in the degradation phase of the adhesive after the damage has started and might avoid imminent failure of it.

As for the RADIOSS simulations also in LS-DYNA the DCB test was replicated and developed for the three studied thicknesses. The same parameters explained previously to describe the adhesive card in the SLJ section were used to develop the adhesive card

to work also for this condition of loading and represent quite well the experimental curves.

In the following diagram the obtained results will be shown.

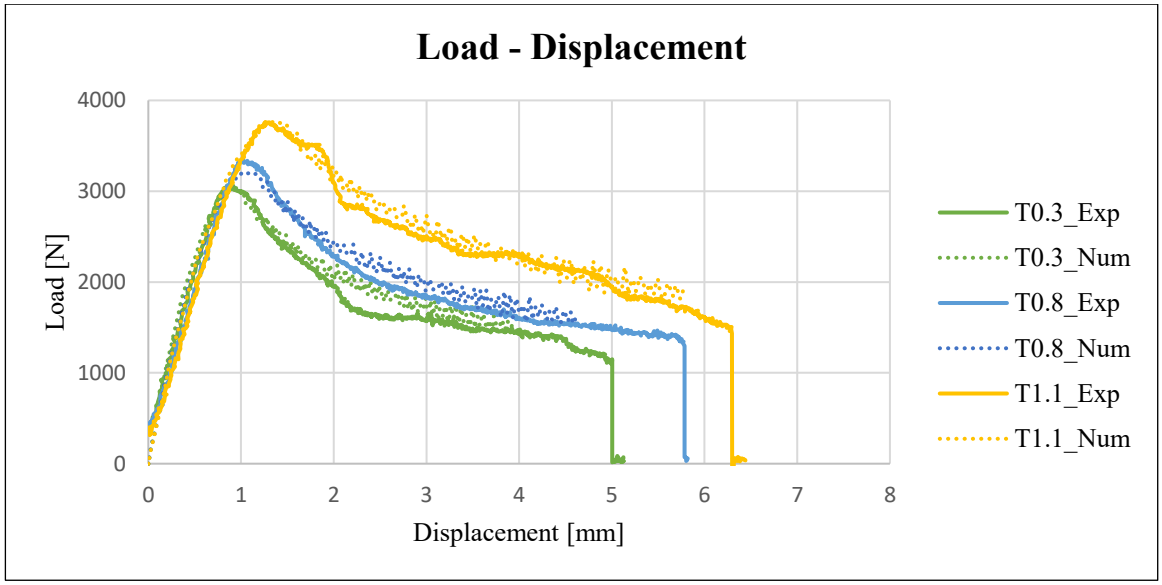

Figure 98. Experimental vs Numerical - DCB

Similar results as for RADIOSS have been obtained here, where the numerical curve represents quite closely the experimental one, especially in the first elastic part where load increases up to the first element failure. The peak load reached in the simulation is comparable with the actual results, as well as the propagation of the crack phase in which the damage of the adhesive elements continues. To obtain numerical curves close to the experimental ones all of the parameters shown in this chapter have been tuned starting from the experimental data gathered during the tests. The experimental curve is more scattered due greater amount of imperfections, voids and non linearities that are not included in the model, but despite this, the trend is accurately resembled.

Conclusion and future development

The primary goal of this thesis work has been the investigation of the mechanical properties of a structural bi-component epoxy adhesive, which is a widespread type in the automotive industry, especially in the last few decades a lot of research has been done to study alternative connections and adhesive joining is one of them.

The research has been divided into a first experimental phase, in which several mechanical tests have been performed (including dog bone samples on pure adhesive, Double Cantilever Beam on metal substrates and Single Lap Joints on carbon fibre substrates) and in a second numerical simulation phase, in which the experimental tests have been replicated with the use of FEA to simulate the adhesive connection and develop numerical models that represented the tested cases.

Preparation of all the specimens has been performed following appropriate Standards for each test, as well as for testing procedures. Experimental data have been elaborated to determine all the required mechanical properties, showing a mid/high mechanical resistance for the studied adhesive, which fulfilled all the expected parameters given in the manufacturer's datasheet.

Then numerical simulation was performed with the help of two different software (RADIOSS and LS-DYNA), the adhesive card modelling was tuned with the experimental data found and a good correlation between experimental tests and numerical simulation has been reached, as shown in the dedicated chapter. This allowed us to have a precise model of the adhesive, especially in RADIOSS, where results were closer to the experimental data in most of the cases. This difference could be due to the formulation of the adhesive card, since many more input parameters were needed in RADIOSS, which meant more variability and greater freedom in tuning it, to achieve the wanted results. While a simpler card has been used in LS-DYNA, it has been reliable and representative of the experimental curves in most of the tested configurations.

Further development of dedicated adhesive cards could improve even more the numerical results to adapt and better tune the card, especially in LS-DYNA where a simple triangular cohesive failure law seemed to not represent well the adhesive behaviour for some configurations and a trapezoidal or exponential curve could improve model reliability.

On top of this, an actual application of real components could help to validate the simulation models and have a clearer picture of the obtainable results. Since SLJ tests involve both normal and tangential loading on the adhesive they have been used to validate the adhesive models in this research, but of course an application where the loading is mixed and applied on a real component could be representative of a more complete study case.

Bibliography

[1] L.F.M. da Silva, A. Öchsner, and R. D.Adams, *Handbook of adhesion technology*. Springer, 2011.

[2] Consuelo Fritz and Juan Francisco Olivera, *Nanocellulose in heterogeneous water-based polymerization for wood adhesives.* 2022.

[3] *Global greenhouse gas emissions by the transportation sector*, https://transportgeography.org/contents/chapter4/transportation-and-environment/greenhouse-gas-emissions-transportation/

[4] R.D. Adams, *Adhesive bonding: Science, technology and applications.* Woodhead publishing limited and CRC Press, 2005.

[5] D. Fazel, M.H. Kadivar, H. Zohoor, M. Farid and M.R. Hematiyan, *Failure procedure in epoxy adhesive joining composite plates*. Springer, 2020.

[6] *Adhesive joints*, https://www.substech.com/dokuwiki/doku.php?id=adhesive_joints

[7] *SikaPower – 1277 product datasheet,* https://industry.sika.com/content/dam/dms/gb01/7/sikapower_-1277.pdf

[8] *SikaPower – 1277 product* https://gbr.sika.com/en/industry/structural-bonding/pre-powder-coating/sikapower-1277.html

[9] L.F.M. da Silva, P.J.C das Neves, R. D.Adams and J.K Spelt, *Analytical models of adhesively bonded joints*. International Journal of Adhesion and Adhesives, 2009.

[10] L.F.M. da Silva and R.D.S.G. Campilho, *Design of adhesively-bonded composite joints.* Fatigue and Fracture of Adhesively-Bonded Composite Joints, 2015.

[11] L.F.M. da Silva, E.A.S. Marques, and R.D.S.G. Campilho, *Handbook of adhesion technology*. Springer, 2018.

[12] L. Goglio and R.D.S.G. Campilho, *Strength prediction of adhesively-bonded joints*. Taylor & Francis Group, CRC Press, 2016.

[13] R.D.S.G. Campilho, M.D. Banea, J.A.B.P. Netoì and L.F.M. da Silva, *Modelling adhesive joints with cohesive zone models: effect of the cohesive law shape of the adhesive layer.* International Journal of Adhesion and Adhesives, 2013.

[14] P. Hu, X. Han, L.F.M. da Silva and W.D. Li, *Strength prediction of adhesively bonded joints under cyclic thermal loading using a cohesive zone model*. International Journal of Adhesion and Adhesives, 2012.

[15] I. Katsivalisa, O.T. Thomsena, S. Feihb and M. Achinthaa, *Development of cohesive zone models for the prediction of damage and failure of glass/steel adhesive joints.* International Journal of Adhesion and Adhesives, 2020.

[16] Cohesive zone modeling – triangular law, https://pub.mdpi-res.com/polymers/polymers-11-01531/article_deploy/html/images/polymers-11-01531-g004.png?1569585807

[17] *Development of cohesive zone models for 3M™ structural adhesives.* 3M Scotch Weld guide.

[18] *Introduction to modeling structural adhesives.* 3M Scotch Weld guide.

[19] D. S. Dugdale, *Journal of the Mechanics and Physics of Solids*, 1960.

[20] G. I. Barenblatt, *Journal of Applied Mathematics and Mechanics*, 1959.

[21] R. Fernandes and R.D.S.G. Campilho, *Testing different cohesive law shapes to predict damage growth in bonded joints loaded in pure tension*. The Journal of Adhesion, 2017.

[22] HyperWorks 2017 RADIOSS Reference guide. Altair® HyperWorks®, 2017.

[23] LS-DYNA® KEYWORD USER'S MANUAL VOLUME II, 2021.